CCDC DAC-TR-2020-040
July 2020

Whole-Body Postmortem Human Subject (PMHS) Testing Technical Report: Tests Conducted in Support of Injury Prediction Capabilities Development – Test Series WS10, WS11, and WS12

by Constantine Demetropoulos, John Cavanaugh, Kyle Ott, Jonathan Rupp, David Drewry III, Matthew Montoya, David R. Barnes, and Kathryn L. Loftis

DISCLAIMER

The findings in this report are not to be construed as an official Department of the Army position unless so specified by other official documentation.

WARNING

Information and data contained in this document are based on the input available at the time of preparation.

TRADE NAMES

The use of trade names in this report does not constitute an official endorsement or approval of the use of such commercial hardware or software. The report may not be cited for purposes of advertisement.

CCDC DAC-TR-2020-040
July 2020

Whole-Body Postmortem Human Subject (PMHS) Testing Technical Report: Tests Conducted in Support of Injury Prediction Capabilities Development – Test Series WS10, WS11, and WS12

Constantine Demetropoulos, Kyle Ott, David Drewry III, and Matthew Montoya
The Johns Hopkins University Applied Physics Laboratory

John Cavanaugh
Wayne State University

Jonathan Rupp
University of Michigan Transportation Research Institute

David R. Barnes
SURVICE Engineering Company

Kathryn L. Loftis
CCDC Data & Analysis Center

REPORT DOCUMENTATION PAGE

Form Approved
OMB No. 0704-0188

1. REPORT DATE	2. REPORT TYPE	3. DATES COVERED *(From - To)*
July 2020	Technical Report	2013–2019

4. TITLE AND SUBTITLE
Whole-Body Postmortem Human Subject (PMHS) Testing Technical Report: Tests Conducted in Support of Injury Prediction Capabilities Development – Test Series WS10, WS11, and WS12

5a. CONTRACT NUMBER
W911QX-17-D-0006

5b. GRANT NUMBER

5c. PROGRAM ELEMENT NUMBER

6. AUTHOR(S)
Constantine Demetropoulos, John Cavanaugh, Kyle Ott, Jonathan Rupp, David Drewry III, Matthew Montoya, David R. Barnes, and Kathryn L. Loftis

5d. PROJECT NUMBER

5e. TASK NUMBER

5f. WORK UNIT NUMBER

7. PERFORMING ORGANIZATION NAME(S) AND ADDRESS(ES)
Director
U.S. Army CCDC Data & Analysis Center
6896 Mauchly Street
Aberdeen Proving Ground, MD

8. PERFORMING ORGANIZATION REPORT NUMBER
CCDC DAC-TR-2020-040

9. SPONSORING / MONITORING AGENCY NAME(S) AND ADDRESS(ES)

10. SPONSOR/MONITOR'S ACRONYM(S)

11. SPONSOR/MONITOR'S REPORT NUMBER(S)

12. DISTRIBUTION / AVAILABILITY STATEMENT
DISTRIBUTION STATEMENT A. Approved for public release; distribution is unlimited.

13. SUPPLEMENTARY NOTES

14. ABSTRACT
The Warrior Injury Assessment Manikin (WIAMan) Program conducted three series of three whole-body postmortem human subject (PMHS) tests (nine tests total) to evaluate the biomechanical response to simulated under-body blast. This report presents the results of the nine whole-body PMHS tests. The test fixture, instrumentation, kinematic analysis, test description, and resulting injury descriptions and estimated injury timing is detailed for each of the test series.

15. SUBJECT TERMS
WIAMan, PMHS, whole-body, under-body blast, UBB, AIS, injury timing, biomechanical response

16. SECURITY CLASSIFICATION OF:			17. LIMITATION OF ABSTRACT	18. NUMBER OF PAGES	19a. NAME OF RESPONSIBLE PERSON
a. REPORT	b. ABSTRACT	c. THIS PAGE			Kathryn L. Loftis
UNCLASSIFIED	UNCLASSIFIED	UNCLASSIFIED	SAME AS REPORT	156	19b. TELEPHONE NUMBER *(include area code)* (410) 306-0344

Standard Form 298 (Rev. 8-98)
Prescribed by ANSI Std. Z39.18

Table of Contents

Table of Contents

List of Figures

List of Figures

List of Figures

List of Tables

List of Tables

Executive Summary

Three series of three whole-body postmortem human subject (PMHS) tests (nine tests total) were conducted to evaluate the biomechanical response to simulated under-body blast. Test conditions were chosen to produce theater-relevant injuries to the pelvic ring, foot-ankle complex, and lumbar spine that could support a subsequent effort to assess the performance of the Warrior Injury Assessment Manikin (WIAMan) injury assessment risk curves for these body regions.

The three sets of floor and seat velocity profiles used in these tests were selected to be representative of under-body blast loading conditions that occur at the upper range of the specifications established for the WIAMan program, where minimal PMHS data previously existed. Key measurements made in these tests included floor and seat accelerations, forces applied to the foot and pelvis, accelerations and angular velocities measured at discrete locations on PMHS components, and strain gauges and acoustic emission measurements to identify fracture timing.

Results of the test series met the objectives of producing pelvis, foot/ankle, and lumbar injuries, which provided data that can be used to evaluate WIAMan injury assessment risk curves. Of the nine PMHS tests, five resulted in pelvic ring fractures, five resulted in eight foot-ankle fractures (i.e., two unilateral and three bilateral fractures), and one produced a femur fracture. Eight of the nine tests produced data that are suitable for injury assessment risk curve capabilities development efforts, with the remaining test having a delayed floor loading and a different floor pulse. Future work may consider repeating this last test so that a minimum of three valid tests exist at each of the three test conditions used in this study.

1. INTRODUCTION

The Warrior Injury Assessment Manikin (WIAMan) program is an Army-sponsored initiative to develop an advanced anthropomorphic test device (ATD) to predict injuries for seated vehicle occupants in under-body blast (UBB). As part of this program, the first comprehensive set of biomechanical response and injury tolerance data has been collected under high-rate vertical loading representative of that experienced by seated vehicle occupants in UBB.

Biomechanical response and tolerance data have been collected from tests of whole postmortem human subjects (PMHSs) and PMHS components. The first set of whole-body PMHS tests served to characterize overall human biomechanical response for the purpose of developing biofidelity response corridors (BRCs). These tests were conducted at lower severity input conditions, as the goal was not to produce injury but to establish specifications for human kinematics and the interactions between humans and the seat environment to act as performance targets for the WIAMan ATD.

Human Injury Probability Curves (HIPCs), which are probabilistic dose-response relationships that relate the magnitude of a mechanical quantity to the risk of injury (typically fracture), were developed from component PMHS tests. Match-paired tests of ATD and PMHS components were performed to relate human injuries to WIAMan ATD component responses. Match-paired testing was performed with the WIAMan ATD using the whole-body PMHS test BRC input conditions primarily to evaluate biofidelity. A secondary use of these tests was to evaluate the Injury Assessment Reference Curves (IARCs) developed from match-paired component tests. However, because BRC whole-body PMHS tests were conducted at lower severity conditions, it was not possible to assess the WIAMan IARCs over the full range of UBB-relevant conditions that were defined by experiments conducted by the US Army.

This report presents the results of an individual series of nine whole-body PMHS tests that served to collect whole-body response data under injurious loading conditions. Information in this report focuses only on the whole-body PMHS tests. IARC assessment is being performed in an independent Army effort. Match-paired WIAMan ATD tests for the conditions used in the tests described in this report will also be reported separately. Analyses of combined results will be performed and described in a subsequent report. The level of detail in the current report is such that a future user could accurately and completely understand methods and key results related to the current PMHS whole-body test series, including injuries, injury timing, and kinematics.

1.1 Test Objectives

In addition to the collection of injury data in whole-body PMHS tests across the full range of UBB-relevant conditions where no whole-body response data previously existed, this test series had two other main objectives:

1. Produce injuries to body regions for which injuries had not yet been produced in whole-body tests or for which insufficient quantities of injuries were available to assess the performance of IARCs.
2. Produce theater-relevant injury patterns.

Figure 1 provides additional information on the injury patterns produced in BRC tests. Of note, multiple injuries were produced in the lumbar spine. However, only a single pelvis injury was produced, and no injuries were produced in the foot/ankle. For these reasons, a focus of the current series of tests was to produce pelvis and foot/ankle fractures, and ideally additional femur fractures.

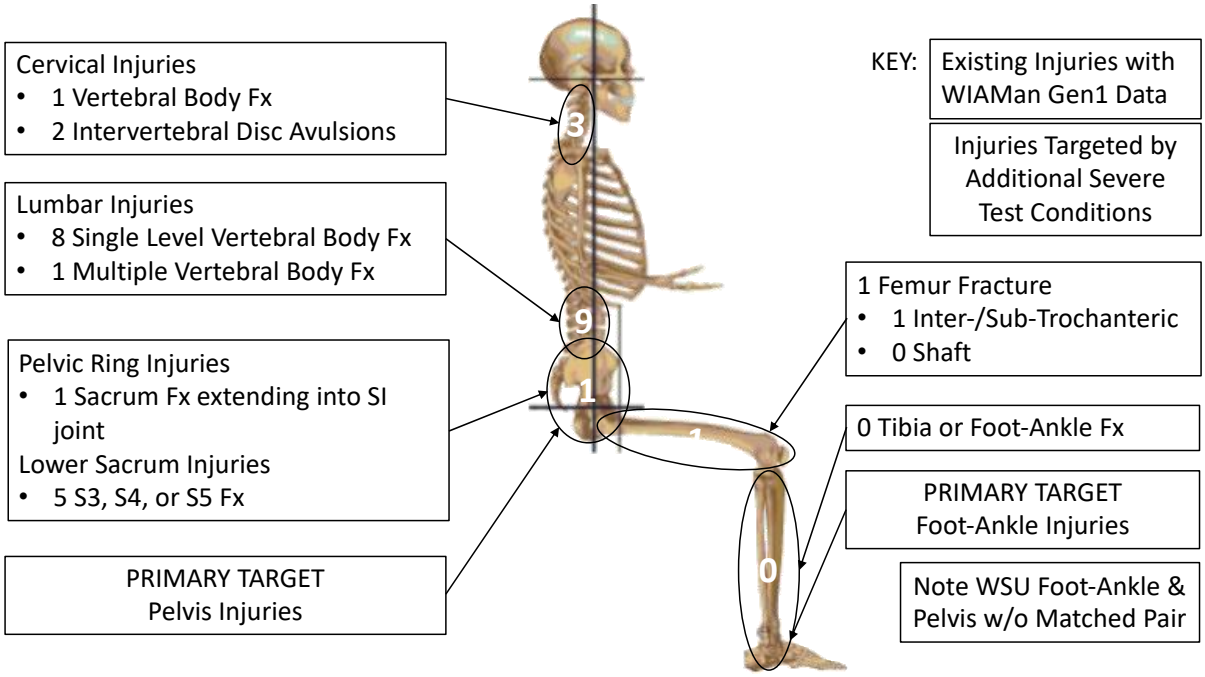

Figure 1. Whole-body PMHS injuries with existing WIAMan Gen1 match-paired data

1.2 Test Series Overview

Table 1 provides the test conditions used in the three current test series of three whole-body PMHS tests. WS10 was run at the Johns Hopkins University Applied Physics Laboratory (JHU-APL), WS11 was run at the Wayne State University (WSU) Bioengineering Center, and WS12 was run at the University of Michigan Transportation Institute (UMTRI), as noted in the table.

Floor and seat pulses for these tests were selected based on inputs used in component testing that was associated with a range of injury and noninjury conditions for the foot/ankle and pelvis such that combined nine tests (i.e., three tests at each of three conditions) had the potential to generate injuries based on component testing and prior whole-body BRC experiments. Efforts were also made to distribute conditions across the full range of UBB-relevant conditions to address injuries that occur across the range of input conditions, thus minimizing overlap of coverage for a given test condition. Another key factor in the selection of test conditions was that physical match-paired experiments with the WIAMan existed for two of the three proposed tests, minimizing the need for additional ATD testing. WIAMan Gen1 data existed prior to PMHS tests for WS10, while WIAMan TD2G (a later version of the WIAMan Technical Demonstrator) data existed prior to PMHS tests for WS11. Although WIAMan TD2G could not substitute for WIAMan Gen1 data, a safely completed test on the WIAMan TD2G was a strong indication the WIAMan Gen1 could be used in this condition.

Table 1. Targeted Test Conditions

Test Series ID #	Performer	Floor Peak Velocity (m/s)	Floor TTP Velocity (ms)	Seat Peak Velocity (ms)	Seat TTP Velocity (ms)	PPE	Posture	Seat Padding
WS10	JHU-APL	15.5	2.5	10.0	7.5	MED	90/90/90	V10
WS11	WSU	13.0	2.5	9.0	5.0	MED	90/90/90	V10
WS12	UMTRI	10.0	2.5	6.5	7.5	MED	90/90/90	Rigid

Figure 2 shows the target peak seat and floor velocities and the associated times to peak (TTPs) for the three conditions used in the current test series and previous component and whole-body BRC injury/no-injury test outcomes. Of note, only a single whole-body test conducted by WSU prior to the current series produced pelvis fracture, and the input conditions for that test were sufficiently severe that the fracture was out of scope for injury severity and matched-pair testing. For this reason, seat padding was used in the WS10 and WS11 test conditions. The WS12 condition was tested using a rigid seat to raise peak applied pelvis forces into the potentially injurious zone.

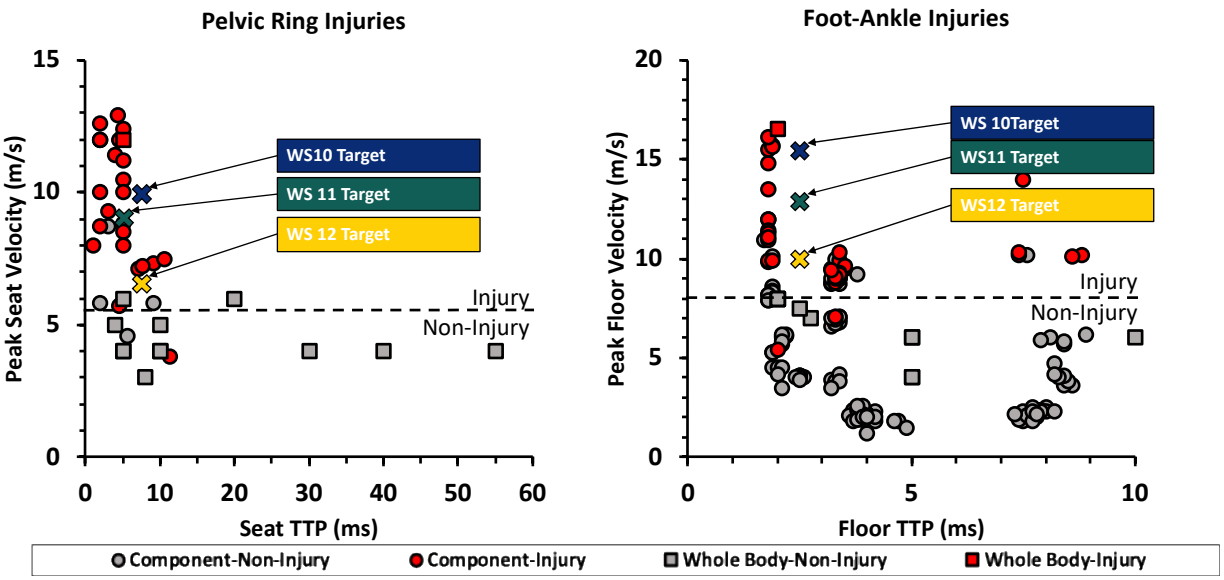

Figure 2. Test conditions of WS10 (JHU-APL), WS11 (WSU), and WS12 (UMTRI) relative to the full range of UBB-relevant conditions and previous component and whole-body test results

The following sections provide additional details on the WS10, WS11, and WS12 test series. Methods and results for each test series are presented separately but in similar format. The results of match-paired WIAMan Gen1 testing will be provided in a subsequent report.

2. WS10 SERIES (JHU-APL)

2.1 Methods

2.1.1 APL Test Fixture

The JHU-APL test device, the Vertically Accelerated Load Transfer System (VALTS), is a vertical sled system designed to generate a range of high-velocity, short-duration input pulses. Standing at a total height of 10.5 m, the VALTS has the capacity to simultaneously vertically accelerate two seated surrogates that may be ATD, PMHS, or both (Figure 3). The VALTS has one 1.27- × 1.52-m primary platform to which a seat system is mounted, and two secondary 0.36- × 0.59-m platforms located in front of the primary platform that serve as the right and left occupant floor plates. Both floor plates are independently programmed and driven from each other and are also actuated independently from the primary platform. The total achievable travel of the primary platform is 3.1 m, while the floor platforms are constrained between displacement limits that restrict travel to 0.05 m. The VALTS achieves high-impact energies by pneumatically propelling precision-guided ballistic masses into both the primary and secondary platforms. The ballistic masses are propelled by a single 25.4-cm-diameter, high-pressure nitrogen actuator for the primary platform and two 10.2-cm-diameter nitrogen actuators for each of the secondary platforms. Elastomers with a linear response are placed between the ballistic mass and the platform bases to produce the desired pulse duration, while the pneumatic pressure system controls the impact speed. Input velocities on the VALTS ranged from 2 to 10 m/s with durations from 2 to 35 ms for the primary (seat) platform and from 2 to 16.5 m/s with durations from 1 to 10 ms for the secondary (floor) platforms. Additionally, isolation of the different test platforms allows for independent timing of the applied loads, which supports the study of differential timing between floor and seat. Pneumatic air brakes are incorporated within the VALTS linear bearings to either control the descent of the primary platform or to prevent slam-down after a test. For this study, only the initial accelerative portion of loading is of interest with simultaneous floor and seat loading.

A V10 seat cushion was placed between the subject and the seat. The V10 cushion is 0.457 × 0.457 m and consists of two pieces of Poron (192.22 kg/m^3) (0.012 m), one piece of Ethafoam 4101FR (35.2 kg/m^3) (0.057 m), and three pieces of Poron (144.17 kg/m^3) (0.012 m). The total thickness of the cushion was 0.121 m. The surface of the cushion was covered with a layer of gaffer's tape.

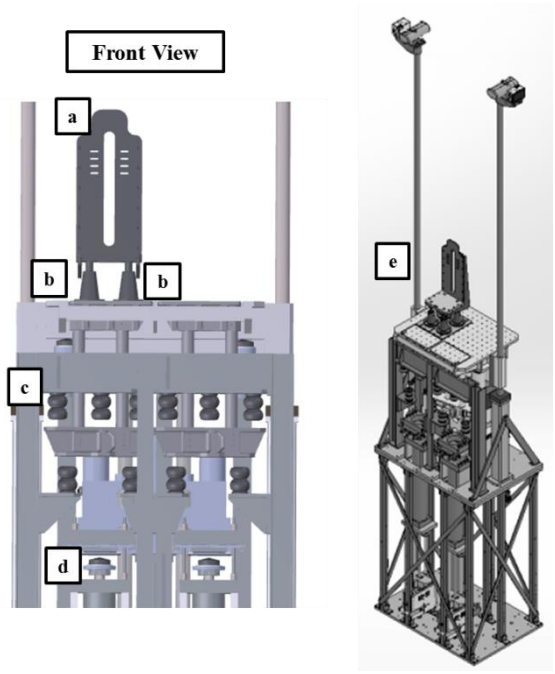

a) Seat system
b) Floor platforms
c) Displacement limiting stops
d) Linear elastomers
e) Isometric view of primary platform

Figure 3. Rendering of the Vertically Accelerated Load Transfer System (VALTS) in front and isometric views

2.1.2 Instrumentation Locations and Transducer Types

The test fixture incorporated an array of uniaxial load cells and accelerometers at the occupant-seat and occupant-footplate interfaces (Figure 4). The seat load cell configuration included uniaxial load cells at the sacrum, left and right ischium, and left and right thigh, allowing for the analysis of seat load distribution between the component seat plates (Rupp et al., 2016) as well as the ability to sum the individual loads to calculate a total seat force. Footplate load cells measured the forefoot and heel forces that could be used to calculate total floor force. Associated accelerometers measured footplate acceleration and were used for mass correction of loads, as listed in Table 2. Fixture velocities were calculated by integrating acceleration signals and the floor and seat, respectively.

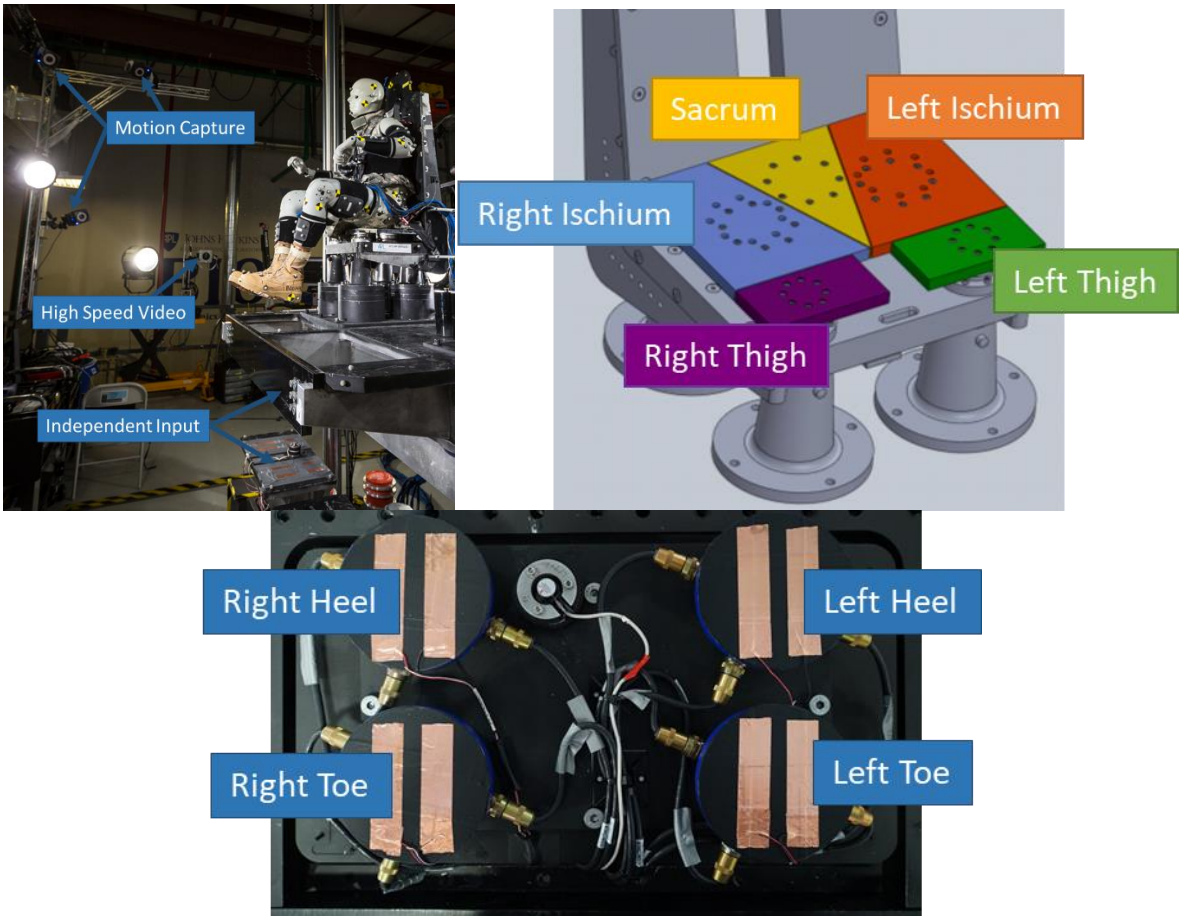

Figure 4. Rig instrumentation locations

Table 2. Masses and Instrumentation Used for Mass Compensation

Location	Plate Mass (kg)	Load Cell Names	Load Cell Model	Accelerometer Name	Accelerometer Model
Left heel	0.6	L Heel FOR	5210XYZ	Floor ACC	Endevco_72701A-20k
Right heel	0.6	R Heel FOR	5210XYZ	Floor ACC	Endevco_72701A-20k
Left forefoot	0.6	L Toe FOR	5210XYZ	Floor ACC	Endevco_7264D-2000
Right forefoot	0.6	R Toe FOR	5210XYZ	Floor ACC	Endevco_7264D-2000
Sacrum	2.2	Sacrum FOR	LWPF1-50kN	Sacrum ACC	Endevco_7270A-6k
Left IT	3.3	L Ischium FOR	LWPF1-50kN	L Ischium ACC	Endevco_7270A-6k
Right IT	3.3	R Ischium FOR	LWPF1-50kN	R Ischium ACC	Endevco_7270A-6k
Left thigh	1.3	L Thigh FOR	LWPF1-20kN	L Thigh ACC	Endevco_7270A-6k
Right thigh	1.3	R Thigh FOR	LWPF1-20kN	R Thigh ACC	Endevco_7270A-6k

PMHS instrumentation included six-degrees-of-freedom (6DOF) sensors (6DX, Diversified Technical Systems, Inc.), uniaxial accelerometers (7264 and 7270A, Endevco), acoustic emission sensors (Nano 30, Physical Acoustics), and strain gauges (KFW-2-350-D17-11, Kyowa). The types and locations of these sensors and the orientations of strain gauges are

provided in Table 3 and Figure 5. The 6DX sensors measured X-, Y-, and Z-accelerations (A_x, A_y, and A_z, respectively) and X-, Y-, and Z-angular rates (AR_x, AR_y, and AR_z, respectively). The 6DX sensors were rigidly mounted to the skull (3 cm superior to the Frankfort Plane at the level of the tragion) using screws with Helicoil thread inserts, thoracic vertebrae (T1, T5, T8, T12, and L3), sacrum (S1–S3 level), superior pubic rami, distal femurs, and proximal tibias. Screws were placed in the bone for mounting these subjects, with the exception of the pubic ramus in which hose clamps were used to mount the sensors. The distal femur 6DX sensors were located proximal to the distal femur at a distance of 25% of the total femur length. The proximal tibia 6DX sensors were located distal to the most proximal portion of the bone at a distance of 25% of the total tibia length. The 7270A accelerometers, which measure A_z, were installed on the medial surface of the left and right calcaneus and oriented parallel to the leg long axis. Modified 7264 accelerometers with one flange removed were installed on the cervical bodies of C2 and C4 just lateral of the mid-sagittal plane in the superior-inferior direction. A computed tomography (CT) scan was conducted after instrumentation but prior to testing to document sensor positions relative to the skeleton.

Table 3. Subject Instrumentation Locations

6DX	Strain Gage[a]	Acoustic Emission Sensor	7264/7270A Uniaxial Accelerometer
Head	Left Rib 10	T6	C2
Sternum	Right Rib 10	T8	C4
Left Superior Pubic Ramus	Left ASIS	T10	Left Calcaneus
Right Superior Pubic Ramus	Right ASIS	L1	Right Calcaneus
Left Distal Femur	Left Superior Pubic Ramus	L3	…
Right Distal Femur	Right Superior Pubic Ramus	L4	…
Left Proximal Tibia	Left Proximal Femur	Left Iliac Wing	…
Right Proximal Tibia	Right Proximal Femur	Right Iliac Wing	…
T1	Left Distal Femur	Left Tibia	…
T5	Right Distal Femur	Right Tibia	…
T8	Left Proximal Tibia	Left Calcaneus	…
T12	Right Proximal Tibia	Right Calcaneus	…
L3	Left Distal Tibia	…	…
Sacrum (S1–S3)	Right Distal Tibia	…	…
…	Left Calcaneus	…	…
…	Right Calcaneus	…	…

[a] Strain gauges were placed along the long axes of long bones, along the circumferential direction of ribs, along the direction of the pelvic ring for the pubic ramus, along the direction of the iliac crest for the anterior superior iliac spine (ASIS), and fore to aft for the calcaneus locations.

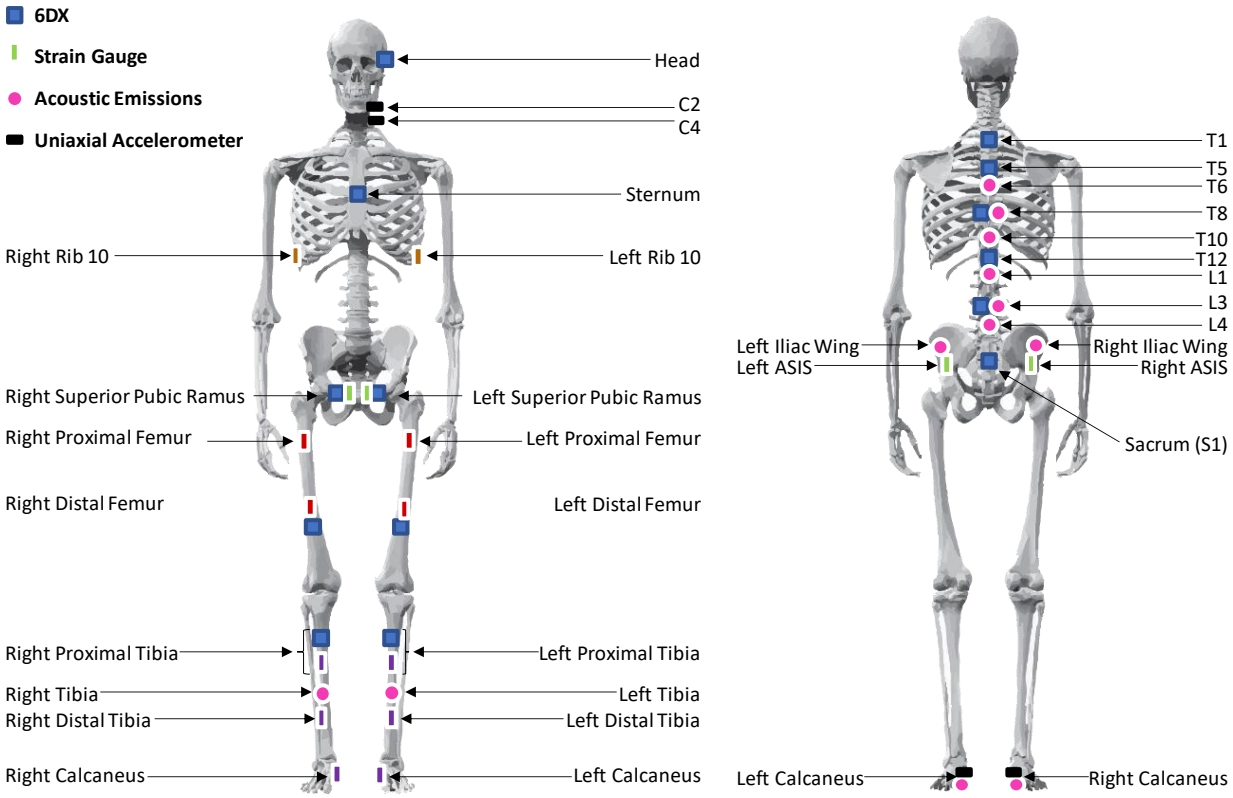

Figure 5. Subject instrumentation locations

2.1.3 Kinematic Analysis

Spherical markers (rigidly installed in bone through the use of screws to the bone or affixed to rigidly attached mounts through tapped holes in the mounts) or quadrant marker stickers (adhered to surface of clothing or personal protective equipment [PPE]) were placed at various skeletal and surface landmarks for kinematic tracking. Tracked locations included the head (three spherical markers at various locations of the face, see Table 4), shoulders (spherical markers at left and right acromion), pelvis (subject specific clamps attached to the posterior superior iliac spine bilaterally), femur (quadrant markers proximal and distal, and spherical markers), knee (motion transformed to this location using coordinate measurement data), proximal tibia (quadrant markers attached to 6DX sensor mount, and spherical markers), and boots (left and right forefoot, left and right hindfoot, left and right lateral malleolus) (Tables 4 and 5). Various points on the fixture were tracked to define and translate the coordinate system as it moved through the tracking frame (Table 6) (Knee motion transformed using coordinate measurement data from femur motion, Table 5). Motion tracking and calibration were performed using motion analysis software (VICON).

Table 4. Rigidly Installed Kinematic Marker Locations

<table>
<tr><td> 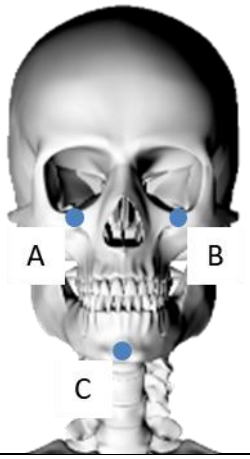
</td><td> 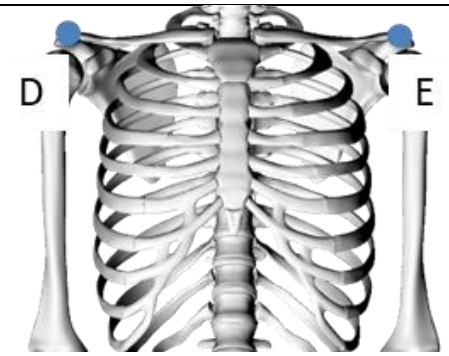
</td><td> 
</td></tr>
<tr><td>A) Head_Anterior_Lateral_Right
B) Head_Anterior_Medial_Left
C) Head_Anterior_Medial</td><td>D) Shoulder_Right_Lateral
E) Shoulder_Left_Lateral</td><td>G) Femur_Right_Anterior[a]
H) Femur_Left_Anterior[a]</td></tr>
<tr><td colspan="2"> 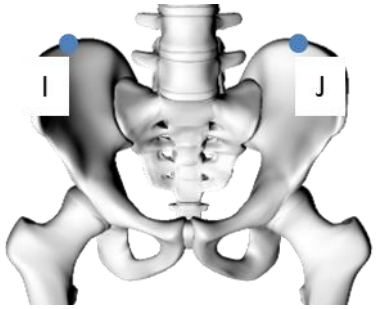
</td><td> 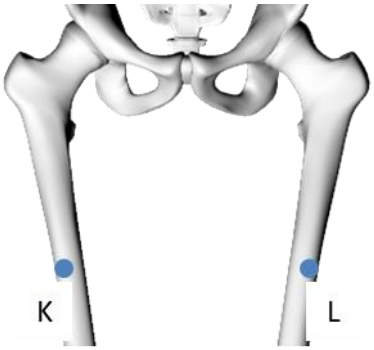
</td></tr>
<tr><td colspan="2">I) Pelvis_Right_PSIS
J) Pelvis_Left_PSIS</td><td>K) RThigh_Prox_Femur
L) LThigh_Prox_Femur</td></tr>
</table>

[a] Measured points transformed to knee using collected coordinate measurement device points.

Table 5. Kinematic Surface Marker Locations

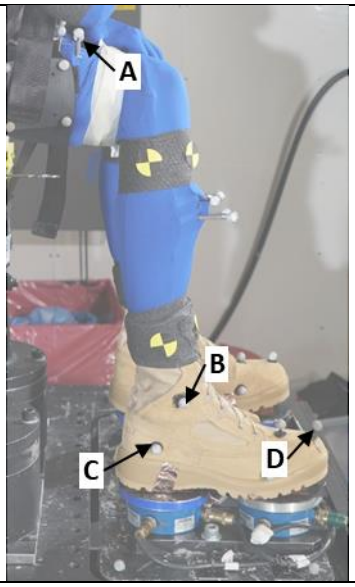

A) Knee_Right_Lateral [a]
B) Boot_Right_Lateral_Superior
C) Boot_Right_Lateral_Posterior
D) Boot_Right_Lateral_Anterior

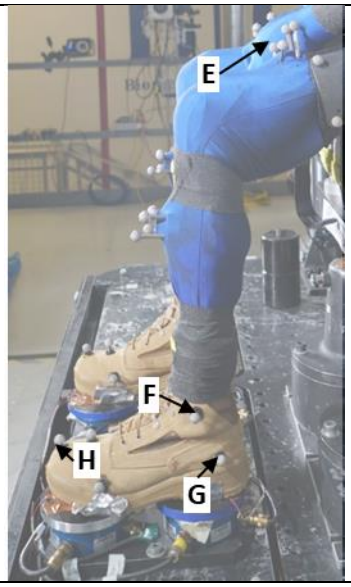

E) Knee_Left_Lateral [a]
F) Boot_Left_Lateral_Superior
G) Boot_Left_Lateral_Posterior
H) Boot_Left_Lateral_Anterior

[a] Knee motion transformed using coordinate measurement data from femur motion.

Table 6. Rig Kinematic Marker Locations

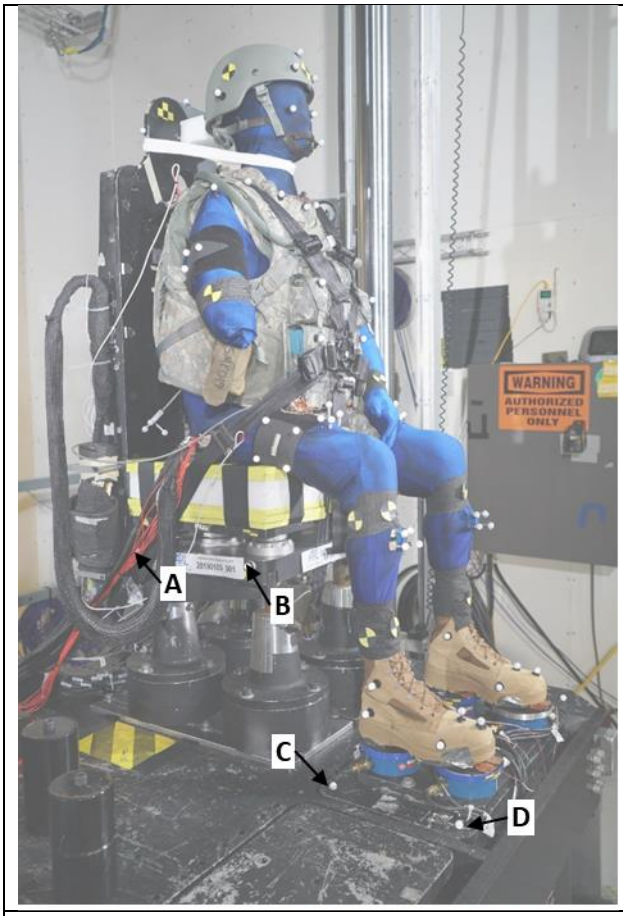

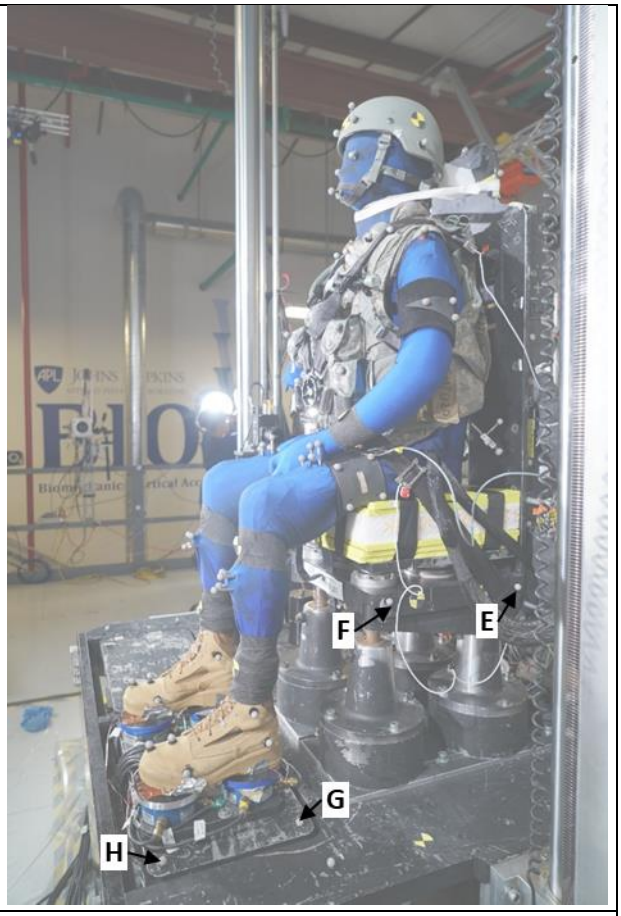

A) Seatpan_Right_Aft [a]	E) Seatpan_Left_Aft
B) Seatpan_Right_Fore	F) Seatpan_Left_Fore
C) Rig_Right_Aft	G) Floor_Left_Aft
E) Floor_Right_Fore	H) Floor_Left_Fore

[a] Exact locations of seatpan aft and floor fore may vary between tests based on visibility from camera views.

The location of the head center of gravity (CG) was calculated at each point in time using the skeletal surface markers shown in Table 4 based on the head CG location relative to these markers calculated using CT data with the procedure defined in the W0084 technical guidance document (Bass et al., 2016). For this calculation, it was assumed that the head CG does not change during the event. Foot angle was also calculated using the landmarks listed in Table 7.

Table 7. Calculated Kinematic Descriptions

Location	Description	Image
Head_ Center	Calculated position using a rigid body transformation from rigidly installed kinematic markers on head (Table 4) and head center of gravity calculated from CT scan	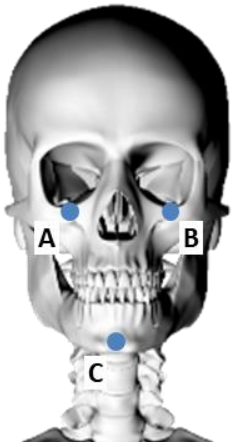
Boot_Knee_ Right	Included foot angle between Knee_Right_Lateral to Boot_Right_Lateral_Superior and Boot_Right_Lateral_Posterior to Boot_Right_Lateral_Anterior	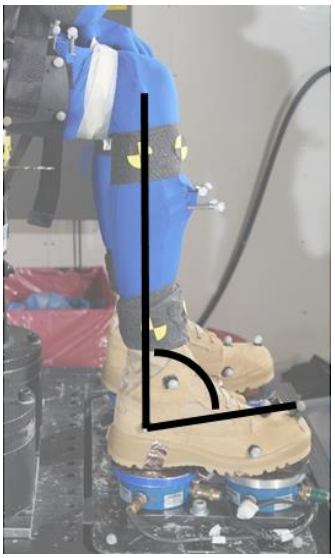
Boot_Knee_ Left	Included foot angle between Knee_Left_Lateral to Boot_Left_Lateral_Superior and Boot_Left_Lateral_Posterior to Boot_Left_Lateral_Anterior	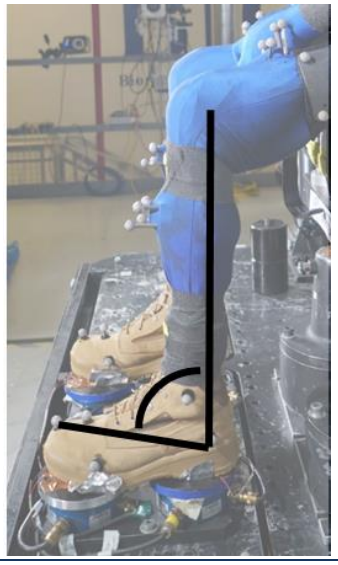

2.1.4 Subject Characteristics

Table 8 provides the characteristics of the three subjects tested by JHU-APL for the WS10 series. All subjects were within predefined acceptable ranges. Appendix A provides standard subject anthropometry measured in accordance with reference document W0080, *Minimum Pretest Anthropometry Requirements for Scaling* (Bass et al., 2013).

Table 8. Subject Characteristics with Inclusion Criteria

Test Series ID	Subject	Age (yrs)	Gender	Height (cm)	Weight (kg)	BMI	T-Score (L1–L4)
WS10-001	16-10009	59	M	182.9	86.2	26.0	1.0
WS10-002	1612325R	54	M	170.2	72.1	24.9	0.1
WS10-003	F182258	65	M	177.8	80.7	25.5	0.0
Acceptance Criteria	…	18 - 80	M	165 - 186	64 - 106	18 - 35	-1.0 - +2.5

2.1.5 Subject Positioning

Subject positioning was based on the relative locations of skeletal surface landmarks, together with seated X-ray images. Figure 6 shows the target postures and highlights important joint angles and relative positions of landmarks. Landmarks were identified through palpation. Landmarks on the pelvis were determined through a lateral X-ray while seated on the test rig. Pelvis angle was defined as the angle of the line formed by the midpoint between the left and right anterior superior iliac spines (mid-ASIS) and the pubic symphysis landmark compared in reference to vertical.

A 3-D coordinate measurement device (Romer Absolute Arm, Cobham, Great Britain) was used to measure the position of the PMHS prior to each test. During the positioning process, three dimensional locations were recorded at various landmarks and checked against target-relative orientations. When measurements fell outside of tolerance, the PMHS was adjusted accordingly and remeasured until within tolerance or as close to the target range as PMHS anatomy permitted. Tape was used to secure each PMHS head in the proper posture by running a strip or multiple strips of tape from the PMHS head and/or helmet to a rigid location on the test fixture. Tape mounting locations varied with each test, but tape was typically affixed to the PMHS chin, nose, and helmet (see Figure 5 for examples). For each PMHS, the minimum number of strips of tape that were sufficient to secure the head in the proper posture was applied. Tape was precut approximately 90% across immediately prior to each test such that the tape severed during the loading event. In all tests, all strips of tape were completely severed at the beginning of the loading event. PMHS head motion did not appear to be influenced by the tape placement. Final coordinates were documented immediately before each test.

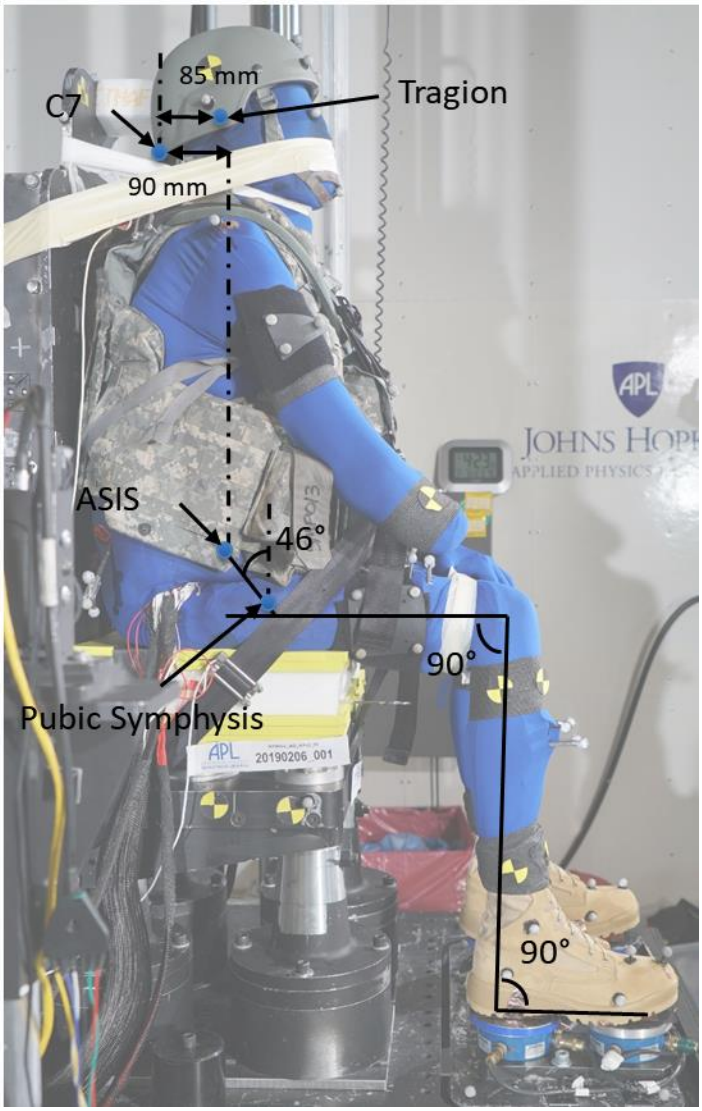

Figure 6. Target posture

Target and actual postures for all tests are shown in Table 9. Target postures were based on the postures assumed by midsize male Soldiers seated in a military vehicle seat with a vertical back and horizontal seat cushion (based on Reed & Ebert [2013]). Positioning was performed following the procedure described by Rupp and Reed (2015). When positioning subjects, the highest priority was given to matching pelvis angle, head position and angle, and foot and knee angles. Lower priority was given to acromion position, as some subjects were missing forearms, preventing the use of the arm to control shoulder position.

Table 9. Subject Positioning

Measurement	Description	Target Range		WS10-001	WS10-002	WS10-003
		Low	High			
Pelvis Angle	Angle of line from mid-ASIS to pubic symphysis in the XZ-plane with respect to vertical	35°	45°	42.5°	43.3°	38.7°
ASIS Fore-Aft Distance	A-P difference of left and right ASIS landmarks	-10 mm	10	0	3.7	-2
ASIS Vertical Distance	Vertical difference of left and right ASIS landmarks	-10 mm	10	7	-9	-6
Mid-ASIS Aft of Cervicale	Fore-aft distance from average of left and right ASIS landmarks to most posterior aspect of C7	80 mm	100	80	92.85	91
Acromion Fore-Aft Difference	Fore-aft difference between left and right acromion landmarks	-20 mm	20	-12	-17	-4
Acromion Vertical Distance	Vertical difference between left and right acromion landmarks	-20 mm	20	-19	-8	-3
Cervicale Aft of Tragion	Fore-aft distance from average of left and right tragion to most posterior aspect of C7	75 mm	95	77	89	93
Infraorbitale Superior of Tragion	Vertical distance from mid-infraorbitale to mid-tragion	5 mm	15	14	13	13
Boot Heel Separation	Distance between centers of boot heels	285 mm	305	304	295	295

2.1.6 Personal Protective Equipment, Boot, and Belt Fitting Procedures

PPE, including the advanced combat helmet (ACH), improved outer tactical vest (IOTV), and Belleville 390 DES men's hot weather desert tan combat boots (Belleville Boot Company, Belleville, IL) were fitted to the PMHS in accordance with reference documents W0058 (*Helmet Fitting Procedures*), W0059 (*IOTV Fitting Procedures*), and W0060 (*Boot Fitting Procedures*), respectively (WIAMan Biomechanics Team, 2013a, 2013b, 2013c). The routing and fitting of the five-point seatbelt restraint harness were performed in accordance with reference document W0070 (*Belt Fitting Procedures*) (WIAMan Biomechanics Team, 2013d).

2.1.7 Data Processing

All signals were processed following the procedures used for BRC development. Accelerometers and seat/floor load cell data were filtered using a low-pass fourth-order digital phaseless Butterworth filter using a cutoff frequency of 3 kHz. Angular rate data were filtered using a cutoff frequency of 1650 Hz. DTS 6DX transducer measurements were transformed to standardized locations relative to skeletal anatomic landmarks using the procedure developed by the Signal Conversion Tiger Team (SCoTT) reported by Slykhouse et al. (2019). Seat and floor velocities were calculated by integrating Z-axis accelerometers located under the center of the seat and under the center of the left and right feet.

Times to peak velocity for the floor and seat were calculated using methods defined by Spink (2014). These methods involve a baseline shift and integration of the acceleration time history, the peak (largest negative) velocity within a time frame of interest, and identification of all local

minima less than 90% of the absolute peak. The local minimum just prior to the absolute peak is selected as the new peak velocity, and points corresponding to 5%, 20%, and 95% of the final peak velocity are determined. If the velocity history exhibits a monotonic fall between 5% and 20%, the velocity slope is calculated between the points at 5% and 95% of the peak velocity. If the velocity history is not monotonic between 5% and 20%, the data point immediately following the last positive derivative in the window is identified and used to replace zero as the baseline for the 5% calculation. The start and end times are determined by calculating the times at which the equation defining the velocity slope is equal to zero and peak velocity, respectively. The time to peak is the difference between the calculated ending and starting times.

During test execution of the WS10-002 and WS10-003, two separate data acquisition failures occurred, resulting in the loss of some data channels. For WS10-002, lost channels included the following 6DX sensors: left femur, right ramus, S1, L3, and T12. For WS10-003, the channels lost included the following sensors: floor and rig acceleration, floor load cells, seat load cells, and C2 and C4 acceleration. For WS10-003, kinematic marker tracking was used to determine the system input velocity.

2.1.8 Injury Assessment and Injury Timing Analysis

Acceleration, angular rate, strain, and acoustic emission data were all viewed qualitatively to provide an estimate of injury timing for each test. These estimates are subject to error, as signals in the region of injury often contain more than one event that could be interpreted as the time of injury. In general, fracture timing was identified as the time following an acoustic burst where there was a corresponding spike or change in direction of an acceleration pulse. Approximate allowances were made for the time needed for sound to travel between the fracture location and the acoustic emission sensor. However, for situations where fracture occurred at a location that was remote from an acoustic emission sensor or accelerometer, fracture timing was estimated over a window based on accelerometer responses. Figure 7 shows an illustrated example of how sacrum fracture timing was estimated based on the time of the acoustic burst measured by a nearby mounted sensor and the measurements of a nearby mounted accelerometer.

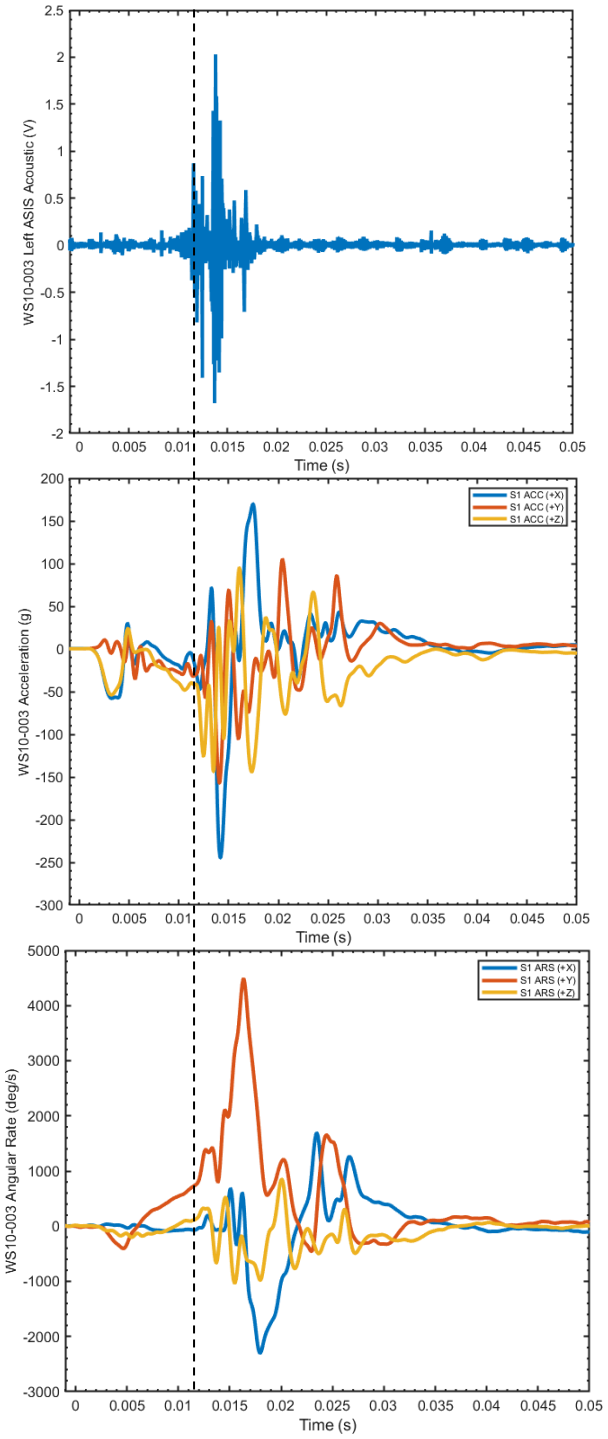

Figure 7. Example of plots used to determine injury timing for sacrum fracture in WS10-003: sacrum acoustic emission (top), sacrum acceleration (middle), and sacrum angular rate (bottom)

2.2 Results

2.2.1 Test Conditions

Table 10 compares floor and seat conditions for each of the three tests in the WS10 series to targets, and Figure 8 shows the corresponding velocity-time histories. Note that for the third test the peak velocity and TTP for floor and seat were estimated based on kinematic marker tracking data and are imprecise due to limited sampling rates. However, the other two tests had similar input velocities and TTPs. For this reason, actual input velocities and TTPs for test WS10-003 are assumed to be closer to the first two tests. The following two statements describe tests WS10-001 and WS10-002. Floor peak velocities ranged from 14.7 to 15.1 m/s with a target of 15.5 m/s, and TTP of floor velocity ranged from 2.7 to 2.8 ms with a 2.5-ms target. Seat pulses ranged from 9.6 to 9.7 m/s with a target of 10.0 m/s, and TTPs of seat velocity ranged to 7.5 ms with a target of 7.5 ms. Figure 8 provides floor and seat velocity histories used to determine peak velocity and TTP with both tests showing good repeatability.

Table 10. Test Conditions: Targeted and Achieved

Test Series ID	Floor Peak Velocity (m/s)	Floor TTP (ms)	Seat Peak Velocity (m/s)	Seat TTP (ms)	PPE	Posture	Seat Padding
WS10-001	15.1	2.8	9.7	7.5	MED	90/90/90	V10
WS10-002	14.7	2.7	9.6	7.3	MED	90/90/90	V10
WS10-003	15.0 [a]	4 [a]	9.5 [a]	9 [a]	MED	90/90/90	V10
Target	15.5	2.5	10.0	7.5	MED	90/90/90	V10

[a] Estimated based on kinematic marker tracking data.
Note: MED = medium.

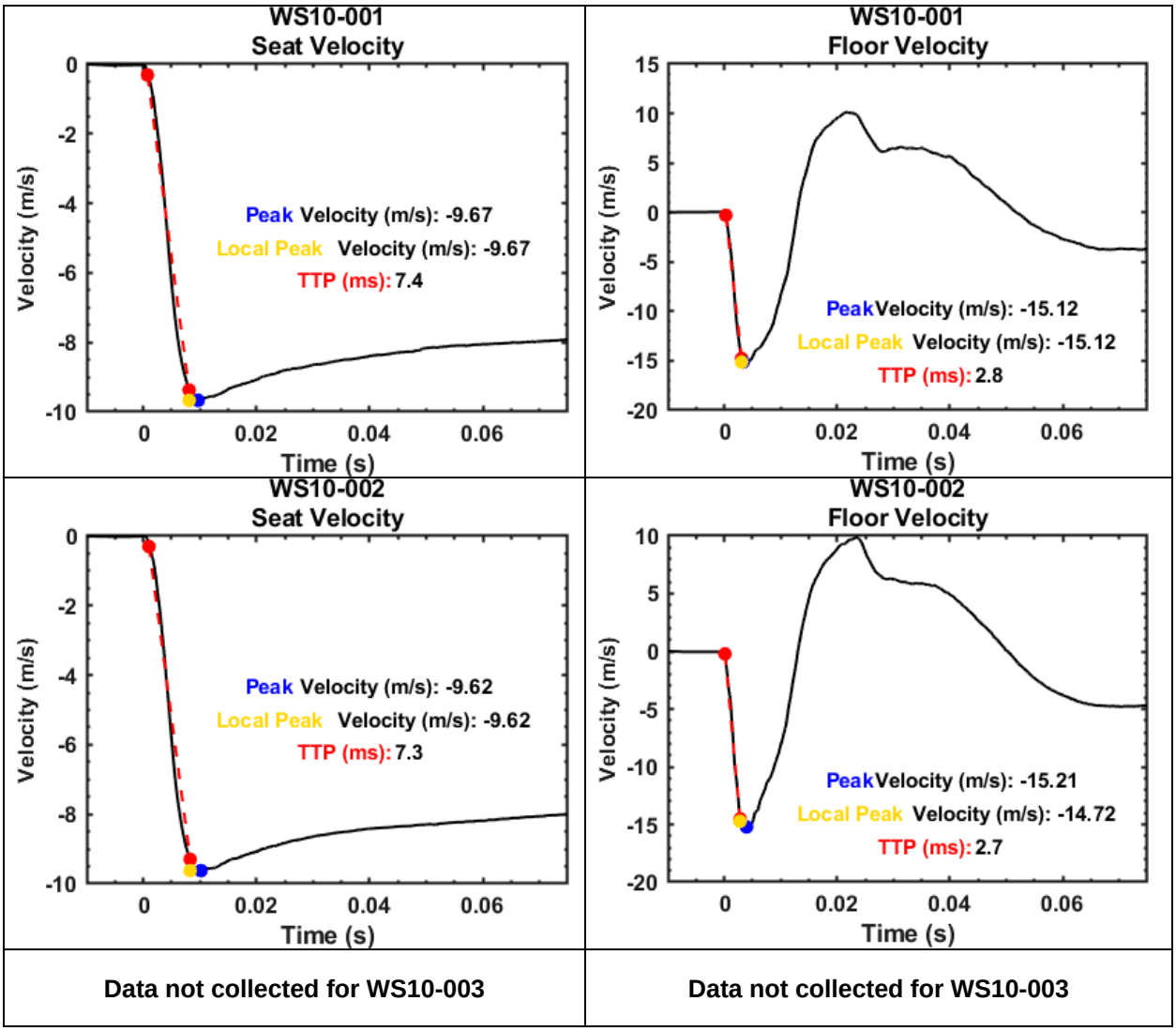

Figure 8. Seat and floor velocity time histories with peak and time to peak

2.2.2 Injury Outcomes

Tables 11–14 provide the injuries and associated Abbreviated Injury Scale (AIS) 2015 codes for the lower extremities, pelvis, lumbar spine, and thoracic spine, respectively. All three subjects sustained substantial injuries in the lower extremities, pelvis, and lumbar, as seen in Figure 9. Additionally, all three subjects sustained substantial rib fractures with WS10-002 having the most extensive rib fractures. WS10-002 also had the most spinous process fractures of any subject. Both seated X-ray and CT images of this subject demonstrate a qualitatively straighter spine than the other two subjects tested in this series. Fractures of the spine were limited compared to the previous test series. Illustrations of pelvis fracture patterns are shown in Figures 10–12. Images of all fractures, as well as key pre- and posttest radiology to document injury patterns, are provided in Appendix A. Injury patterns were consistent with those reported from

combat theater events by Danelson et al. (2018) with the exception of the rib fractures that were not widely reported.

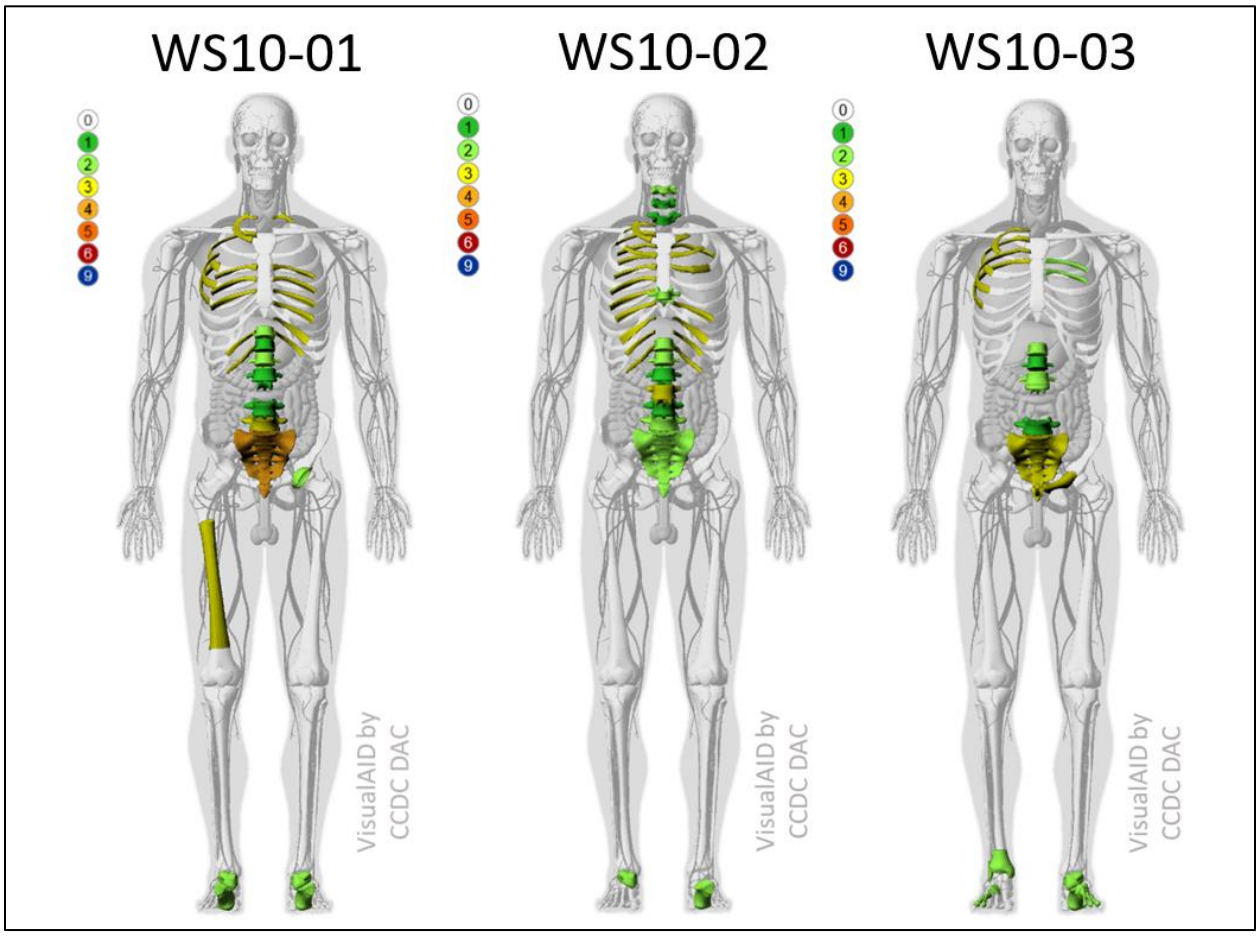

Figure 9. WS10 Visual Anatomical Injury Descriptor (VisualAID) injury visualization

Table 11. Lower Extremity Injuries

	AIS 2015	Description	Injury Classification
WS10-001	**Right:** Calcaneus fracture (AIS 857371.2) Talus fracture (AIS 857251.2) Femur fracture (AIS 857271.3) **Left:** Calcaneus fracture (AIS 857371.2) Talus fracture (AIS 857251.2)	Calcaneus: unstable fracture of left/right calcaneus extending into >3 articular surfaces Talus: simple posterior chip fractures Femur: mid-shaft bending wedge fracture	Severe calcaneus fracture (Sanders Type IV) Simple talus fracture (Hawkins I) Wedge femur fracture (OTA 42-B2)
WS10-002	**Right:** Talus fracture (AIS 857261.2) **Left:** Calcaneus fracture (AIS 857371.2)	Calcaneus: unstable fracture of calcaneus extending into >3 articular surfaces Talus: simple anterior chip fractures	Severe calcaneus fracture (Sanders Type IV) Simple talus fracture (Hawkins I)
WS10-003	**Right:** Calcaneus fracture (AIS 857371.1) Cuneiform fracture (AIS 857551.2) Metatarsal fracture (4–5) (AIS 857173.2) Pilon fracture (AIS 854371.2) Fibula fracture (AIS 854461.2) **Left:** Calcaneus fracture (AIS 857371.2) Talus fracture (AIS 857251.2) Cuboid fracture (AIS 857600.2) Cuneiform fracture (AIS 857561.2) Metatarsal fracture (3–5) (AIS 857173.2)	**Right:** Calcaneus: stable fracture of calcaneus extending into 1 articular surface Cuneiform: stable fracture mid to inferior body Metatarsal: displaced fractures to metatarsals 4–5 Pilon: comminuted fracture Fibula: wedge fracture **Left:** Calcaneus: stable fracture of calcaneus extending into >3 articular surfaces Talus: simple anterior chip fractures Cuboid: stable fracture mid body Cuneiform: stable fracture mid body Metatarsal: displaced fractures to metatarsals 3–5	**Right:** Mild calcaneus fracture (Sanders Type I) Pilon: comminuted fracture Fibula: wedge fracture **Left:** Severe calcaneus fracture (Sanders Type IV) Simple talus fracture (Hawkins I) Cuboid: stable fracture mid body Cuneiform: stable fracture mid body Metatarsal: displaced fractures to metatarsals 3–5

Table 12. Pelvis Injuries

	AIS 2015	Description
WS10-001	Pelvic ring fracture: Complete disruption (AIS 856171.4) Acetabulum fracture (AIS 856200.2)	Bilateral fracture of S1–S5 consistent with vertical shear fracture to the acetabulum
WS10-002	Bilateral sacrum fracture S3, stable (AIS 856151.2)	Bilateral stable fracture of the sacrum at the level of S3
WS10-003	Pelvic ring fracture: Complete disruption, Left superior pubic ramus fracture: displaced, Pubic symphysis fracture (AIS 856161.3)	Bilateral fracture of S1–S5 consistent with vertical shear Complete fracture of the left superior pubic ramus fracture of the pubic symphysis

Table 13. Lumbar Spine Injuries

	AIS 2015	Description
WS10-001	L5 burst fracture, major height loss (AIS 650634.3) L4 spinous process fracture (AIS 650618.1) L2 left/right transverse process fracture (AIS 650620.1) L1 burst fracture, minor height loss (AIS 650632.2)	Major burst fracture at L5 involving substantial height loss Minor anterior body fracture at L1 L2 avulsion type transverse process fractures
WS10-002	L5 left/right transverse process fracture (AIS 650617.2) L5 spinous process fracture (AIS 650617.2) L4 spinous process fracture (AIS 650618.2) L3 burst fracture, major height loss (AIS 650634.3) L2 left transverse process fracture (AIS 650620.2) L1 right transverse fracture (AIS 650617.2) L1 spinous process fracture (AIS 650617.2)	Multiple spinous process fractures Major burst fracture at L3 involving substantial height loss L2 and L1 avulsion type transverse process fractures
WS10-003	L5 anterior body fracture, minor height loss (AIS 650632.2) L5 left transverse process fracture (AIS 650620.1) L2/L3 disc disruption (AIS 650699.2) L2 anterior body fracture, minor height loss (AIS 650632.2) L1 right transverse process fracture (AIS 650620.1)	Both L2 and L5 anterior body fractures were minor L5 and L1 avulsion type transverse process fractures Complete disc disruption between L2 and L3, non-displaced

Table 14. Torso and Cervical Spine Injuries

	AIS 2015	Description
WS10-001	T11 anterior body fracture (AIS 650432.2) T12 right transverse process fracture (AIS 650420.1) Right rib 3, 6, 7, 9, 12 Postero-lateral fracture (AIS 450203.3) Left rib 2, 4, 5, 10, 11 Postero-lateral fracture (AIS 450203.3)	Severe T11 anterior body fracture without height loss Mid to upper thoracic postero-lateral rib fractures bi-laterally
WS10-002	T8 anterior body fracture (AIS 650432.2) C4 anterior body fracture (AIS 650232.2) T1 spinous process fracture (AIS 650418.2) C6 spinous process fracture (AIS 650218.2) Bilateral rib 1-12 Postero-lateral fracture (AIS 450203.3)	Minor T8 and C4 anterior body fractures Postero-lateral rib fractures bi-laterally across all rib levels
WS10-003	T12 superior body fracture (AIS 650432.2) Right rib 2-5 Postero-lateral fracture (AIS 450203.3) Left rib 5-6 Postero-lateral fracture (AIS 450203.3)	T12 superior lateral body fracture without height loss Limited amount of postero-lateral rib fractures bi-laterally

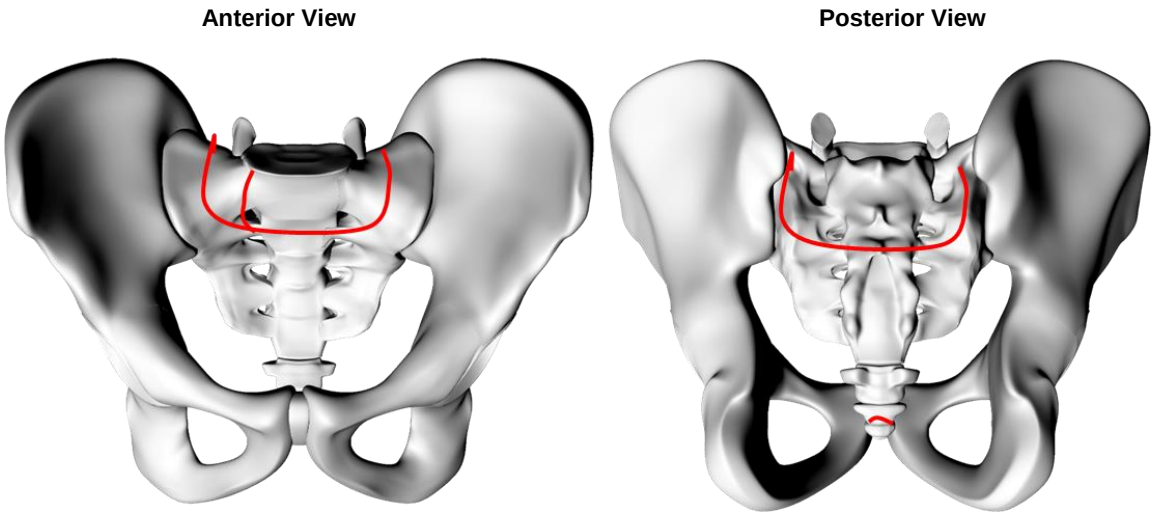

Figure 10. WS10-001 pelvis injury diagrams

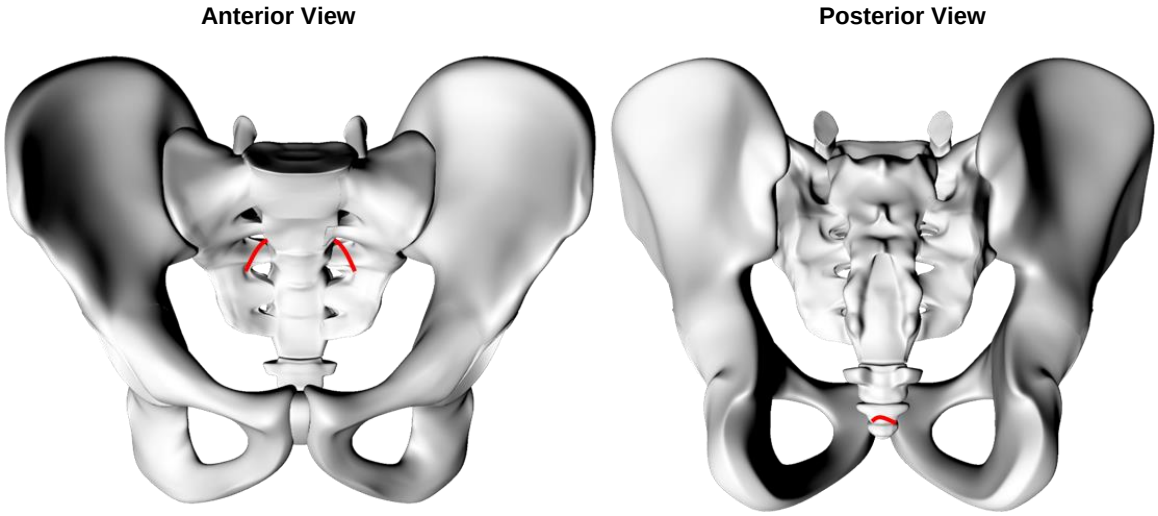

Figure 11. WS10-002 pelvis injury diagrams

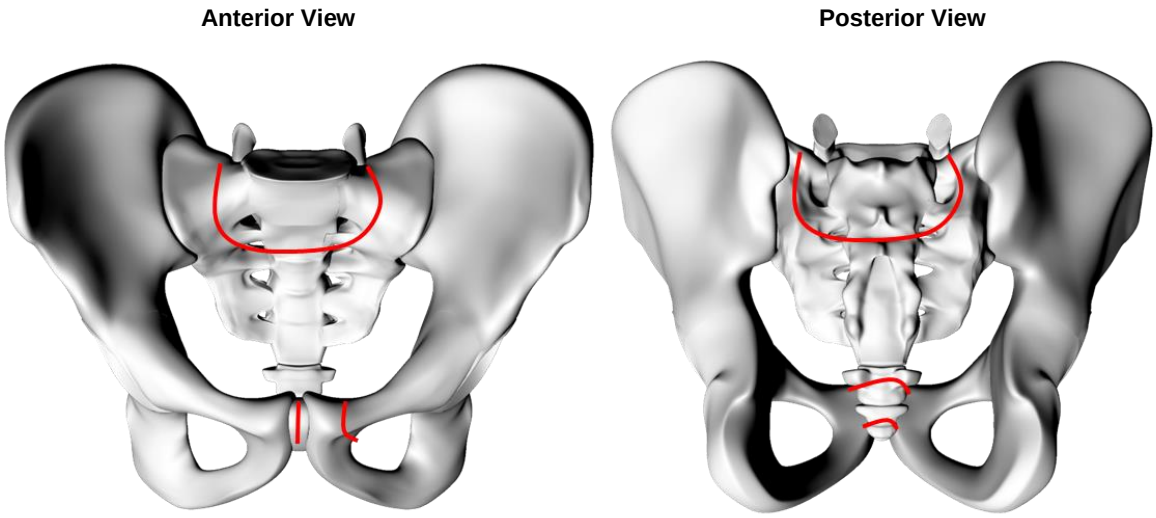

Figure 12. WS10-003 pelvis injury diagrams

2.2.3 Injury Timing

Figure 13 illustrates the notional fracture timing estimated from the analysis of acoustic emissions (AE), strain gauge, accelerometer, and angular rate sensor (ARS) data relative to key fixture and PMHS responses. Due to the number of ribs injured during these tests, and oftentimes lack of direct instrumentation mounted to these locations, injury timing represented here should be considered a best estimate. The most significant fractures were listed here. Minor injuries, such as transverse or spinous process factures, were not included.

Consistent with expectations, calcaneus fractures generally occurred prior to 5 ms and were closely aligned with the time of peak floor force. Pelvic ring fractures also generally occurred around the time of peak seat force. Consistent with the results of previous tests, vertebral body fractures tended to occur after the time of peak seat force, with thoracic spine fracture occurring after lumbar fractures. Maximum torso compression was estimated from acromion displacement relative to the seat and was subsequent to rib fractures.

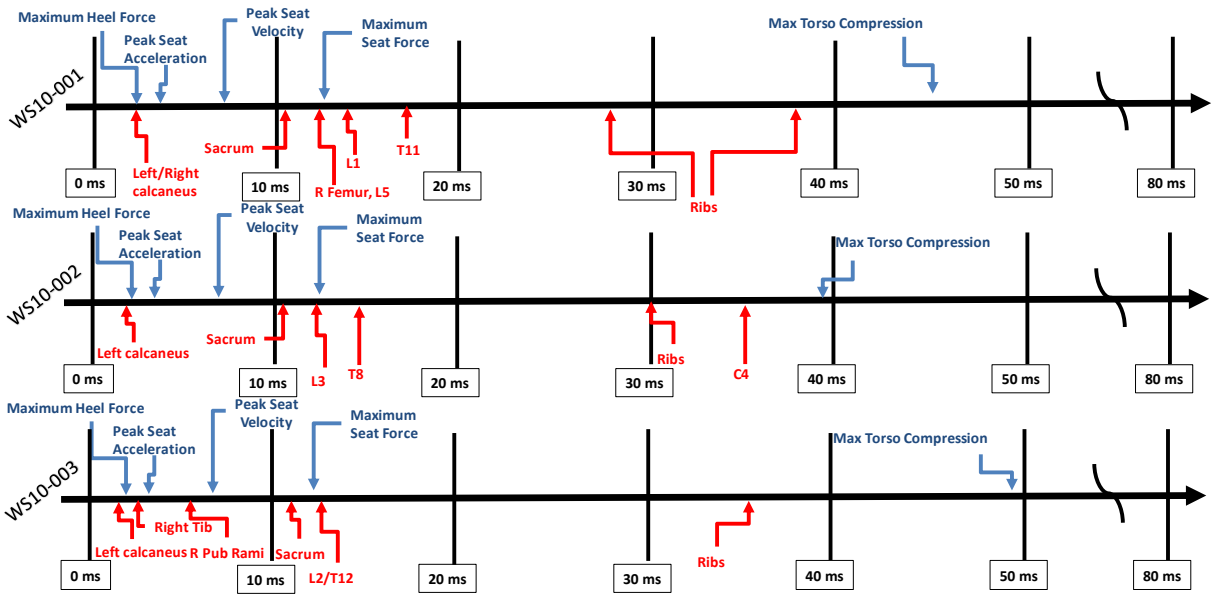

Figure 13. Injury timing relative to key events displayed as a timeline

2.2.4 Key Sensor Responses

Key sensor responses are shown in Figures 14–20. The spike in seat force for test WS10-001 (Figure 14) is indicative of a cable yank and does not affect the peak value. The large oscillations in the signal response subsequent to the initial S1 acceleration (Figures 18 and 19) correlate well with the timing of injuries that occurred during these tests as indicated previously in Figure 6. Finally, the positive sacrum rotation in the Y direction is indicative of posterior pelvic rotation that was observed in many of the whole-body tests. Both WS10-01 and WS10-03 had similar overall responses with WS10-03 having a smaller magnitude of rotation.

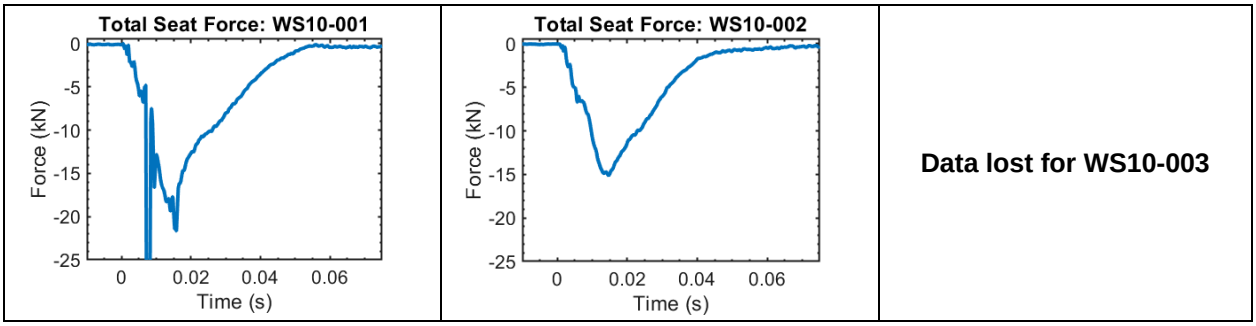

Figure 14. Seat force responses

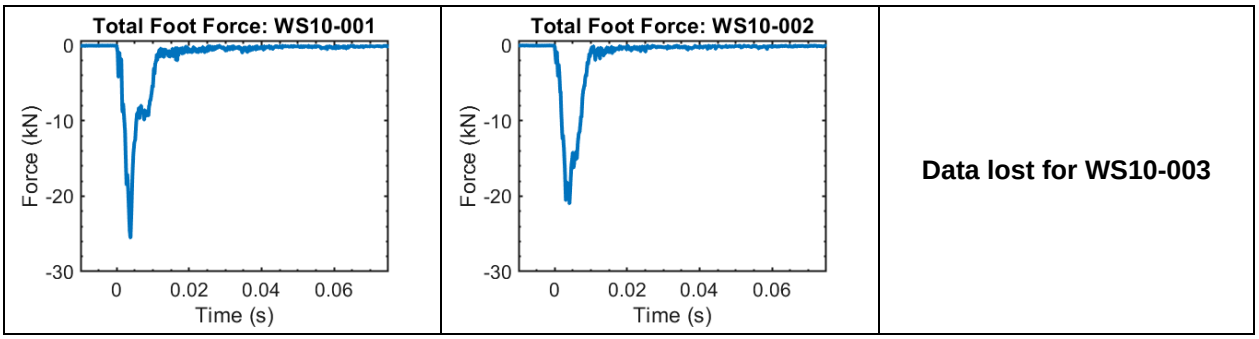

Figure 15. Floor force responses (sum of heel and forefoot loads)

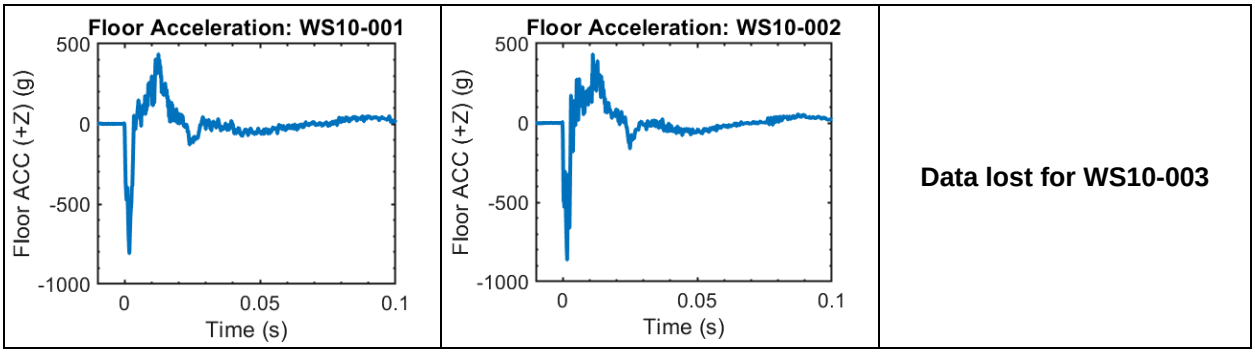

Figure 16. Floor vertical acceleration measurements (from heel plate accelerometer)

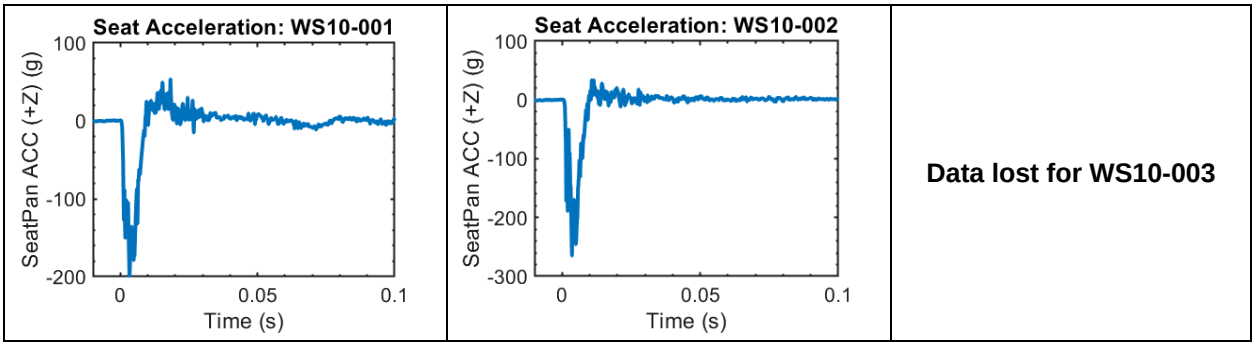

Figure 17. Seat vertical acceleration measurements

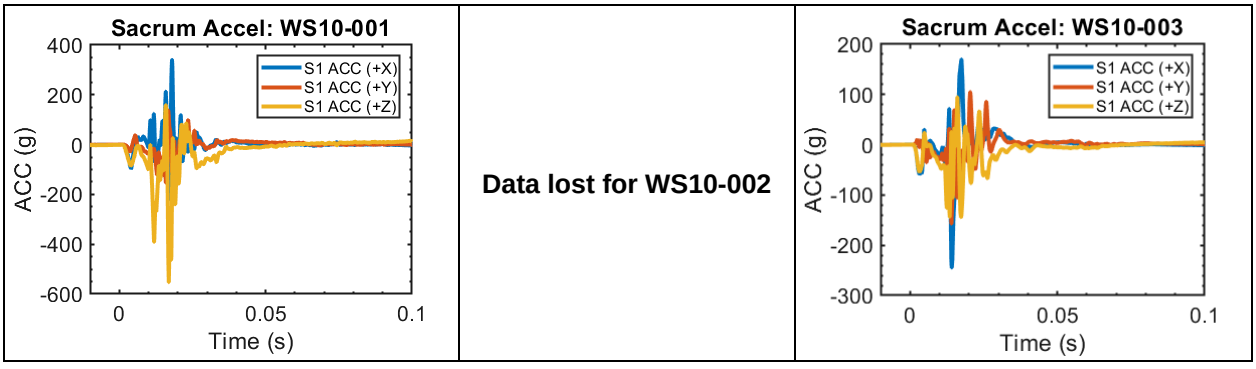

Figure 18. Sacrum acceleration measurements

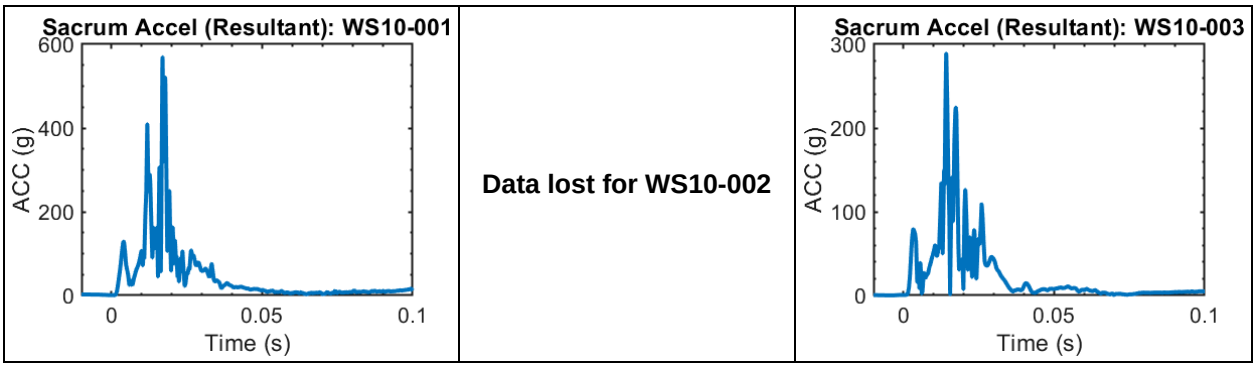

Figure 19. Resultant sacrum acceleration measurements

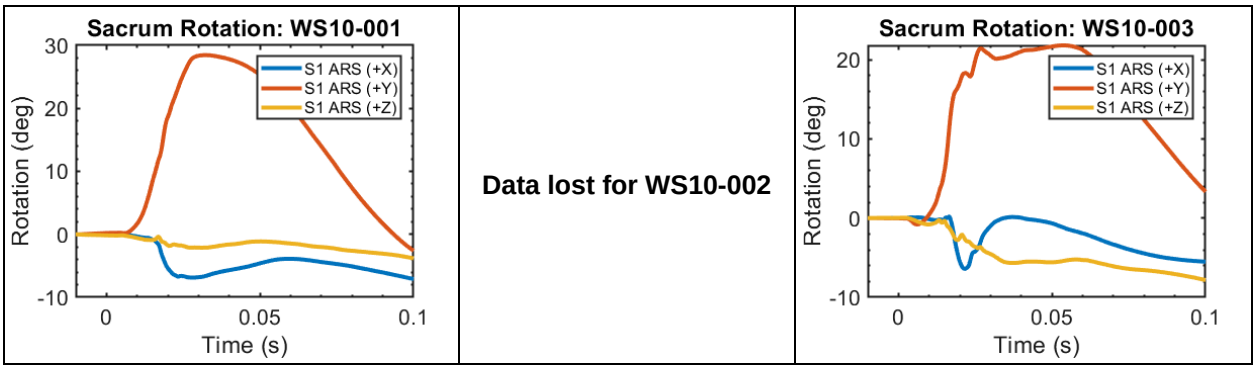

Figure 20. Pelvis (sacrum) rotation

2.2.5 Whole-Body Kinematics

Figures 21–23 provide X-Z (sagittal) and Y-Z (coronal) plane trajectories of markers attached to the knee, boot, shoulder, and head, as well as the frontal plane trajectories of the marker attached to the anterior knee for the first 100 ms. Observed trajectories have similar characteristics to those from tests in similar postures with less severe input conditions, although the magnitude of displacements in the WS10 series tests are much greater. For WS10-001, the right femur was fractured, which affected knee and foot kinematics. All trajectories shown in Figures 21–23 are relative to the seat.

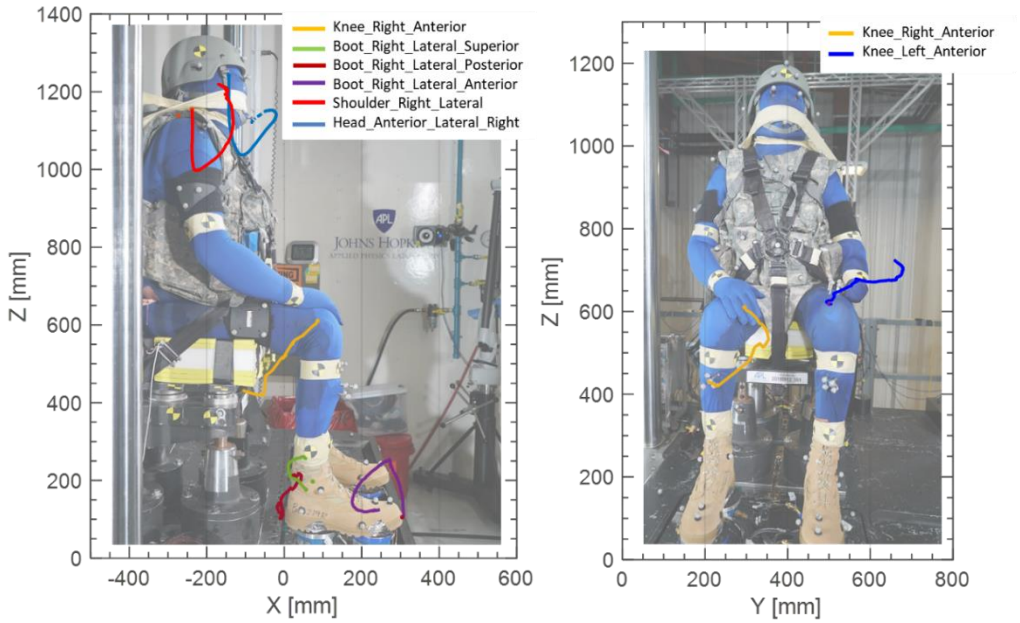

Note that for WS10-001, the right femur was fractured DURING TESTING, which affected knee and foot kinematics.
All motions are relative to a fixed point on the seat frame.

Figure 21. X-Z plane marker trajectories for knee, boot, shoulder, and head (left) and Y-Z marker trajectories for the anterior knee (right) from test WS10-001 overlaid with image showing initial position of the PMHS

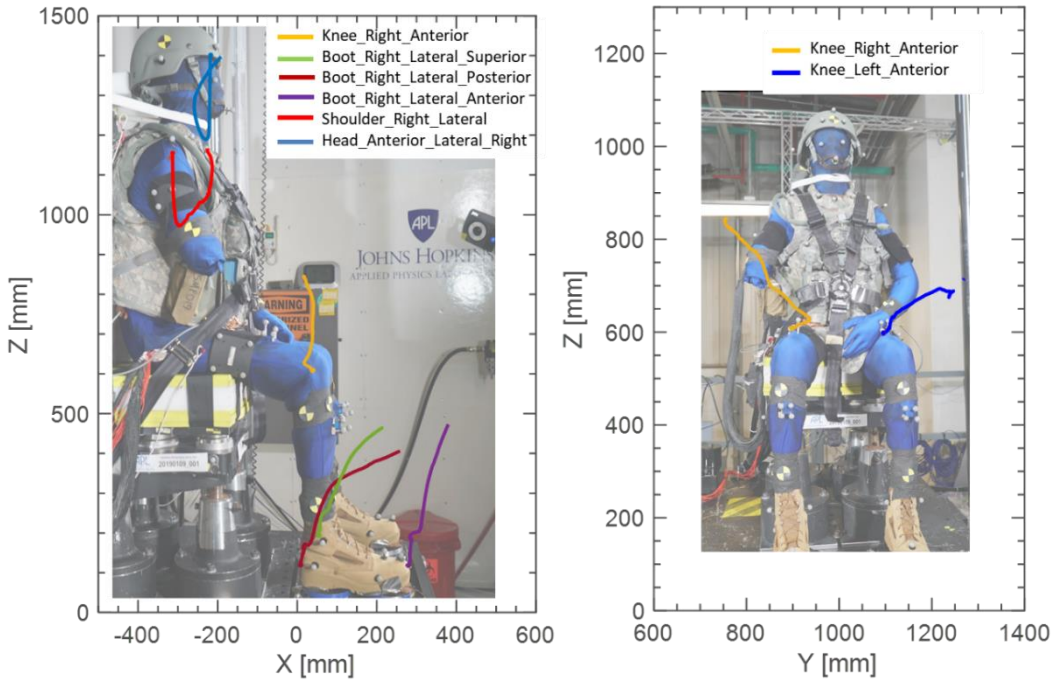

All motions are relative to a fixed point on the seat frame.

Figure 22. X-Z plane marker trajectories for knee, boot, shoulder, and head (left) and Y-Z marker trajectories for the anterior knee (right) from test WS10-002 overlaid with image showing initial position of the PMHS

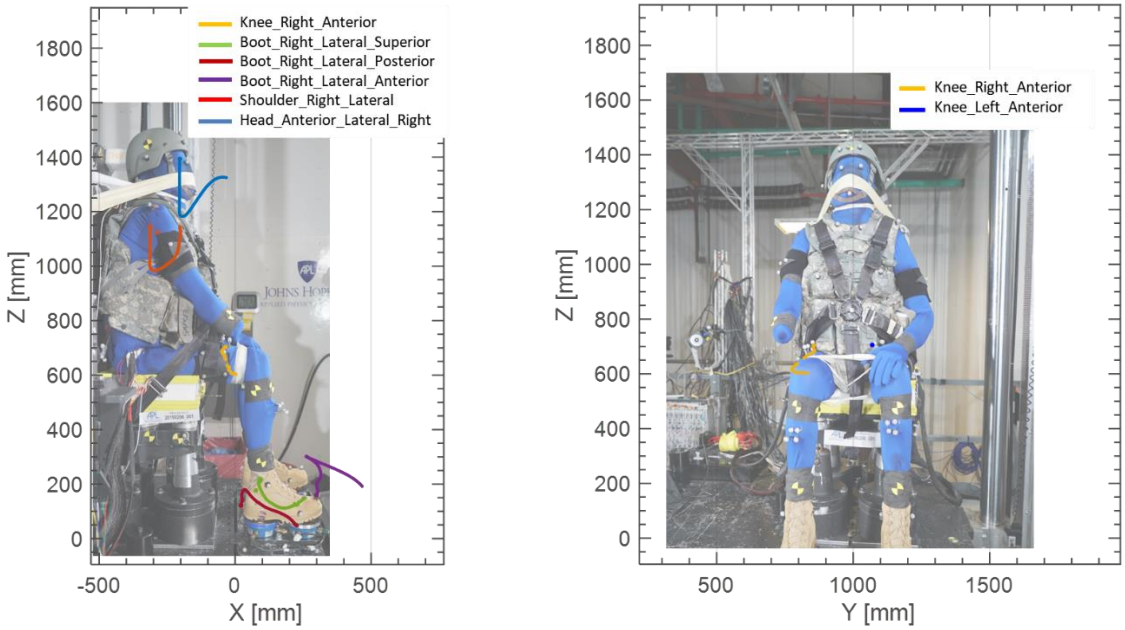

Note that knee left motion was occluded by the subject's arm during this test.
All motions are relative to a fixed point on the seat frame.

Figure 23. X-Z plane marker trajectories for knee, boot, shoulder, and head (left) and Y-Z marker trajectories for the anterior knee (right) from test WS10-003 overlaid with image showing initial position of the PMHS

3. WS11 SERIES (WSU)

3.1 Methods

3.1.1 WSU Test Fixture

The WSU test fixture is an aluminum, horizontal, decelerative system comprising a sled deck (WHAM IV), a rigid seat on rails, and a movable footplate (Figure 24). Two rails are mounted to the sled deck, parallel to the long axis of the sled. A rigid seat fixture is positioned with the seat back parallel to the sled deck and on top of the rails. A pneumatic system accelerates the sled system from the initial stationary position down the 23.75-m track. The target velocity at the seat is determined by the pressure used to accelerate the horizontal sled system. Honeycomb blocks, mounted on the barrier (Figure 25), are used to decelerate the seat fixture. Two snubbers (RCOS 3X 12 BS 04 Efdyn Inc., OK) are used to decelerate the sled deck. A movable floor assembly produced an independent floor pulse. The 0.406- × 0.406- × 0.0063-m floor plate pulse duration is tuned with elastomers (GBA-20 MEPC Inc., IL) that also return some energy allowing for floor velocities greater than the incoming seat velocity. Table 15 shows the test parameters, corresponding honeycomb block specifications, and the number of elastomers used for achieving the target pulse.

A V10 seat cushion was placed between the subject and the seat. The V10 cushion is (0.457 × 0.457 m) and consists of two pieces of Poron (192.22 kg/m^3) (0.012 m), one piece of Ethafoam 4101FR (35.2 kg/m^3) (0.057 m), and three pieces of Poron (144.17 kg/m^3) (0.012 m). The total thickness of the cushion was 0.121 m. The surface of the cushion was covered with a layer of gaffer's tape.

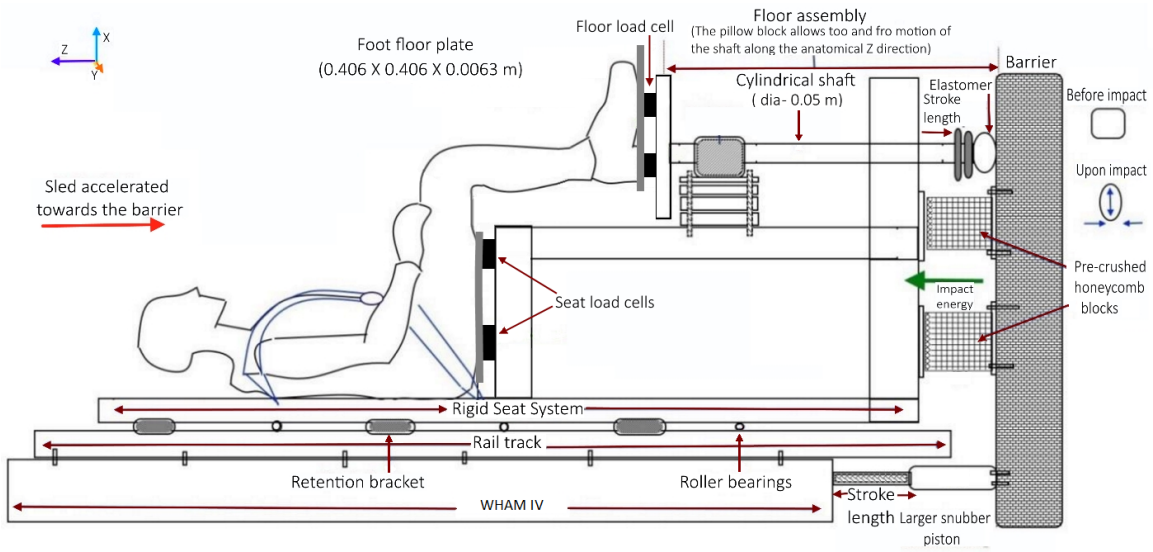

Figure 24. WSU horizontal sled system with the occupant positioned on the seat with a five-point belt

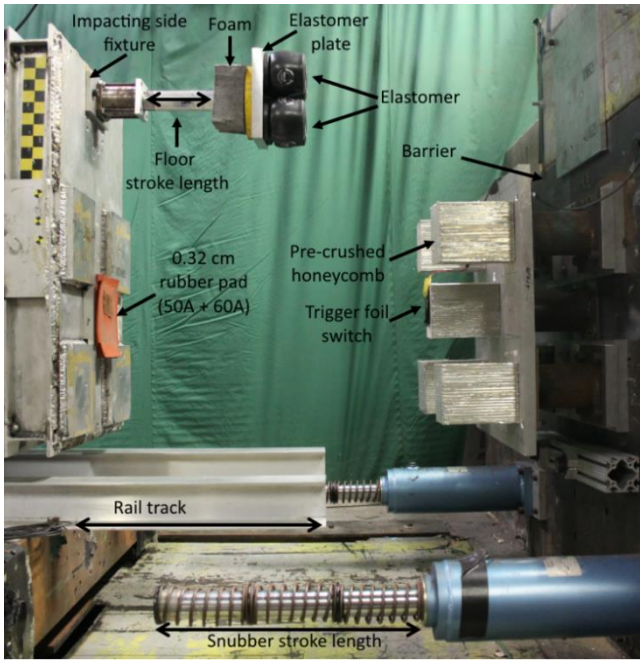

Figure 25. The two large-capacity snubbers mounted to the barrier are used to decelerate the sled deck, while the precrushed aluminum honeycomb blocks attached to the barrier are used to decelerate the seat fixture and produce a target time to peak for the seat

Table 15. WS11 Test Parameters and Specifications

Test ID	WS11
Sample size	3
WSU test IDs	WSU 12, WSU 13, WSU 14
Seat input	9 m/s in 5 ms
Floor input	13 m/s in 2.5 ms
PPE (ACH + IOTV)	Medium
Posture	Nominal (90/90/90)
Seat padding	V10 Cushion
Hexcell block dimensions (m) (#)	0.133 x 0.133 x 0.178 (5)
Precrushed depth (m)	0.005
Crush strength (Pa)	6.10 x 106
Hexcell cell dimensions (m)	0.004 x 0.003 x 0.0015
Number of elastomers	4 (GBA-20)
Floor stroke (m)	0.089

3.1.2 Instrumentation Locations and Transducer Types

The test fixture contained an array of uniaxial load cells and accelerometers at the occupant-seat and occupant-floor interfaces (Table 16 and Figure 26). The seat load cell configuration included uniaxial load cells at the sacrum plate, left and right ischium plates, and left and right thigh plates, allowing for an analysis of seat load distribution between the components (Rupp et

al., 2016) as well as the ability to sum the individual loads to calculate a total seat force. Floor load cells and accelerometers measured the total floor force and floor acceleration. Each foot consisted of a separate fore- and hind-foot load cell–accelerometer pair, such that the components of the floor load could be evaluated for each foot, as well as total loads. Fixture velocities were calculated by integrating acceleration signals.

Table 16. Masses and Instrumentation Used for Mass Compensation

Location	Plate Mass (kg)	Load Cell Names	Load Cell Model	Accelerometer Name	Accelerometer Model
Left heel	1.29	Hindfoot_Left	Interface LWPF1-50k	Hindfoot_Left	Endevco 72701A-20k
Right heel	1.29	Hindfoot_Right	Interface LWPF1-50k	Hindfoot_Right	Endevco 72701A-20k
Left forefoot	1.42	Forefoot_Left	Interface LWPF1-20k	Forefoot_Left	Endevco 72701A-6k
Right forefoot	1.42	Forefoot_Right	Interface LWPF1-20k	Forefoot_Right	Endevco 72701A-6k
Sacrum	1.90	Sacrum_Center	Interface LWPF1-50k	Seatpan_Sacrum	Endevco 72701A-20k
Left IT	2.97	Ischium_Left	Interface LWPF1-50k	Seatpan_Ischium_Left	Endevco 72701A-20k
Right IT	2.91	Ischium_Right	Interface LWPF1-50k	Seatpan_Ischium_Right	Endevco 72701A-20k
Left thigh	1.30	Femur_Left	Interface LWPF1-20k	Seatpan_Femur_Left	Endevco 72701A-6k
Right thigh	1.30	Femur_Right	Interface LWPF1-20k	Seatpan_Feumr_Right	Endevco 72701A-6k

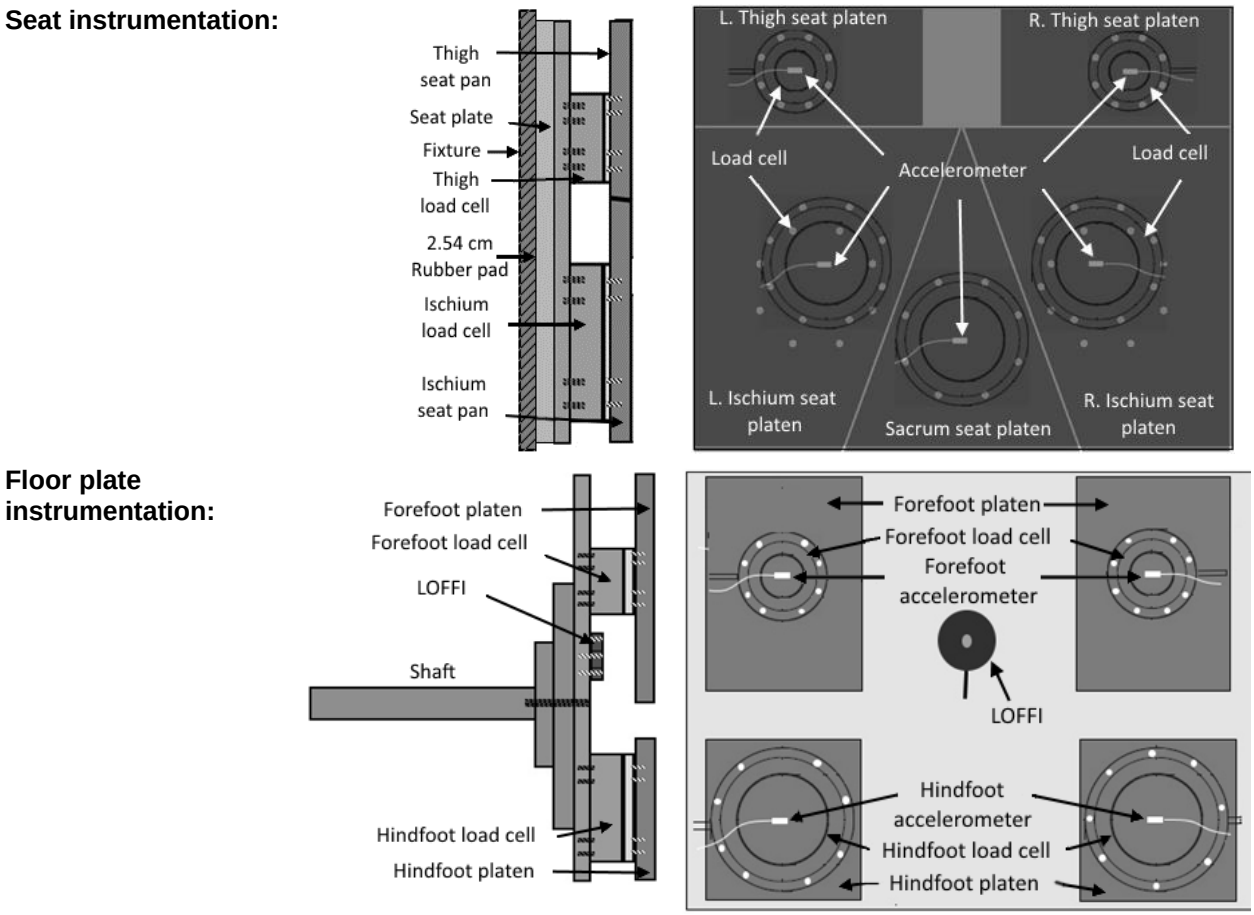

Figure 26. Rig instrumentation locations

PMHS instrumentation included 6DOF sensors (6DX, Diversified Technical Systems, Inc., CA), uniaxial accelerometers (7270A, Endevco), acoustic emission sensors (Nano 30, Physical Acoustics Corporation, NJ), and uniaxial strain gauges (C2a-06-0621w-350, Vishay, NC). The types and locations of these sensors and the orientations of strain gauges are provided in Table 17 and Figure 27. The 6DX sensors measured X-, Y-, and Z-accelerations (A_x, A_y, and A_z, respectively) and X-, Y-, and Z-angular rates (AR_x, AR_y, and AR_z, respectively). The 6DX sensors were rigidly mounted to the skull (3 cm superior to the Frankfort plane at the level of the tragion), the sternum, the thoracic vertebrae (T1, T5, T8, and T12), and the sacrum (S1–S3 level) using screws. The 6DX sensors were rigidly mounted to the right superior pubic ramus, the distal femurs, and the distal tibiae using worm gear clamps. The distal femur and tibia 6DX sensors were located proximal to the most distal portion of the bone at a distance of 0.2–0.3 and 0.15–0.25 of the total femur and tibia lengths, respectively. Linear accelerometers (7270A, Endevco, CA) (installed to measure A_z) were installed on the medial surface of the left and right calcaneus. A CT scan was conducted after instrumentation but prior to testing document sensor positions relative to the skeleton.

Table 17. Subject Instrumentation Locations

6DX	Strain Gage[a]	Acoustic Emission Sensor	7270A Accelerometer
Head	Left ASIS	T4	Left Calcaneus
Sternum	Right ASIS	T7	Right Calcaneus
Right Superior Pubic Ramus	Left Superior Pubic Ramus	T9	
Left Distal Femur	Right Superior Pubic Ramus	T11	
Right Distal Femur	Left Distal Femur	L1	
Left Distal Tibia	Right Distal Femur	L2	
Right Distal Tibia	Left Proximal Tibia	L4	
T1	Right Proximal Tibia	Sacrum	
T5	Left Distal Tibia	Left Iliac Wing	
T8	Right Distal Tibia	Right Iliac Wing	
T12	Left Calcaneus	Left Calcaneus	
Sacrum (S1–S3)	Right Calcaneus	Right Calcaneus	

[a] Strain gauges were placed along the long axes of long bones, the circumferential direction of ribs, along the direction of the pelvic ring for the pubic ramus, along the direction of the iliac crest for the ASIS, and fore to aft for the calcaneus locations.

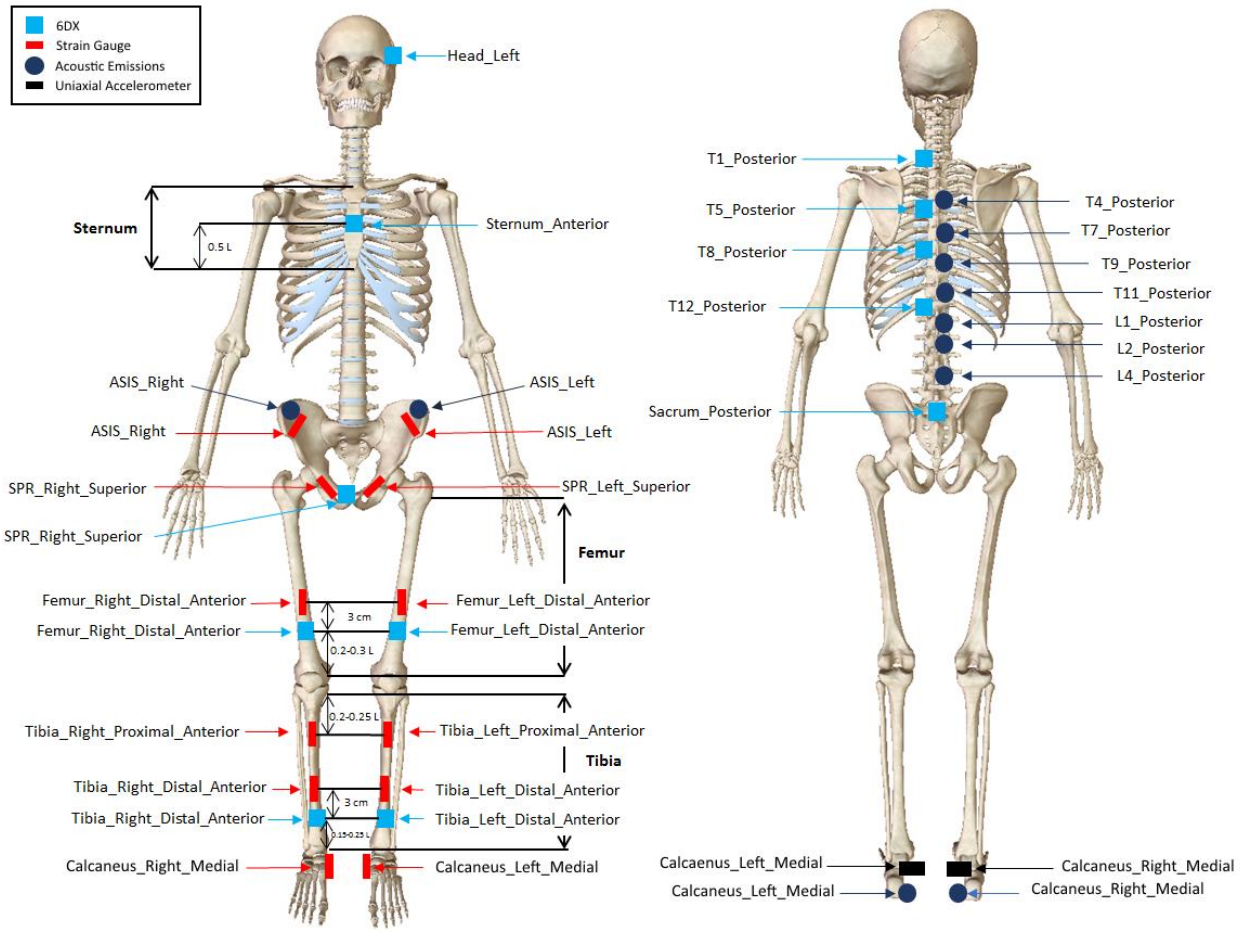

Figure 27. Subject instrumentation locations

3.1.3 Kinematic Analysis

Circular quadrant marker stickers (adhered to the surface of the body suit or PPE) were placed at various skeletal or surface landmarks for kinematic tracking. Tracked locations included the head (markers at the left and right tragion and left and right infraorbitale), shoulders (markers at the left and right acromion), knees (markers at the left and right patella, and left and right lateral femoral condyles), and boots (left and right forefoot, left and right hind foot, left and right lateral malleolus) (Tables 18–20).

Various points on the fixture were tracked to define and translate the coordinate system as it moved through the camera frame (Table 21). Motion tracking and calibration were performed using motion analysis software (TEMA, Image Systems Motion Analysis).

Table 18. Surface Marker Anatomical Locations

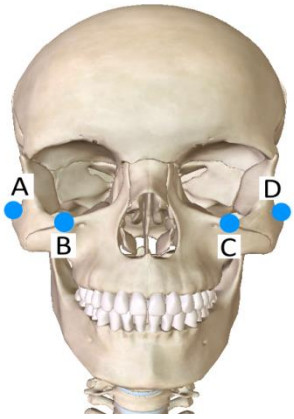	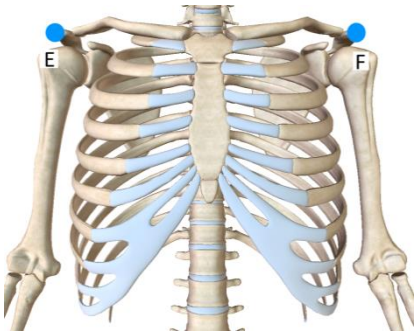	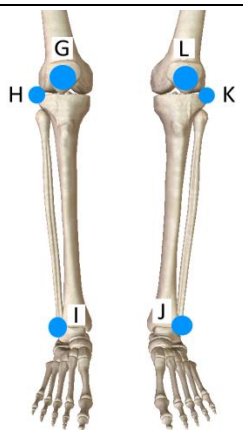
A) Tragion_Right_Lateral B) Infraorbitale_Right C) Infraorbitale_Left D) Tragion_Left_Lateral	E) Acromion_Right_Lateral F) Acromion_Left_Lateral	G) Patella_Right_Anterior H) Epicondyle_Right_ Lateral I) Malleolus_Right_ Lateral J) Malleolus_Left_ Lateral K) Epicondyle_Left_ Lateral L) Patella_Left_Anterior

Table 19. Surface Marker Boot Locations

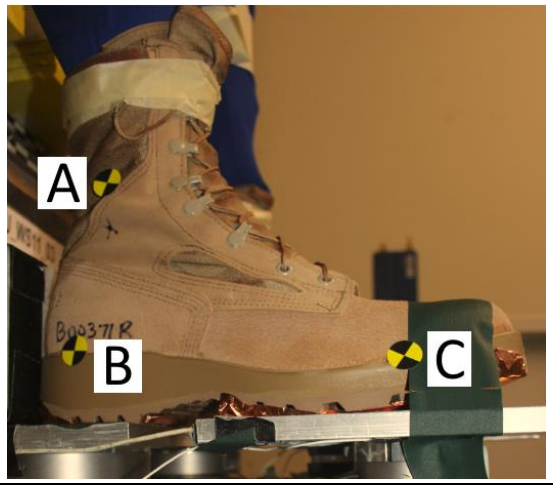	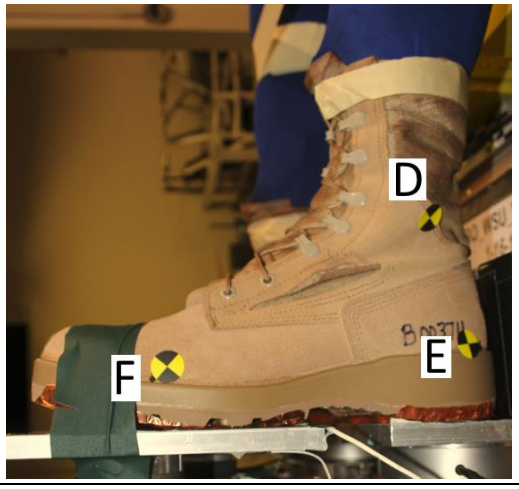
A) Mallelous_Right_Lateral B) Boot_Hindfoot_Right_Lateral C) Boot_Forefoort_Right_Lateral	D) Mallelous_Left_Lateral E) Boot_Hindfoot_Left_Lateral F) Boot_Forefoort_Left_Lateral

Table 20. Rig Kinematic Marker Locations

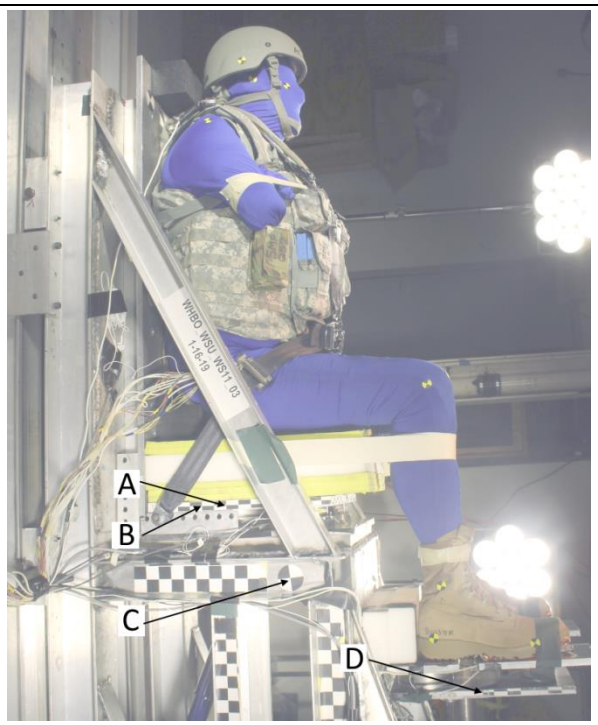

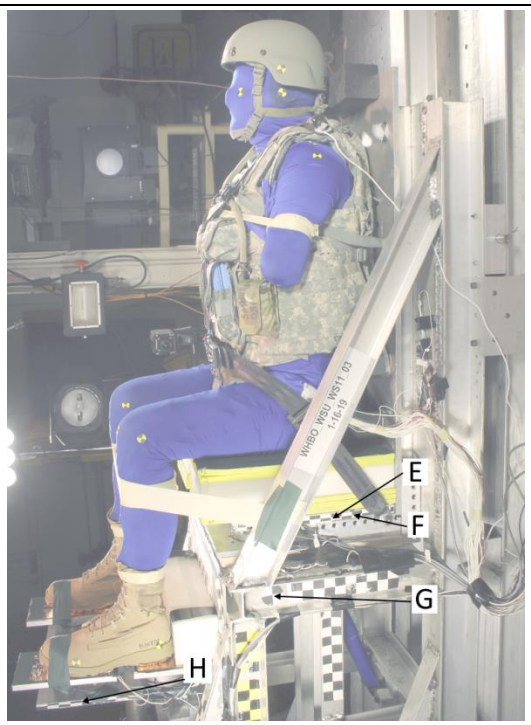

A) Seatpan_Right_Top B) Seatpan_Right_Bottom C) Rig_Right D) Floor_Right[a]	E) Seatpan_Left_Top F) Seatpan_Left_Bottom G) Rig_Left H) Floor_Left[a]

[a] Exact locations of floor plate fore-aft and up-down may vary between tests based on the femur and tibia length of the test subject.

Foot angle was calculated using the landmarks listed in Table 21.

Table 21. Calculated Kinematic Descriptions

Location	Description
Foot_Tibia_Right	Included angle between Epicondyle_Right_ Lateral to Mallelous_Right_Lateral and Boot_Hindfoot_Right_Lateral to Boot_Forefoot_Right_Lateral
Foot_Tibia_Left	Included angle between Epicondyle_Left_ Lateral to Mallelous_Left_Lateral and Boot_Hindfoot_Left_Lateral to Boot_Forefoot_Left_Lateral

3.1.4 Subject Characteristics

Table 22 provides the characteristics of the three subjects tested by WSU for the WS11 series. All subjects were within predefined acceptable ranges, with the exception of the low mass for the subject used in test WS11-02. Due to this subject's age (age 35 at the time of death), the WIAMan Engineering Office (WEO) approved an exception to the inclusion criteria. In

Appendix B, Tables B-1 through B-3 provide standard subject anthropometry measured in accordance to reference document W0080 (Bass et al., 2013).

Table 22. Subject Characteristics with Inclusion Criteria

Test Series ID	Subject ID	Age (yrs)	Gender	Height (cm)	Weight (kg)	BMI	T-Score (L1–L4)
WS11-01	L171491	62	M	170.2	87.5	29.2	-0.4
WS11-02	S172105	35	M	165.7	56.7[a]	20.7	-0.4
WS11-03	S160979	61	M	175.0	88.2	28.8	1.5
Acceptance Criteria	…	18 - 80	M	165 - 186	64 - 106	18 - 35	-1.0 - +2.5

[a] S172105 subject with low mass was approved for use.

3.1.5 Subject Positioning

Subject positioning was based on the relative locations of skeletal surface landmarks. Figure 28 shows the targeted posture conditions and highlights important joint angles and relative positions of landmarks. Landmarks were identified through palpation to locate the skeletal points of interest. Landmarks on the pelvis were determined through the palpation of the pubic symphysis and left and right ASIS, which were accessible by reaching under the IOTV. Pelvis angle was defined as the angle of the line formed between the mid-ASIS point and the pubic symphysis with reference to the vertical axis. All landmark locations were measured by the same staff member.

A 3-D coordinate measurement device (Romer arm 7320I, Hexagon Metrology Inc., CA) was used to measure the position of the PMHS before each test. During the positioning process, 3-D coordinates were recorded for the specified landmarks and checked against target relative coordinates. When landmarks fell outside of the tolerance, the PMHS was adjusted accordingly and remeasured until they were within tolerance. Gaffer's and masking tape were used to secure each PMHS foot in the proper position against the floor plate by running a strip of tape from the PMHS booted forefoot to the floor plate. Tape mounting locations varied with each test (see Table 19 for examples). Similarly, masking tape was used to secure PMHS knee spacing. All positioning tape was precut, approximately 50% across immediately prior to each test such that the tape severed during the loading event. In all tests, all strips of tape were completely severed at the beginning of the loading event. Therefore, PMHS movement of the lower leg and feet did not appear to be influenced by the tape placement. In addition, foam blocks were used between the boot and test fixture, between the pelvis and test fixture, and between the head and test fixture to achieve the target positioning of key anatomical landmarks. These blocks were used for positioning to support the static mass of the body components. The kinematics of PMHS during testing were such that additional load was not applied to the blocks during the loading phase of the event. Final coordinates of anatomic landmarks were documented immediately prior to each test.

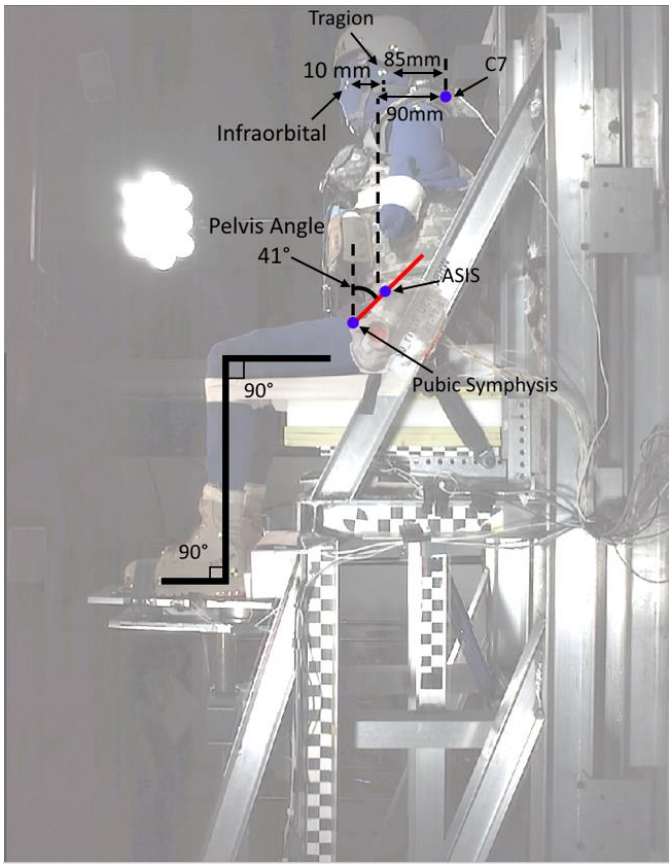

Figure 28. Target position

Target and actual postures for all WS11 tests are shown in Table 23. Target postures were based on the postures assumed by midsize male Soldiers seated in a military vehicle seat with a vertical seat back and horizontal seat cushion angles based upon Reed and Ebert (2013). Positioning was performed following the procedure described by Rupp and Reed (2015). When positioning subjects, the highest priority was given to matching pelvis angle, head position and angle, and foot and knee angles. Lower priority was given to acromion position, as some subjects were missing forearms, preventing the use of the arm to control shoulder position.

Table 23. Subject Positioning

Measurement	Description	Target Range		WS11-01	WS11-02	WS11-03
		Low	High			
Pelvis Angle	Angle of line from mid-ASIS to pubic symphysis in the XZ-plane with respect to vertical	36°	46°	39.6°	41.2°	38.9°
ASIS Fore-Aft Distance	A-P difference of left and right ASIS landmarks	-10 mm	10 mm	3.9	5.1	5.8
ASIS Vertical Distance	Vertical difference of left and right ASIS landmarks	-10 mm	10 mm	1.5	4.1	1.9
Cervicale Aft of Mid-ASIS	Fore-aft distance from average of left and right ASIS landmarks to most posterior aspect of C7	-80 mm	-100 mm	-89.9	-93.9	-94.9
Acromion Fore-Aft Difference	Fore-aft difference between left and right acromion landmarks	-20 mm	20 mm	3.5	0.9	8.3
Acromion Vertical Distance	Vertical difference between left and right acromion landmarks	-20 mm	20 mm	14.4	11.3	14.8
Cervicale Aft of Tragion	Fore-aft distance from average of left and right tragion to most posterior aspect of C7	75 mm	95 mm	79.9	89.9	84.1
Infraorbitale Superior of Tragion	Vertical distance from mid-infraorbitale to mid-tragion	-5 mm	-15 mm	-13.1	-10.3	-5.4
Boot Heel Separation	Distance between centers of boot heels	285 mm	305 mm	294.4	295.4	297.9

3.1.6 PPE, Boot, and Belt-Fitting Procedures

PPE, including an ACH, IOTV, and Belleville 390 DES men's hot weather desert tan combat boots (Belleville Boot Company, Belleville, IL), were fitted to the PMHS in accordance with reference documents W0058, W0059, and W0060, respectively (WIAMan Biomechanics Team, 2013a, 2013b, 2013c). The routing and fitting of the five-point seatbelt restraint harness were performed in accordance with reference document W0070 (WIAMan Biomechanics Team, 2013d).

3.1.7 Data Processing

All signals were processed following the procedures used for BRC development, which include filtering with a low-pass fourth-order digital phaseless Butterworth filter. Accelerometers and seat/floor load cell data were filtered using a 3-dB cutoff frequency of 3 kHz. Angular rate data were filtered using a 3-dB cutoff frequency of 1650 Hz. DTS 6DX transducer measurements were transformed to standardized locations relative to skeletal anatomic landmarks using the procedure developed by SCoTT reported by Slykhouse et al. (2019).

Times to peak velocity for the floor and seat were calculated using the method defined by Spink (2014). This method involves a baseline shift and integration of the acceleration time history, the peak (largest negative) velocity within a time frame of interest, and identification of all local minima less than 90% of the absolute peak. The local minimum just prior to the absolute peak is selected as the new peak velocity and points corresponding to 5%, 20%, and 95% of the final peak velocity are determined. If the velocity history exhibits a monotonic fall between 5% and

20%, the velocity slope is calculated between the points at 5% and 95% of the peak velocity. If the velocity history is not monotonic between 5% and 20%, the data point immediately following the last positive derivative in the window is identified and used to replace zero as the baseline for the 5% calculation. The start and end times are determined by calculating the times at which the equation that defines the velocity slope is equal to zero and peak velocity, respectively. The time to peak is the difference between the calculated ending and starting times.

3.1.8 Injury Assessment and Injury Timing Analysis

Acceleration, angular rate, strain, and acoustic emission data were all viewed qualitatively to provide an estimate of injury timing for each test. These estimates are subject to error, as signals in the region of injury often contain more than one event that could be interpreted at the time of injury. In general, fracture timing was identified as a spike or change in direction of an acceleration pulse immediately after an acoustic burst, if and when AE data were available. Approximate allowances were made for the time for sound to transmit between the location of fracture and the locations of acoustic emission sensor attachment. However, for situations where fracture occurred at a location that was remote from an acoustic emission sensor or accelerometer, fracture timing was estimated over a window based on accelerometer responses. Figure 29 shows an illustrated example of how T5–T6 fracture timing was estimated based on the time of acoustic burst measured by a nearby mounted sensor and the measurements of a nearby mounted accelerometer.

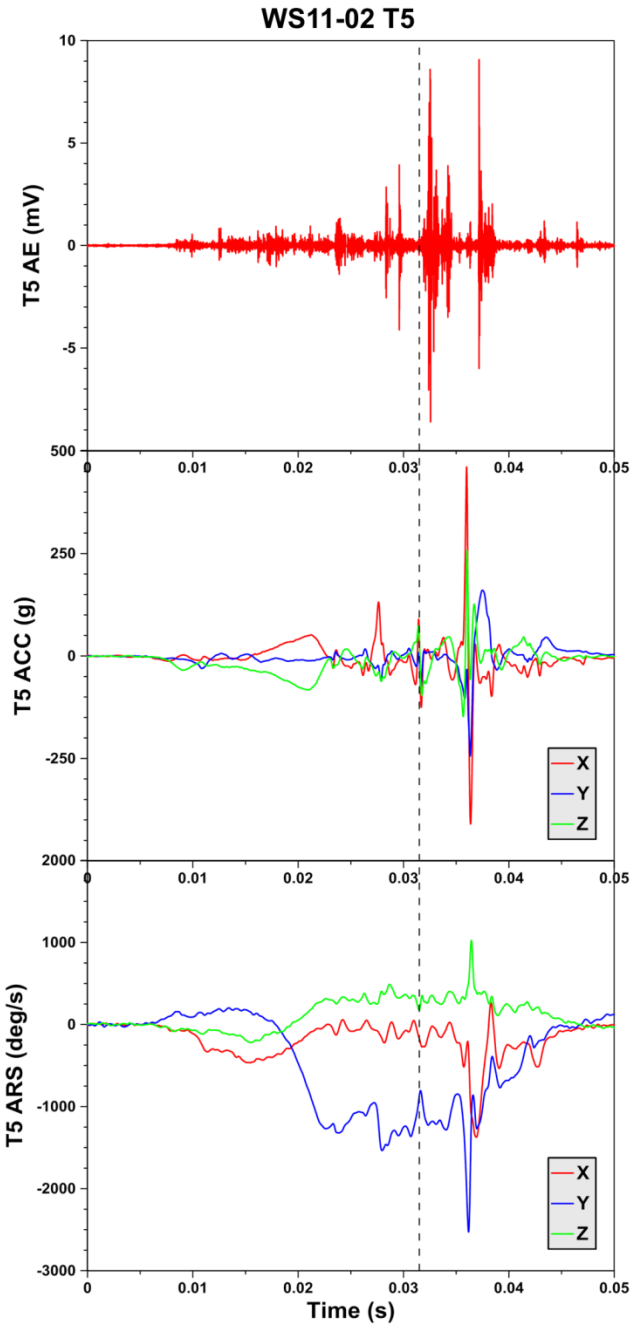

Figure 29. Example of plots used to determine injury timing for T5-T6 fracture in WS11-02 T4 acoustic emission (top), T5 acceleration (middle), and T5 angular rate (bottom). The vertical black dashed line indicates fracture timing.

3.2 Results

3.2.1 Test Conditions

Table 24 shows the floor and seat conditions for each of the three tests in the WS11 series as well as the targets. Floor velocities ranged from 13.4 to 14.3 m/s target, and TTP for floor pulses ranged from 2.4 to 2.6 ms with a target of 2.5-ms WS11-01 and WS11-02, with the exception of WS11-03, for which the floor pulse was 12.1 m/s peak with a TTP of 5.6 ms. During test WS11-03, tape that was used to prevent displacement prior to impact failed prematurely, which reduced floor stroke and peak velocity subsequent to impact. Seat peak velocity ranged from 5.1 to 5.5 m/s with a target velocity of 9 m/s, and TTP for seat pulses ranged from 5.1 to 5.5 ms with a target of 5.0 ms. Figure 30 provides floor and seat velocity histories used to determine peak velocity and TTP.

Table 24. Test Conditions: Targeted and Achieved

Test Series ID	Floor Peak Velocity (m/s)	Floor TTP (ms)	Seat Peak Velocity (m/s)	Seat TTP (ms)	PPE	Posture	Seat Padding
WS11-01	13.4	2.4	9.3	5.1	MED	90/90/90	V10 Cushion
WS11-02	14.3	2.6	9.4	5.5	MED	90/90/90	V10 Cushion
WS11-03	12.1	5.6	9.2	5.3	MED	90/90/90	V10 Cushion
Target	13	2.5	9	5	MED	90/90/90	V10 Cushion

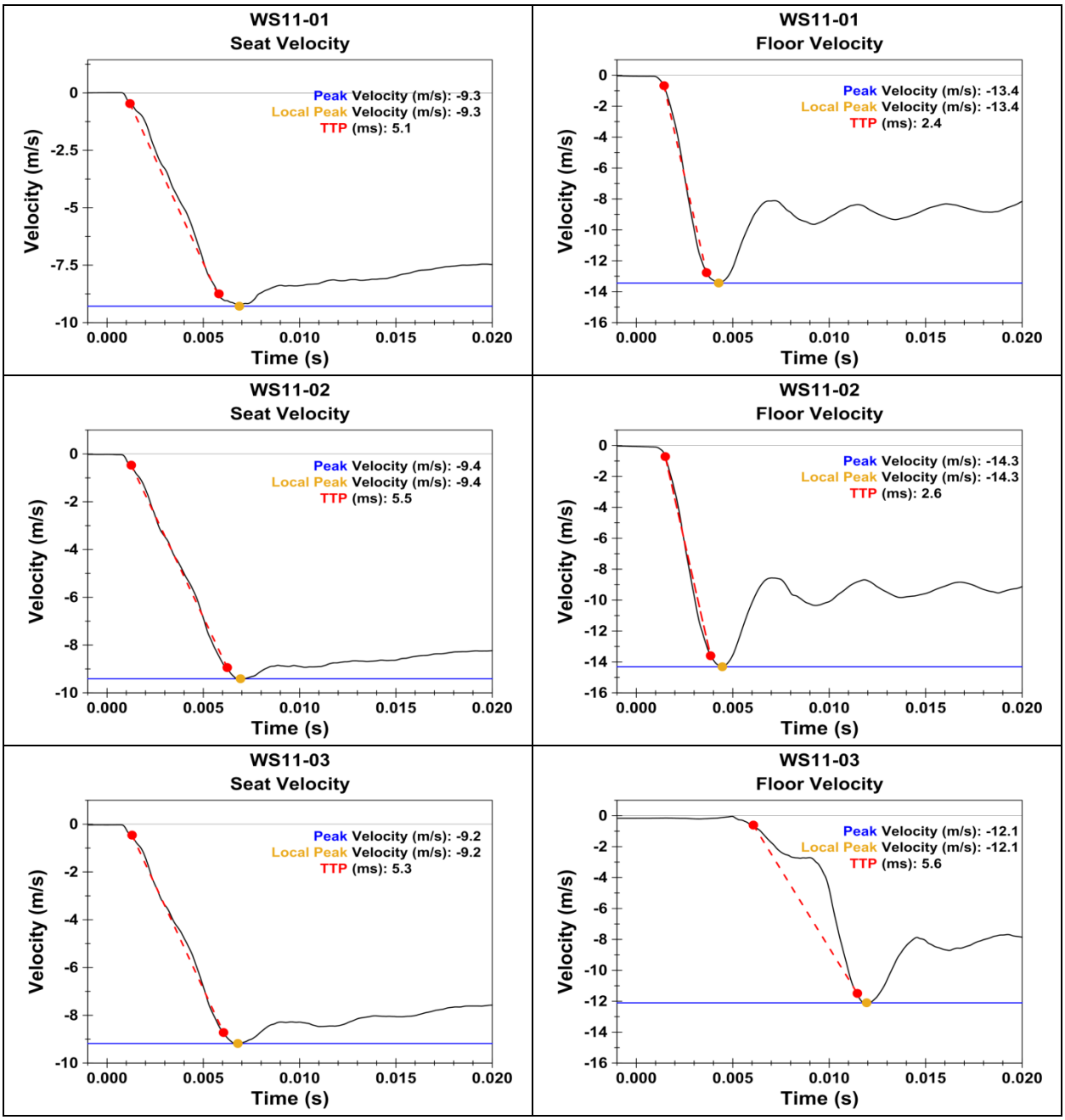

Figure 30. Seat and floor velocity time histories with peak and time to peak

3.2.2 Injury Outcomes

Tables 25–27 provide the injuries and associated AIS 2015 codes for the pelvis, lumbar spine, and thoracic spine, respectively. No lower extremity injuries were produced in the WS11 series, as shown in Figure 31. Isolated pelvis fractures were produced in one test (WS11-01). Pelvis fracture pattern is shown in Figure 32. Images of all fractures and key images of pre-/posttest

radiology documenting injury patterns are provided in Appendix B. Injury patterns were generally consistent with those reported by Danelson et al. (2018) as representative of combat theater events.

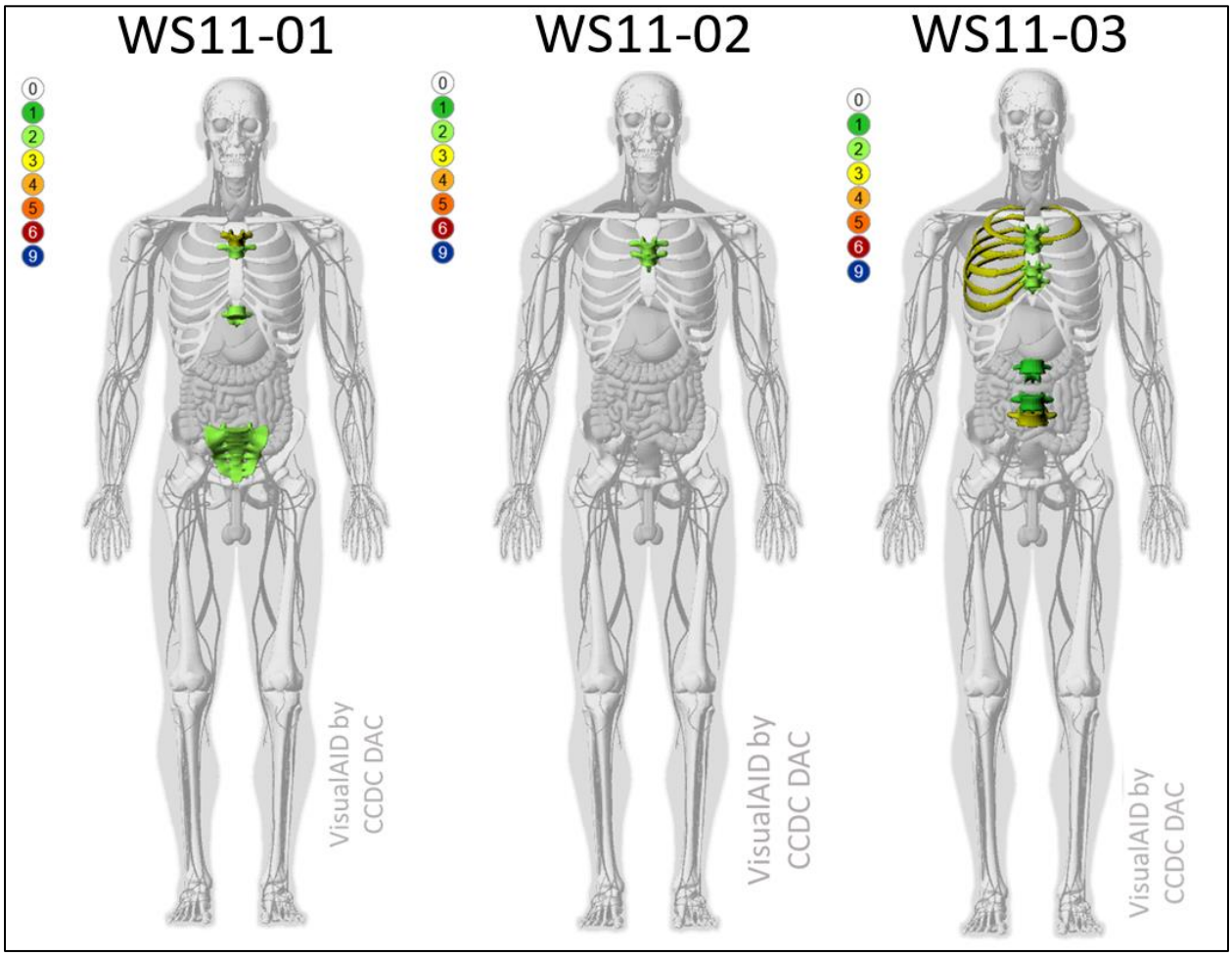

Figure 31. WS11 VisualAID injury visualization

Table 25. Pelvis Injuries

	AIS 2015	Description
WS11-01	Pelvic ring fracture: posterior arch intact; isolated fracture not destroying the integrity of the pelvic ring (AIS 856151.2 00NR)	Comminuted sacrum fracture at S4-S5 level on the left side

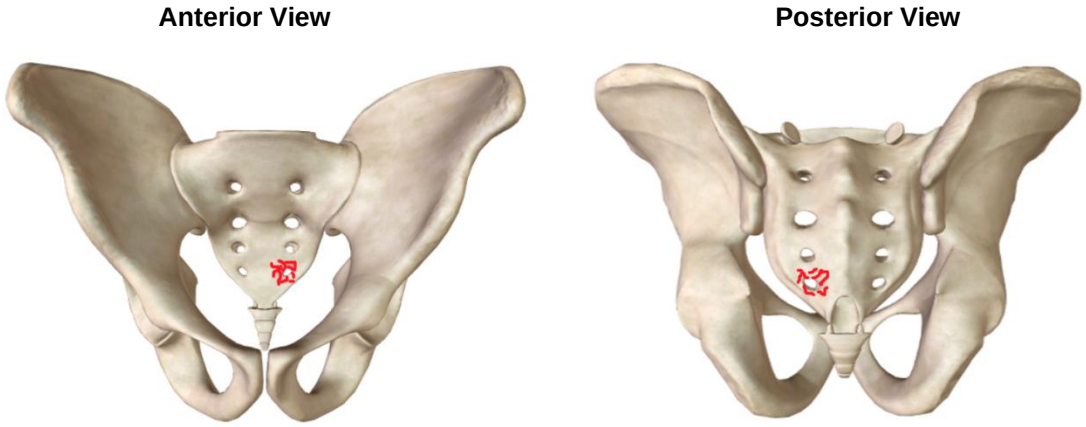

Figure 32. WS11-01 pelvis injury diagrams

Table 26. Lumbar Spine Injuries

	AIS 2015	Description
WS11-03	Vertebral body fracture, major compression (>20% loss of anterior height) (650634.3 0024) Transverse process fracture (AIS 650620.1 1021, AIS 650620.1 2021, AIS 650620.1 1023, AIS 650620.1 2023, AIS 650620.1 1024, AIS 650620.1 2024)	L5 compression fracture (25% loss in anterior height) Bilateral transverse process fractures at L2, L4, and L5

Table 27. Thoracic Spine Injuries

	AIS 2015	Description
WS11-01	Vertebral body fracture, minor compression (<20% loss of anterior height) (AIS 650432.2 0012, AIS 650432.2 0017) Vertebral body fracture, major compression (>20% loss of anterior height) (AIS 650434.3 0011)	T5 compression fracture (2% loss in anterior height) T10 compression fracture (10% loss in anterior height) T4 compression fracture (25% loss in anterior height)
WS11-02	Vertebral body fracture, minor compression (<20% loss of anterior height) (AIS 650432.2 0012, AIS 650432.2 0013)	T5 compression fracture (8.2% loss in anterior height) T6 compression fracture (7.6% loss in anterior height)
WS11-03	Vertebral body fracture, minor compression (<20% loss of anterior height) (AIS 650432.2 0011, AIS 650432.2 0012, AIS 650432.2 0014, AIS 650432.2 0015) Rib cage fracture(s) without flail, (>=3 ribs) (AIS 450203.3 0132, AIS 450203.3 0133, AIS 450203.3 0134, AIS 450203.3 0135, AIS 450203.3 0136, AIS 450203.3 0232)	T4 compression fracture (9% loss in anterior height) T5 compression fracture (16% loss in anterior height) T7 compression fracture (6% loss in anterior height) T8 compression fracture (15% loss in anterior height)

3.2.3 Injury Timing

Figure 33 illustrates fracture timing estimated from the analysis of acceleration, AE, strain gauge, and ARS data relative to key fixture and PMHS responses. Of note, tests WS11-01, WS11-02, and WS11-03 all sustained fractures at the T5 level, where a mount was installed. Although the fracture patterns suggest that they were not caused by the mount, mount installation cannot be conclusively ruled out as a contributing factor.

Consistent with expectations, the isolated sacrum fracture occurred prior to 5 ms and was closely aligned with the time of peak seat force. Consistent with the results of previous tests, spinal body fractures tended to occur after the time of peak seat force, with thoracic spine fracture occurring after lumbar fractures when present.

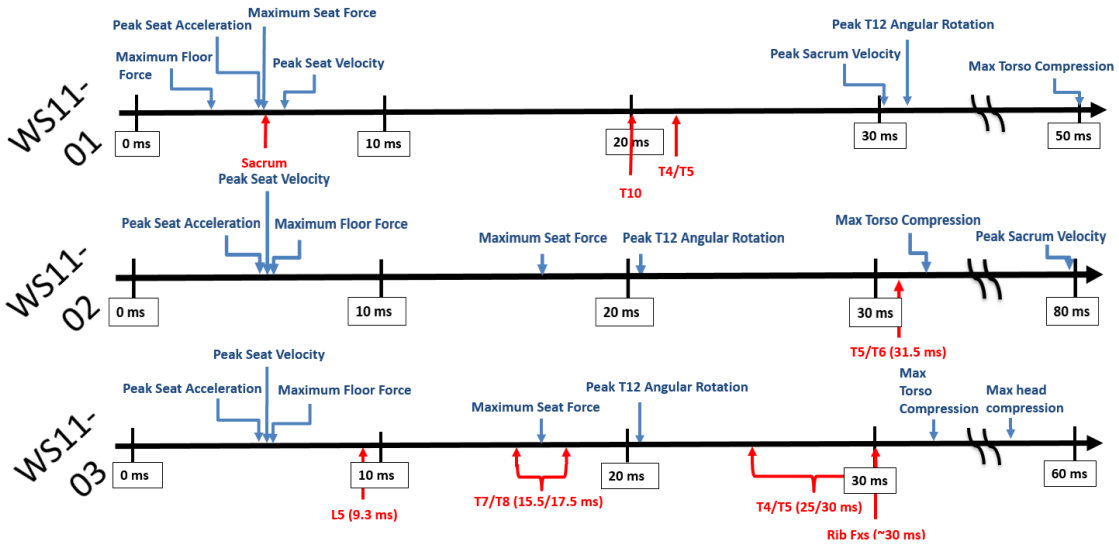

Figure 33. Injury timing relative to key events displayed as a timeline

3.2.4 Key Sensor Responses

Key sensor responses are shown in Figures 34–40. Spikes in sacrum acceleration responses and variability in pelvis rotations across tests are associated with the pelvic ring fractures in WS11-01 and L5 compression fracture in WS11-03.

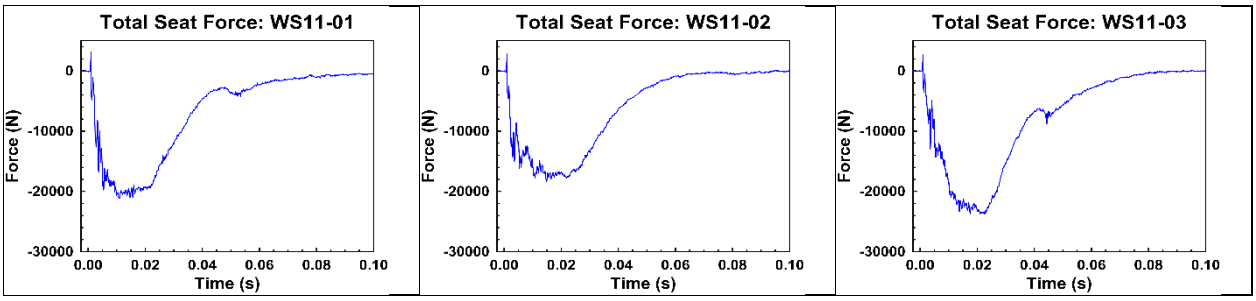

Figure 34. Seat force responses

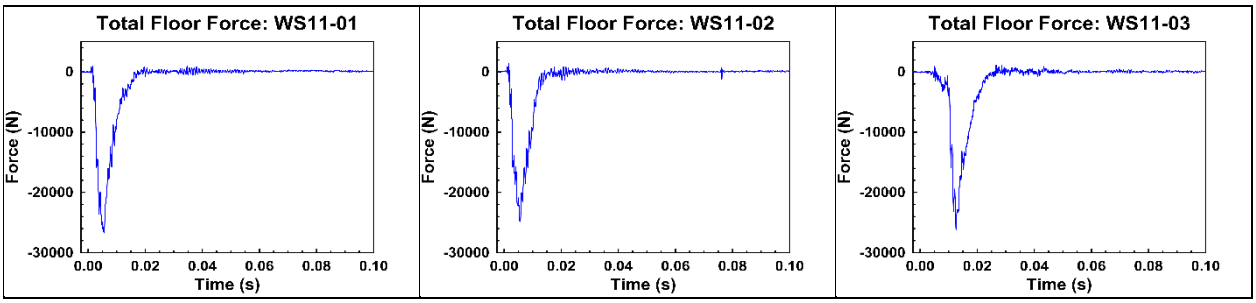

Figure 35. Floor force responses (sum of heel and forefoot loads)

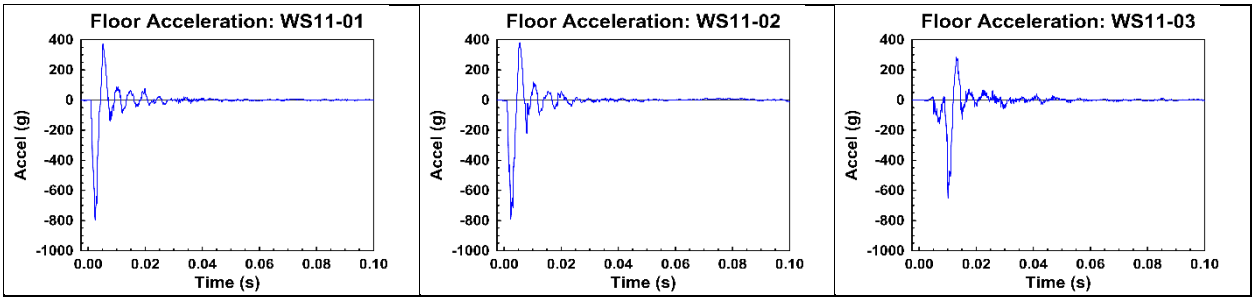

Figure 36. Floor vertical acceleration measurements (from heel plate accelerometer)

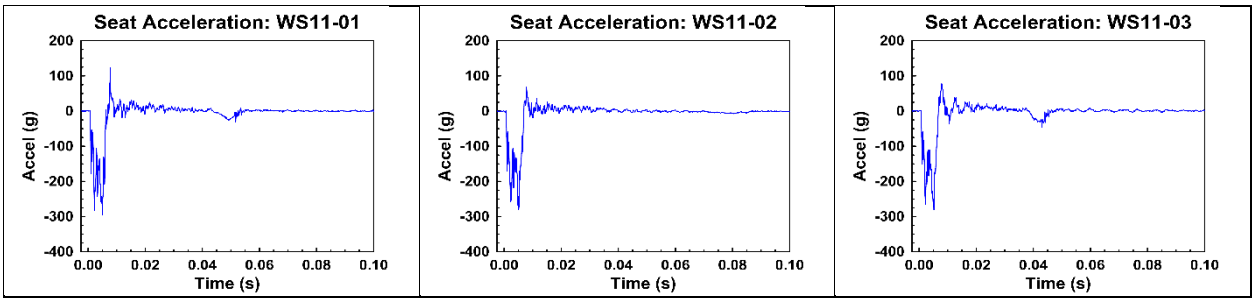

Figure 37. Seat vertical acceleration measurements

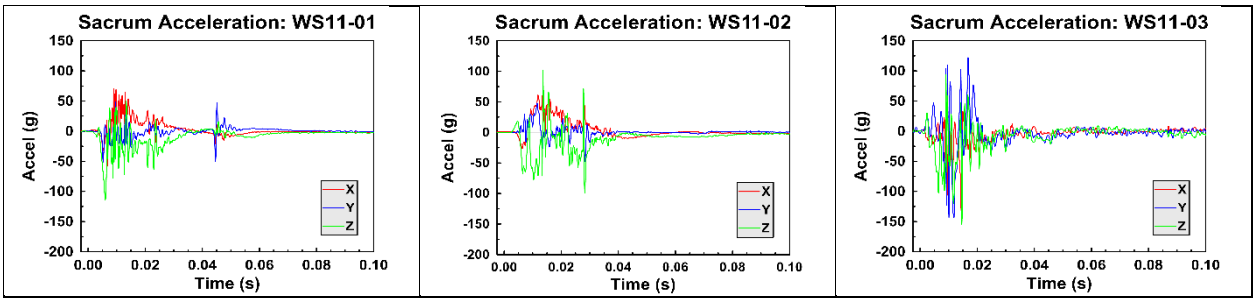

Figure 38. Sacrum acceleration measurements

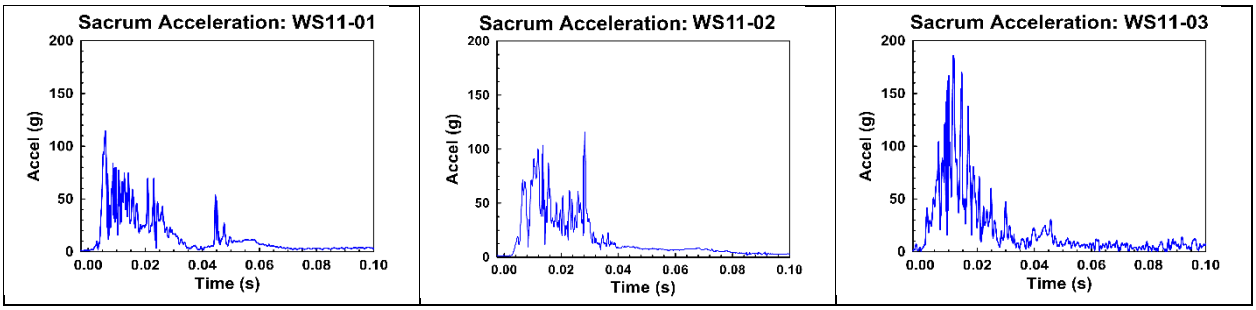

Figure 39. Resultant sacrum acceleration measurements

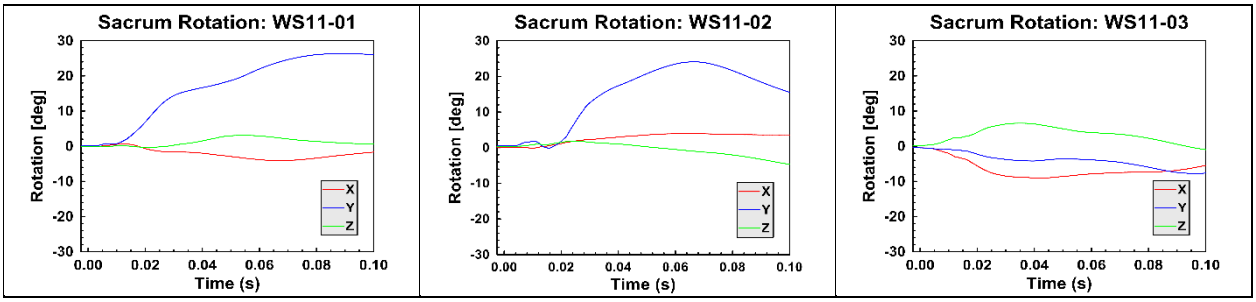

Figure 40. Pelvis (sacrum) rotation

3.2.5 Whole-Body Kinematics

Figures 41–43 provide X-Z (sagittal) and Y-Z (coronal) plane trajectories of markers attached to the boot, knee, shoulder, and head, as well as the frontal plane trajectories of the markers attached to the patella. The observed trajectories have similar characteristics to those from tests in similar postures with less severe input conditions, although the magnitude of the motions in the WS11 series tests are generally greater. All trajectories shown in Figures 41–43 are relative to the seat.

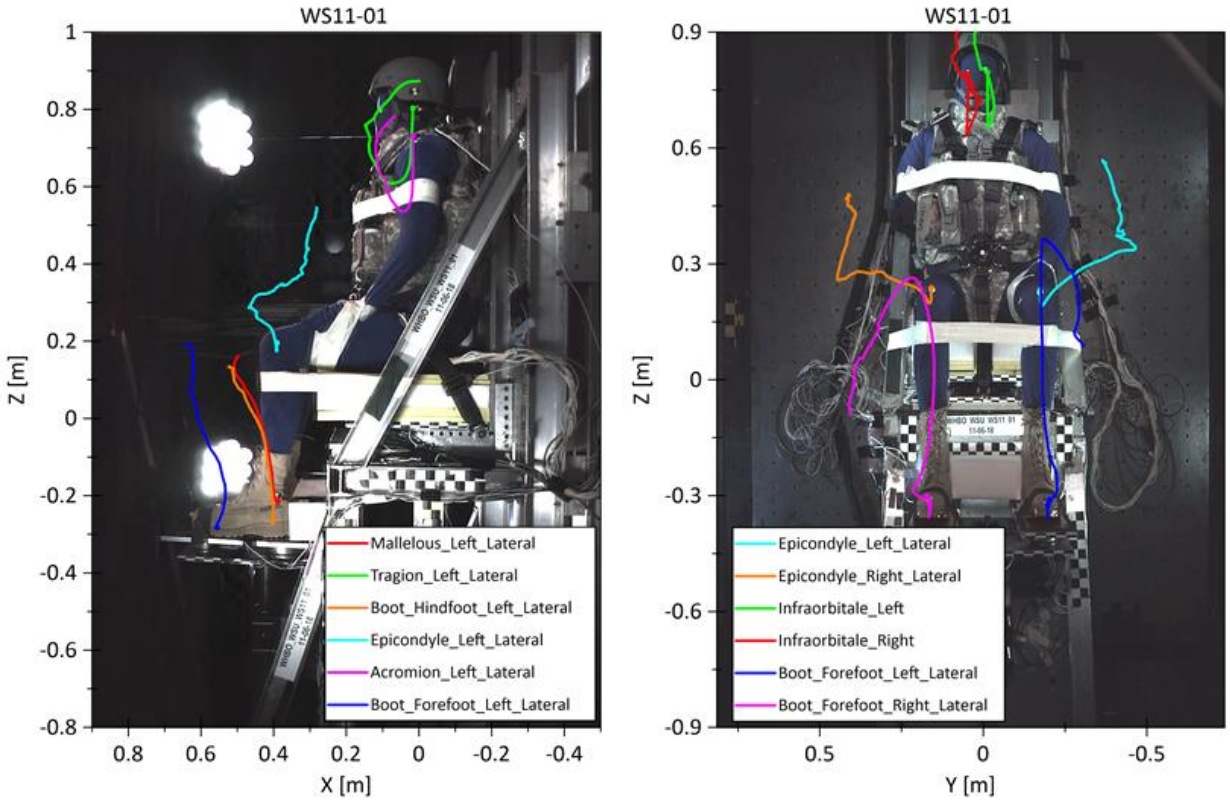

All motions are relative to a fixed point on the seat frame.

Figure 41. X-Z plane marker trajectories for knee, boot, shoulder, and head (left) and Y-Z marker trajectories for the knee, boot, and head (right) from test WS11-01 overlaid with image showing initial position of the PMHS

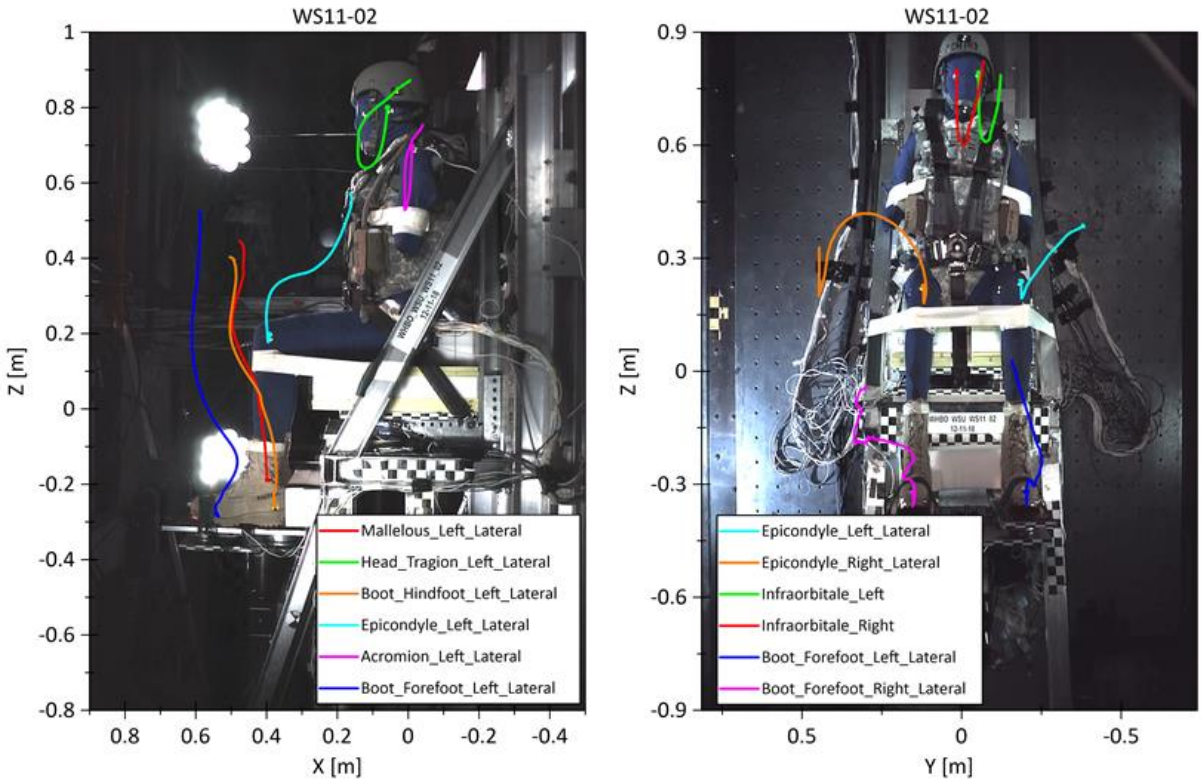

All motions are relative to a fixed point on the seat frame.

Figure 42. X-Z plane marker trajectories for knee, boot, shoulder, and head (left) and Y-Z marker trajectories for the knee, boot, and head (right) from test WS11-02 overlaid with image showing initial position of the PMHS

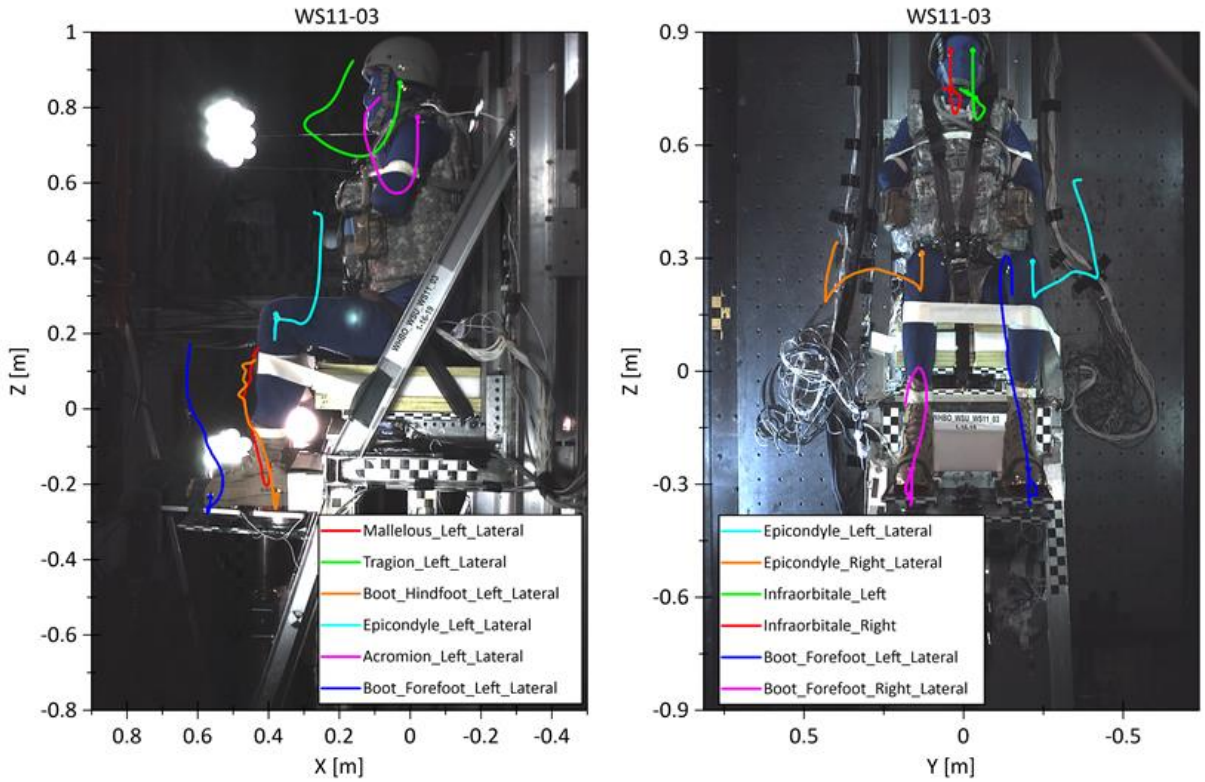

All motions are relative to a fixed point on the seat frame.

Figure 43. X-Z plane marker trajectories for knee, boot, shoulder, and head (left) and Y-Z marker trajectories for the knee, boot, and head (right) from test WS11-03 overlaid with image showing initial position of the PMHS

4. WS12 SERIES (UMTRI)

4.1 Methods

4.1.1 University of Michigan Transportation Institute (UMTRI) Test Fixture

The UMTRI test fixture is a steel vertical drop tower comprising a rigid seat with adjustable height and fore-aft displacement, and a decoupled footplate (Figure 44). The fixture is released from a specified height and accelerated by gravity onto aluminum honeycomb around the base of the fixture and elastomers beneath the footplate. The footplate was attached to the fixture using two nylon bolts designed to break away upon impact, which allowed the footplate to move freely relative to the fixture. The drop height, as well as the amount, type, and distribution of aluminum honeycomb and elastomers, controlled the deceleration pulse magnitude and duration at the seat and footplate.

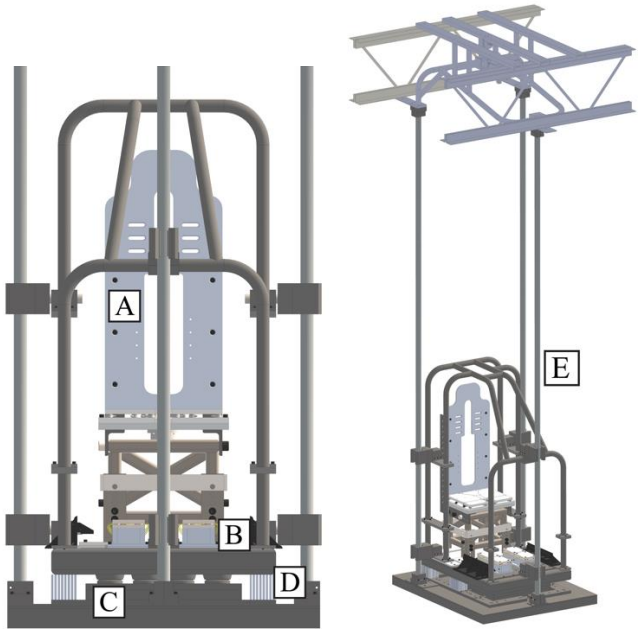

A) Seat system
B) Decoupled foot platform
C) Linear elastomers
D) Aluminum honeycomb
E) Isometric view of primary platform

Figure 44. UMTRI test rig

4.1.2 Instrumentation Locations and Transducer Types

The test fixture contained an array of uniaxial load cells and accelerometers at the occupant-seat and occupant-footplate interfaces (Figure 45). A novel method of incorporating multiple piezoelectric load cells to support individual load sensing plates that may then be summed to evaluate the total load applied to a given plate was used, as described in Rupp et al. (2016). The seat load cell configuration included multiple load sensing plates at the sacrum, left and right ischium, and left and right thigh, allowing for an analysis of seat load distribution between the components, as well as the ability to sum the individual loads to calculate a total seat force (Rupp

et al., 2016). Footplate load cells and accelerometers measured the total floor force and footplate acceleration. Force data were inertially compensated using acceleration data and the mass of the load cell plate (Table 28). Fixture velocities were calculated by integrating acceleration signals.

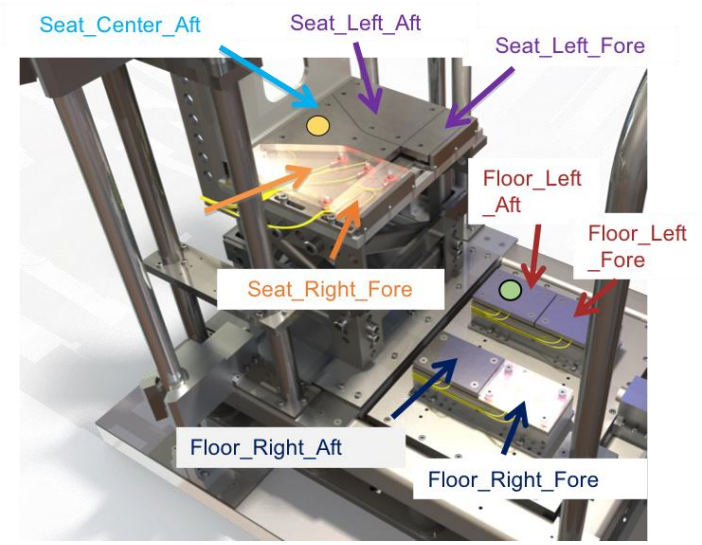

Figure 45. Rig instrumentation locations

Table 28. Masses and Instrumentation Used for Mass Compensation

Location	Plate Mass (kg)	Load Cell Names	Load Cell Model	Accelerometer Name	Accelerometer Model
Left heel	3.36	Floor_Left_Aft_1-4	PCB_202B	Floor_Left_Aft	Endevco_72701A-20k
Right heel	3.36	Floor_Right_Aft_1-4	PCB_202B	Floor_Right_Aft	Endevco_72701A-20k
Left forefoot	1.2	Floor_Left_Fore_1-4	PCB_202B	Floor_Left_Fore	Endevco_7264D-2000
Right forefoot	1.2	Floor_Right_Fore_1-4	PCB_202B	Floor_Right_Fore	Endevco_7264D-2000
Sacrum	3.3	Seatpan_Center_Aft_1-4	PCB_203B	Seatpan_Center_Aft	Endevco_72701A-20k
Left IT	8.0	Seatpan_Left_Aft_1-6	PCB_203B	Seatpan_Left_Aft	Endevco_72701A-20k
Right IT	8.0	Seatpan_Right_Aft_1-6	PCB_203B	Seatpan_Right_Aft	Endevco_72701A-20k
Left thigh	3.3	Seatpan_Left_Fore_1-4	PCB_203B	Seatpan_Left_Fore	Endevco_7264D-2000
Right thigh	3.3	Seatpan_Right_Fore_1-4	PCB_203B	Seatpan_Right_Fore	Endevco_7264D-2000

PMHS instrumentation included 6DOF sensors (6DX, Diversified Technical Systems, Inc.), uniaxial accelerometers (7270A, Endevco), acoustic emission sensors (Nano 30, Physical Acoustics), and uniaxial strain gauges (CEA-06-250UN-350, Mirco-Measurements). The types and locations of these sensors, and the orientations of strain gauges are provided in Table 29 and Figure 46. The 6DX sensors measured X-, Y-, and Z-accelerations (A_x, A_y, and A_z, respectively) and X-, Y-, and Z-angular rates (AR_x, AR_y, and AR_z, respectively). The 6DX sensors were rigidly mounted to the skull (3 cm superior to the Frankfort Plane at the level of the tragion) using Helicoil inserts and screws, thoracic vertebrae (T1, T5, T8, and T12), sacrum (S1-S3

level), left and right iliac wings, superior pubic rami, distal and proximal femurs, and distal and proximal tibias. The distal femur and tibia 6DX sensors were located proximal to the most distal portion of the bone at a distance of 0.2–0.3 and 0.15–0.25 of the total femur and tibia lengths, respectively. The proximal femur and tibia 6DX sensors were located distal to the most proximal portion of the bone at a distance of 0.2–0.3 and 0.2–0.25 of the total femur and tibia lengths, respectively. 6DX sensors at the head, sternum, vertebral bodies, sacrum, and iliac wings were attached by rigid mounts installed in the bone via screws. 6DX sensors at the pubic symphysis, femur, and tibia were installed via hose clamps tightened around the bone. The 7270A accelerometers (that measure A_z) were installed with a gel glue on the medial surface of the left and right calcaneus and oriented parallel to the leg long axis. A CT scan was conducted after instrumentation but prior to testing to document sensor positions relative to the skeleton.

Table 29. Subject Instrumentation Locations

6DX	Strain Gage[a]	Acoustic Emission Sensor	7270A Accelerometer
Head	Left Rib 10	T4	Left Calcaneus
Sternum	Right Rib 10	T7	Right Calcaneus
Left Iliac Wing	Left ASIS	T11	
Right Iliac Wing	Right ASIS	L2	
Left Superior Pubic Ramus	Left Superior Pubic Ramus	L4	
Right Superior Pubic Ramus	Right Superior Pubic Ramus	Sacrum	
Left Proximal Femur	Left Proximal Femur	Left Iliac Wing	
Right Proximal Femur	Right Proximal Femur	Right Iliac Wing	
Left Distal Femur	Left Distal Femur	Left Calcaneus	
Right Distal Femur	Right Distal Femur	Right Calcaneus	
Left Proximal Tibia	Left Proximal Tibia		
Right Proximal Tibia	Right Proximal Tibia		
Left Distal Tibia	Left Distal Tibia		
Right Distal Tibia	Right Distal Tibia		
T1	Left Calcaneus		
T5	Right Calcaneus		
T8			
T12			
Sacrum (S1-S3)			

[a] Strain gauges were placed along the long axes of long bones, the circumferential direction of ribs, along the direction of the pelvic ring for the pubic ramus, along the direction of the iliac crest for the ASIS, and fore to aft for the calcaneus locations.

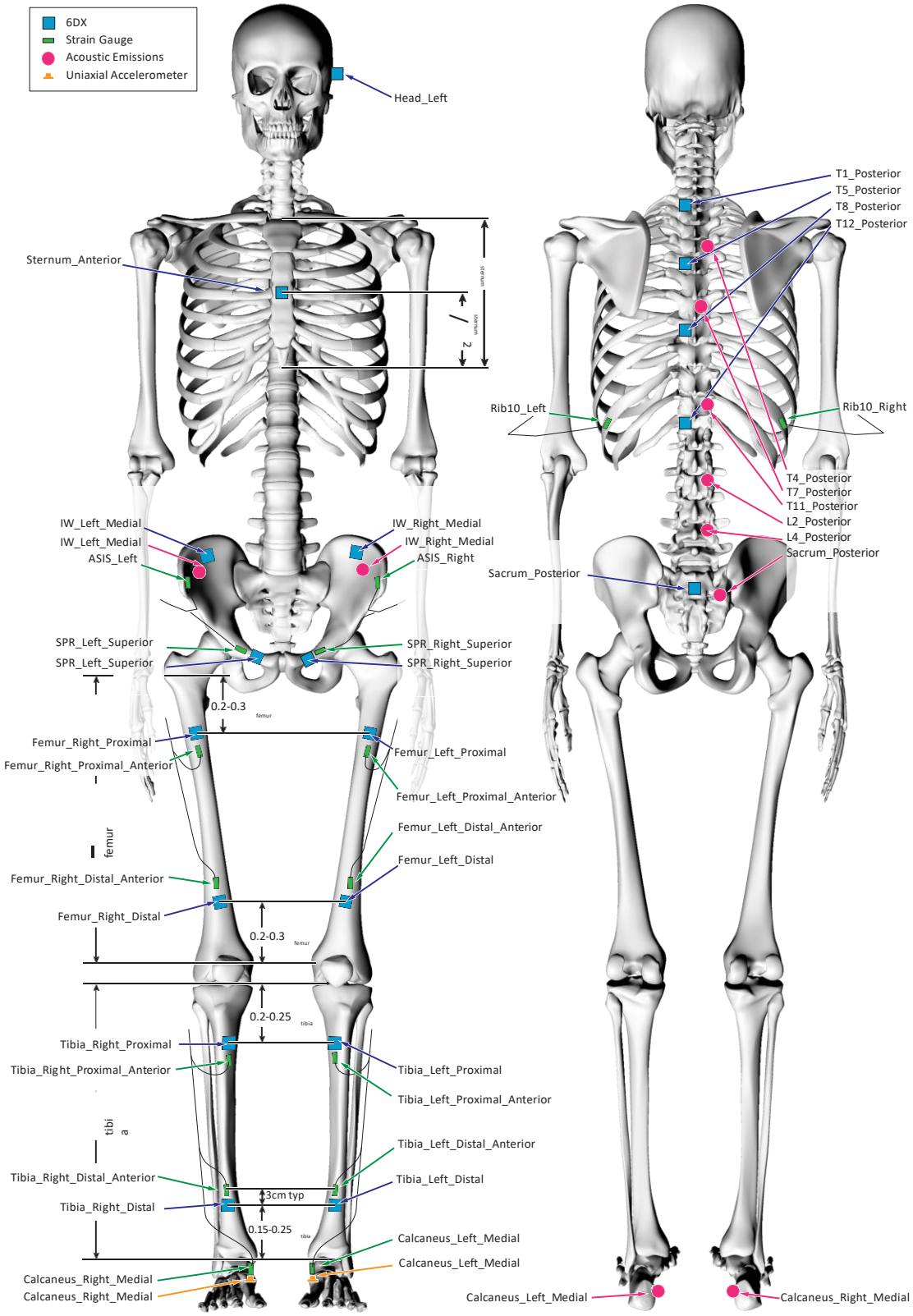

Figure 46. Subject instrumentation locations

4.1.3 Kinematic Analysis

Spherical markers (rigidly installed in bone) or quadrant marker stickers (adhered to the surface of clothing or PPE) were placed at various skeletal or surface landmarks for kinematic tracking. Tracked locations included the head (five spherical markers at various locations of the face), shoulders (spherical markers at left and right acromion), knees (spherical markers at left and right patella, quadrant markers at left and right lateral femoral condyle), and boots (left and right forefoot, left and right hindfoot, left and right lateral malleolus) (Tables 30 and 31). Various points on the fixture were tracked to define and translate the coordinate system as it moved through the camera frame (Table 32). Motion tracking and calibration were performed using motion analysis software (TEMA, Image Systems Motion Analysis).

Table 30. Rigidly Installed Kinematic Marker Locations

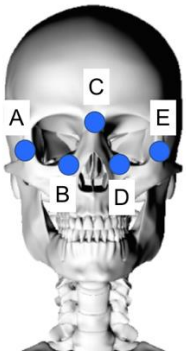	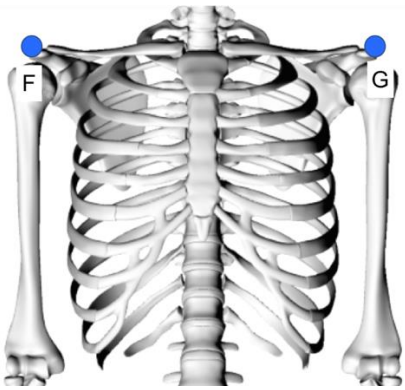	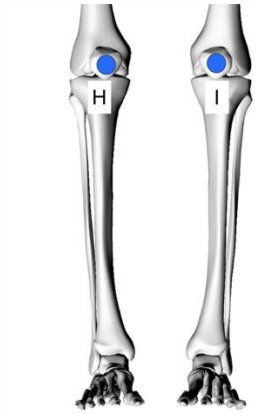
A) Head_Anterior_Lateral_Right B) Head_Anterior_Medial_Right C) Head_Anterior_Medial D) Head_Anterior_Medial_Left E) Head_Anterior_Lateral_Left	F) Shoulder_Right_Lateral G) Shoulder_Left_Lateral	H) Knee_Right_Anterior I) Knee_Left_Anterior

Table 31. Kinematic Surface Marker Locations

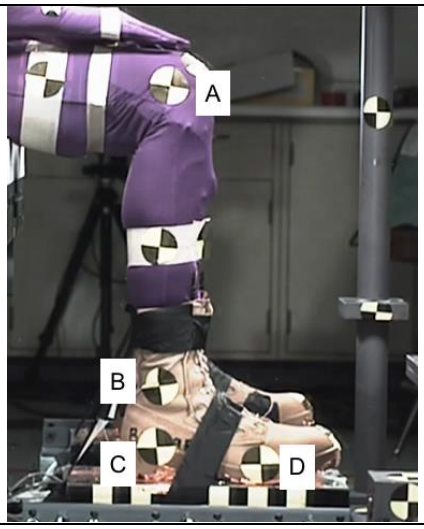

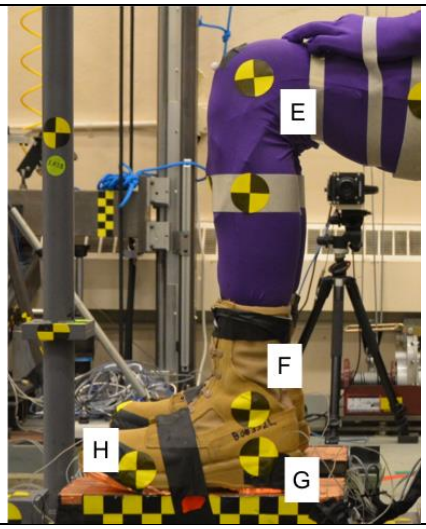

A) Knee_Right_Lateral B) Boot_Right_Lateral_Superior C) Boot_Right_Lateral_Posterior D) Boot_Right_Lateral_Anterior	E) Knee_Left_Lateral F) Boot_Left_Lateral_Superior G) Boot_Left_Lateral_Posterior H) Boot_Left_Lateral_Anterior

Table 32. Rig Kinematic Marker Locations

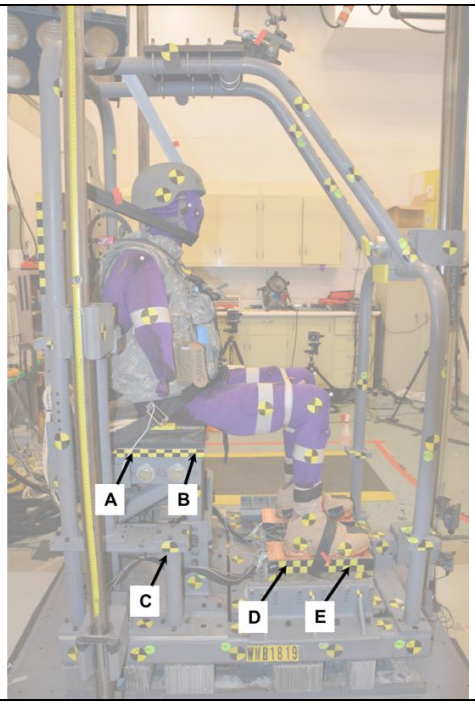

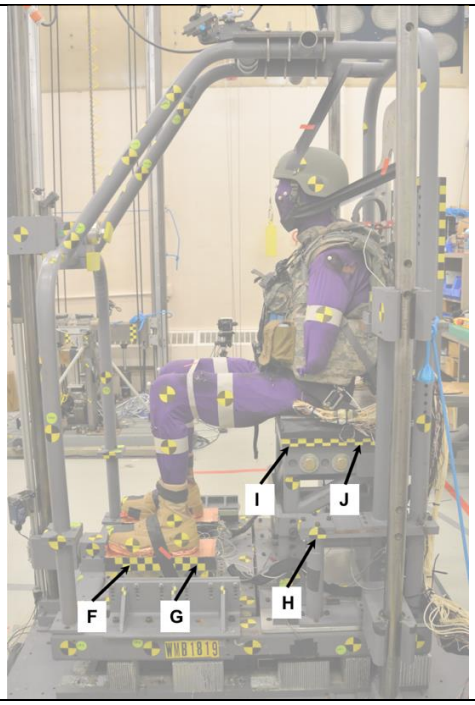

A) Seatpan_Right_Aft [a] B) Seatpan_Right_Fore C) Rig_Right_Aft D) Floor_Right_Aft E) Floor_Right_Fore [a]	F) Floor_Left_Fore [a] G) Floor_Left_Aft H) Rig_Left_Aft I) Seatpan_Left_Fore [a] J) Seatpan_Left_Aft

[a] Exact locations of seatpan aft and floor fore may vary between tests based on visibility from camera views.

The location of the head CG was calculated at each point in time using the skeletal surface markers shown in Table 30 based on the head CG location relative to these markers calculated using CT data with the procedure defined in the W0084 technical guidance document (Bass et al., 2016). For this calculation, it was assumed that head CG does not change over the course of the event. Foot angle was also calculated using the landmarks listed in Table 33.

Table 33. Calculated Kinematic Descriptions

Location	Description
Head_Center	Calculated position using a rigid body transformation from rigidly installed kinematic markers on head (Table 3) and head center of gravity calculated from CT scan
Boot_Knee_Right	Included foot angle between Knee_Right_Lateral to Boot_Right_Lateral_Superior and Boot_Right_Lateral_Posterior to Boot_Right_Lateral_Anterior
Boot_Knee_Left	Included foot angle between Knee_Left_Lateral to Boot_Left_Lateral_Superior and Boot_Left_Lateral_Posterior to Boot_Left_Lateral_Anterior

4.1.4 Subject Characteristics

Table 34 provides the characteristics of the three subjects tested by UMTRI for the WS12 series. All subjects were within predefined acceptable ranges, with the exception of the L1–L4 T-score for the subject used in test WS12-01. This subject had a DEXA T-score below –1.0 but a quantitative computed tomography (QCT) BMD-based T-score of –1.0. Because QCT-based T-scores are more strongly related to tolerance than DEXA-based T-scores and because this subject was younger (age 23 at the time of death), the WEO approved an exception to the inclusion criteria. Appendix C provides standard subject anthropometry measured in accordance to reference document W0080 (Bass et al., 2013).

Table 34. Subject Characteristics with Inclusion Criteria

Test Series ID	Subject	Age (yrs)	Gender	Height (cm)	Weight (kg)	BMI	T-Score (L1–L4)
WS12-01	35249	23	M	172	72	24.5	-1.0[a]
WS12-02	L162663	75	M	178.8	72.6	22.7	0.2
WS12-03	L170249	79	M	171.6	69.4	22.7	0.2
Acceptance Criteria	…	18 - 80	M	165 - 186	64 - 106	18 - 35	-1.0 - +2.5

[a] 35249 L1–L5 T-score performed with QCT; approved for use by the WEO on 25 May 2017.

4.1.5 Subject Positioning

Subject positioning was based on the relative locations of skeletal surface landmarks. Figure 47 shows the target postures and highlights important joint angles and relative positions of landmarks. Landmarks were identified by palpating to locate the skeletal landmark of interest. Landmarks on the pelvis were determined through the palpation of the pubic symphysis and left and right ASIS, which were accessible by reaching under the IOTV. Pelvis angle was defined as the angle of the line formed by the mid-ASIS and pubic symphysis landmarks compared with vertical. All landmark locations were determined by the same staff member.

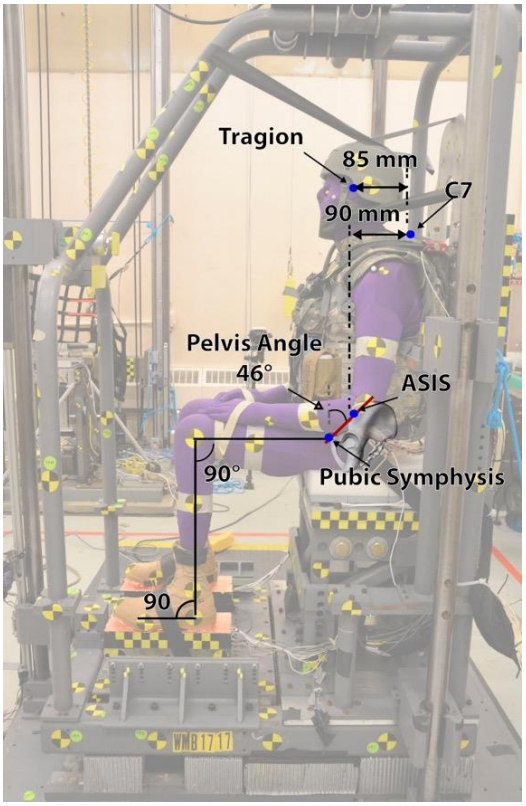

Figure 47. Target position

A 3-D coordinate measurement device (FARO arm) was used to measure the position of the PMHS prior to each test. During the positioning process, 3-D locations were recorded at various landmarks and checked against target relative orientations. When measurements fell outside of tolerance, the PMHS was adjusted accordingly and remeasured until within tolerance or as close to the target range as PMHS anatomy permitted. Gaffer's tape was used to secure each PMHS head in the proper position by running a strip or multiple strips of tape from the PMHS head and/or helmet to a rigid location on the test fixture. Tape mounting locations varied with each test, but tape was typically affixed to the PMHS chin, nose, or helmet (see Table 5, Knee motion transformed using coordinate measurement data from femur motion, for examples). For each PMHS, the fewest strips of tape that were sufficient to secure the head in the proper position

were used. Tape was precut approximately 90% across immediately prior to each test such that the tape severed during the loading event. In all tests, all strips of tape were completely severed at the beginning of the loading event. Therefore, PMHS movement of the head and feet did not appear to be influenced by the tape placement. Final coordinates were documented immediately prior to each test. A similar taping method was used to secure the feet prior to impact.

Target and actual postures for all tests are shown in Table 35. Target postures were based on the postures assumed by midsize male Soldiers seated in a military vehicle seat with a vertical back and horizontal seat cushion angles based upon Reed and Ebert (2013). Positioning was performed following the procedure described by Rupp and Reed (2015). When positioning subjects, the highest priority was given to matching pelvis angle, head position and angle, and foot and knee angles. Lower priority was given to acromion position, as some subjects were missing forearms, preventing the use of the arm to control shoulder position.

Table 35. Subject Positioning

Measurement	Description	Target Range		WS12-01	WS12-02	WS12-03
		Low	High			
Pelvis Angle	Angle of line from mid-ASIS to pubic symphysis in the XZ-plane with respect to vertical	41°	51°	42.7°	44.1°	41.6°
ASIS Fore-Aft Distance	A-P difference of left and right ASIS landmarks	-10 mm	10 mm	-2.8	-0.1	5.3
ASIS Vertical Distance	Vertical difference of left and right ASIS landmarks	-10 mm	10 mm	0.2	-2.19	2.6
Mid-ASIS Aft of Cervicale	Fore-aft distance from average of left and right ASIS landmarks to most posterior aspect of C7	-80 mm	-100 mm	-83.3	-87.6	-97.1
Acromion Fore-Aft Difference	Fore-aft difference between left and right acromion landmarks	-20 mm	20 mm	-1.1	30.8[a]	10.8
Acromion Vertical Distance	Vertical difference between left and right acromion landmarks	-20 mm	20 mm	-9.1	49.6[a]	0.8
Cervicale Aft of Tragion	Fore-aft distance from average of left and right tragion to most posterior aspect of C7	75 mm	95 mm	75.4	76.0	75.3
Infraorbitale Superior of Tragion	Vertical distance from mid-infraorbitale to mid-tragion	-5 mm	-15 mm	-11.5	-11.8	-9.8
Boot Heel Separation	Distance between centers of boot heels	285 mm	305 mm	292.0	289.3	295.6

[a] Due to subject geometry and missing forearms, target positioning for acromion landmarks could not be achieved for WS12-02.

4.1.6 PPE, Boot, and Belt Fitting Procedures

PPE, including an ACH, IOTV, and Belleville 390 DES men's hot weather desert tan combat boots (Belleville Boot Company, Belleville, IL) were fitted to the PMHS in accordance with reference documents W0058 (Helmet Fitting Procedures), W0059 (IOTV Fitting Procedures), and W0060 (Boot Fitting Procedures), respectively (WIAMan Biomechanics Team, 2013a, 2013b, 2013c). The routing and fitting of the five-point seatbelt restraint harness were performed in accordance to reference document W0070 (Belt Fitting Procedures) (WIAMan Biomechanics Team, 2013d).

4.1.7 Data Processing

Similar to BRC development, accelerometers and individual seat/floor load cells were filtered using a low-pass fourth-order digital phaseless Butterworth filter using a cutoff frequency of 3 kHz. Angular rate data were filtered using a cutoff frequency of 1650 Hz. As described in Section 4.1.2, individual uniaxial piezoelectric load cells attached to a given load sensing plate (illustrated in Figure 45) are summed to calculate hindfoot and forefoot loads, as well as loads applied to different parts of the pelvis and thighs. The high-frequency response and lack of damping in these load cells, coupled with the vibration produced by crushing aluminum honeycomb to generate the seat/floor pulses, result in noise in the combined load cell data below 3 kHz; therefore, specific methods developed for this device are used where both the summed loads and the accelerometer used to inertially compensate these loads are filtered using a cutoff frequency of 1 kHz when combined. This method was confirmed during the development of this load sensing system. DTS, 6DX transducer measurements were transformed to standardized locations relative to skeletal anatomic landmarks using the procedure developed by SCoTT reported by Slykhouse et al. (2019). Seat and floor velocities were calculated by integrating Z-axis accelerometers located under the center of the seat and under the center of the left and right feet.

Times to peak velocity for the floor and seat were calculated using the method defined by Spink (2014). This method involves a baseline shift and integration of the acceleration time history, the peak (largest negative) velocity within a time frame of interest, and identification of all local minima less than 90% of the absolute peak. The local minimum just prior to the absolute peak is selected as the new peak velocity, and points corresponding to 5%, 20%, and 95% of the final peak velocity are determined. If the velocity history exhibits a monotonic fall between 5% and 20%, the velocity slope is calculated between the points at 5% and 95% of the peak velocity. If the velocity history is not monotonic between 5% and 20%, the data point immediately following the last positive derivative in the window is identified and used to replace zero as the baseline for the 5% calculation. The start and end times are determined by calculating the times at which the equation that defines the velocity slope are equal to zero and peak velocity, respectively. The time to peak is the difference between the calculated ending and starting times.

4.1.8 Injury Assessment and Injury Timing Analysis

Acceleration, angular rate, strain, and acoustic emission data were all viewed qualitatively to provide an estimate of injury timing for each test. These estimates are subject to error, as signals in the region of injury often contain more than one event, which could be interpreted as the time of injury. In general, the timing of fracture was identified as the time following an acoustic burst where there is a corresponding spike or change in direction of an acceleration pulse. Approximate allowances were made for the time for sound to transmit between the location of fracture and the locations of acoustic emission sensor attachment. However, for situations where fracture occurred at a location that was remote from an acoustic emission sensor or accelerometer, fracture timing was estimated over a window based on accelerometer responses. Figure 48 shows an illustrated example of how sacrum fracture timing was estimated based on the time of acoustic burst measured by a nearby mounted sensor and the measurements of a nearby mounted accelerometer.

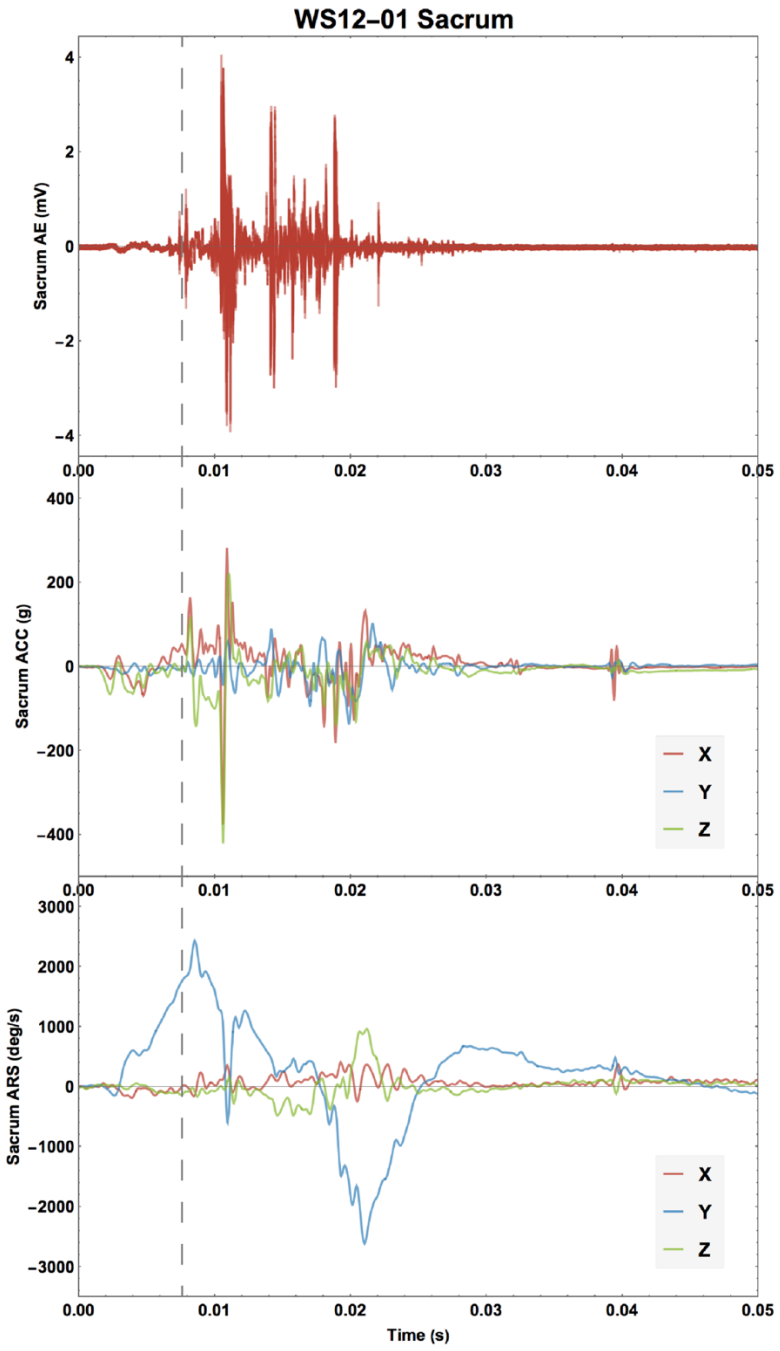

Figure 48. Example of plots used to determine injury timing for sacrum fracture in WS12-01: sacrum acoustic emission (top), sacrum acceleration (middle), and sacrum angular rate (bottom)

4.2 Results

4.2.1 Test Conditions

Table 36 compares floor and seat conditions for each of the three tests in the WS12 series to targets. Figure 49 shows the corresponding velocity histories. Floor velocities met the greater than 9 m/s target and ranged from 10.2 to 10.3 m/s with TTP that ranged from 2.6 to 2.7 ms for a target of 2.5 ms. Seat pulses ranged from 6.4 to 6.5 m/s target with TTP that ranged from 7.0 to 7.2 ms for a target velocity of 6.5 m/s with a 7.5-ms TTP. Figure 49 provides floor and seat velocity histories used to determine peak velocity and TTP.

Table 36. Test Conditions: Targeted and Achieved

Test Series ID	Floor Peak Velocity (m/s)	Floor TTP (ms)	Seat Peak Velocity (m/s)	Seat TTP (ms)	PPE	Posture	Seat Padding
WS12-01	10.2	2.7	6.5	7.2	MED	90/90/90	Rigid
WS12-02	10.3	2.6	6.5	7.1	MED	90/90/90	Rigid
WS12-03	10.3	2.7	6.4	7.0	MED	90/90/90	Rigid
Target	9+	2.5	6.5	7.5	MED	90/90/90	Rigid

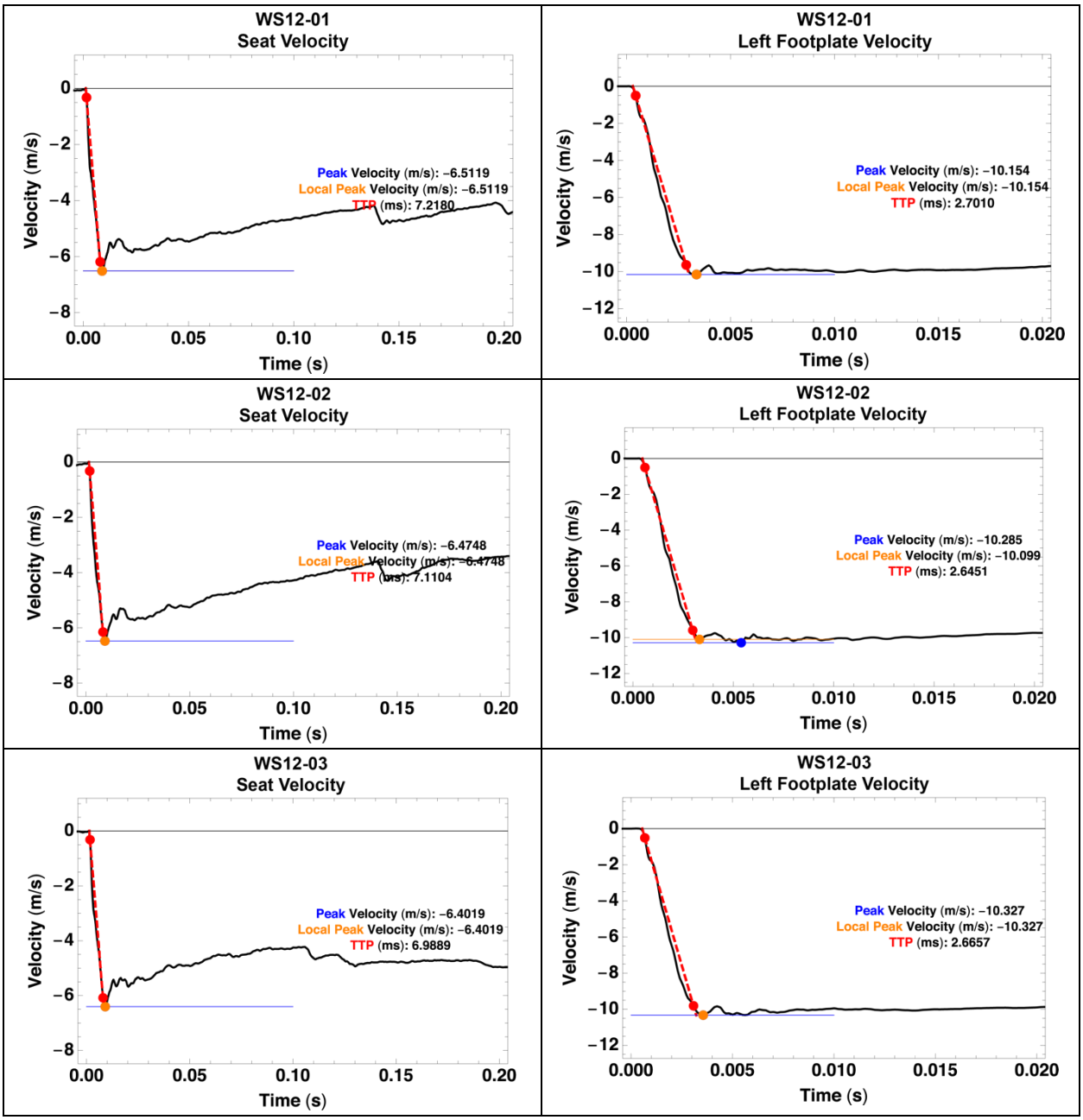

Figure 49. Seat and floor velocity time histories with peak and time to peak

4.2.2 Injury Outcomes

Tables 37–40 provide the injuries and associated AIS 2015 codes for the lower extremities, pelvis, lumbar spine, and thoracic spine, respectively. Of note, two calcaneus fractures, both Sanders Type III AC, were produced, as seen in Figure 50. Unstable pelvis fractures were produced in two tests (WS12-01 and -03). Illustrations of pelvis fracture patterns are shown in Figures 51–53. Images of all fractures and key images pre-/posttest radiology documenting

injury patters are provided in Appendix C. Injury patterns were generally consistent with those reported from combat theater events by Danelson et al. (2018).

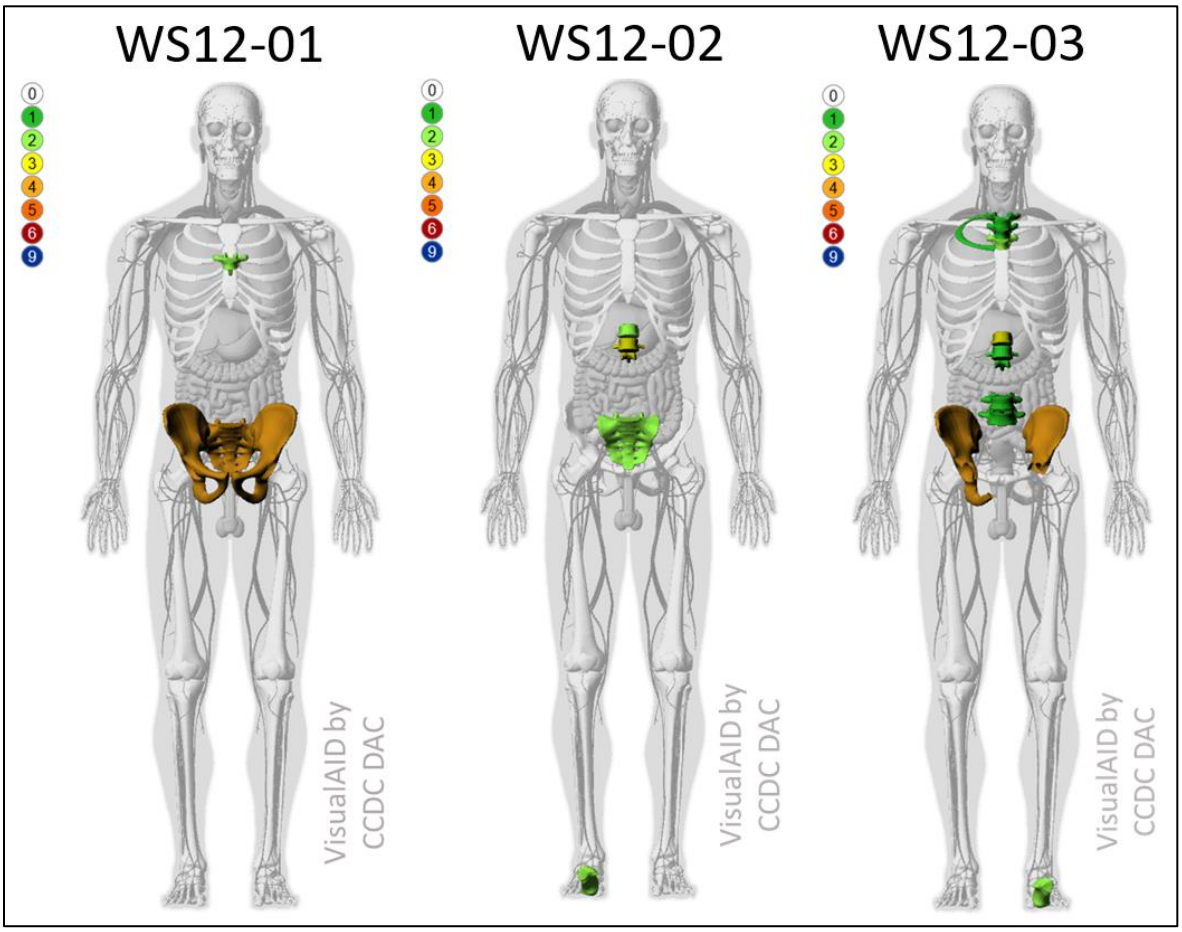

Figure 50. WS12 VisualAID injury visualization

Table 37. Lower Extremity Injuries

	AIS 2015	Description
WS12-01	No injuries	…
WS12-02	Right Calcaneus Fracture (AIS 857371.2 1000)	Unstable fracture of right calcaneus extending into >3 surfaces; Sanders Type III AC
WS12-03	Left Calcaneus Fracture (AIS 857371.2 2000)	Unstable fracture of left calcaneus extending into >3 surfaces; Sanders Type III AC

Table 38. Pelvis Injuries

	AIS 2015	Description
WS12-01	Pelvic ring fracture: bilateral posterior instability (AIS 856171.4 00NR, 10NN, 20NN)	Bilateral fracture of S1–S5 consistent with vertical shear
WS12-02	Pelvic ring stable (AIS 856151.2 00NR)	Bilateral S4/S5 fracture
WS12-03	Complete disruption of posterior arch and floor (AIS 856171.4 10NT, 20NT, 00NW, 10NV, 10NU, 00NR)	Left and right iliac wing fractures Right superior and inferior ramus fractures Right ischial tuberosity fracture Ischial spine fractures, bilateral, possibly avulsion Severe sacrum fracture at and below S3, unstable

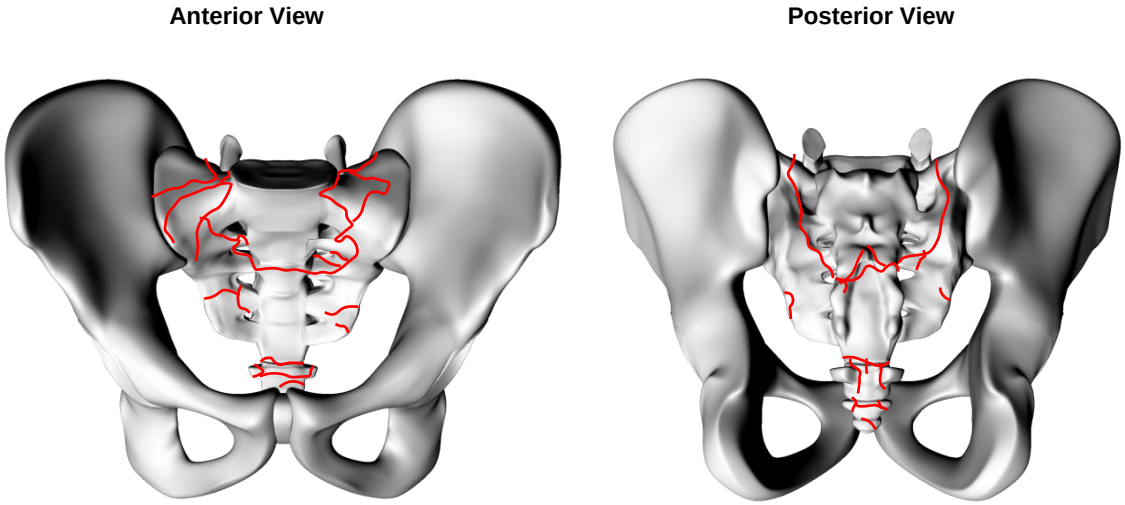

Figure 51. WS12-01 pelvis injury diagrams

Anterior View

Posterior View

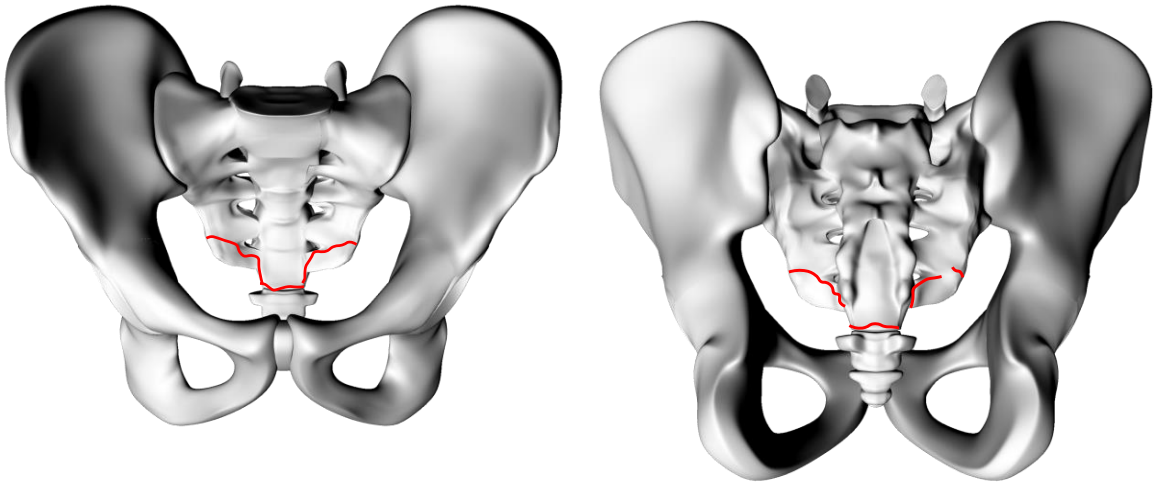

Figure 52. WS12-02 pelvis injury diagrams

Anterior View

Posterior View

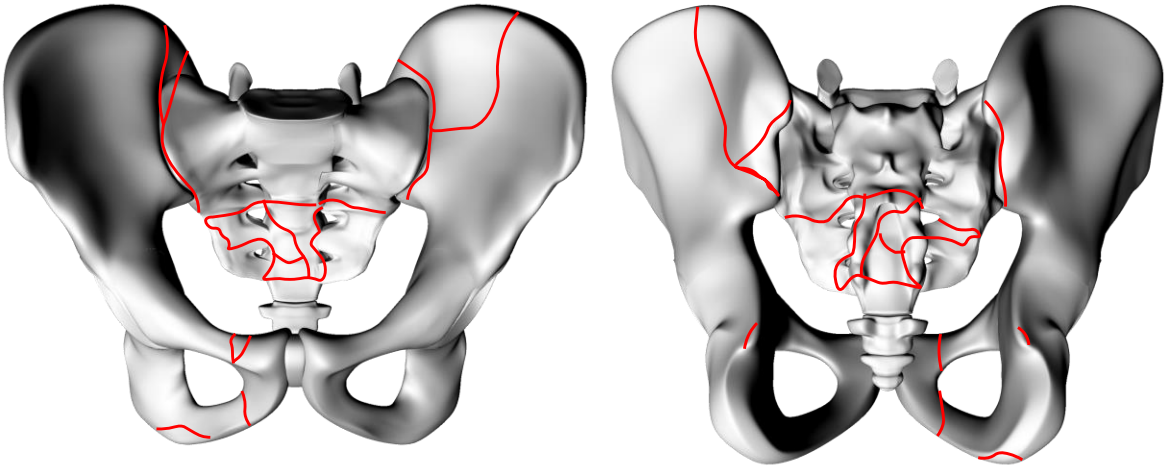

Figure 53. WS12-03 pelvis injury diagrams

Table 39. Lumbar Spine Injuries

	AIS 2015	Description
WS12-01	No Injuries	…
WS12-02	Major compression (>20% height loss) (AIS 650634.3 0020)	L1 vertebral body burst fracture
WS12-03	Transverse process fracture (AIS 650620.1 5020, AIS 650620.1 5023, AIS 650620.1 5024)	Bilateral transverse process fractures at L1, L4 and L5

Table 40. Thoracic Spine Injuries

	AIS 2015	Description
WS12-01	Spinous process fracture (AIS 650418.1 0013)	Avulsion fracture of T6 spinous process
WS12-02	Multiple fractures of same vertebra (AIS 650417.2 0019)	T12 lamina and posterior body fractures (Instrumentation installed at location believed to be a factor)
WS12-03	Vertebral body NFS (AIS 650430.2 0009)	T12 vertebral body burst fracture with posterior element destruction
	Spinous process fracture (AIS 650418.1 0009)	T2 spinous process fracture
	Spinous process fracture (AIS 650418.1 0010)	T3 spinous process fracture
	Multiple fractures of the same vertebra (AIS 650417.2 0011)	T4 lamina and body fracture (T4 partially fused to T3 at spinous process and lamina)

4.2.3 Injury Timing

Figure 54 illustrates fracture timing estimated from the analysis of AE, strain gauge, and ARS data relative to key fixture and PMHS responses. Of note, tests WS12-02 and WS12-03 sustained fractures at T12, where a mount was installed. Although these fracture patterns suggest that they were not caused by the mount, mount installation cannot be conclusively ruled out as a contributing factor.

Consistent with expectations, calcaneus fractures generally occurred prior to 5 ms and were closely aligned with the time of peak floor force. Pelvic ring fractures also generally occurred around the time of peak seat force; however, the isolated sacrum fracture in test WS12-02 occurred earlier in the event. Consistent with the results of previous tests, spinal body fractures tended to occur after the time of peak seat force, with thoracic spine fracture occurring after lumbar fractures.

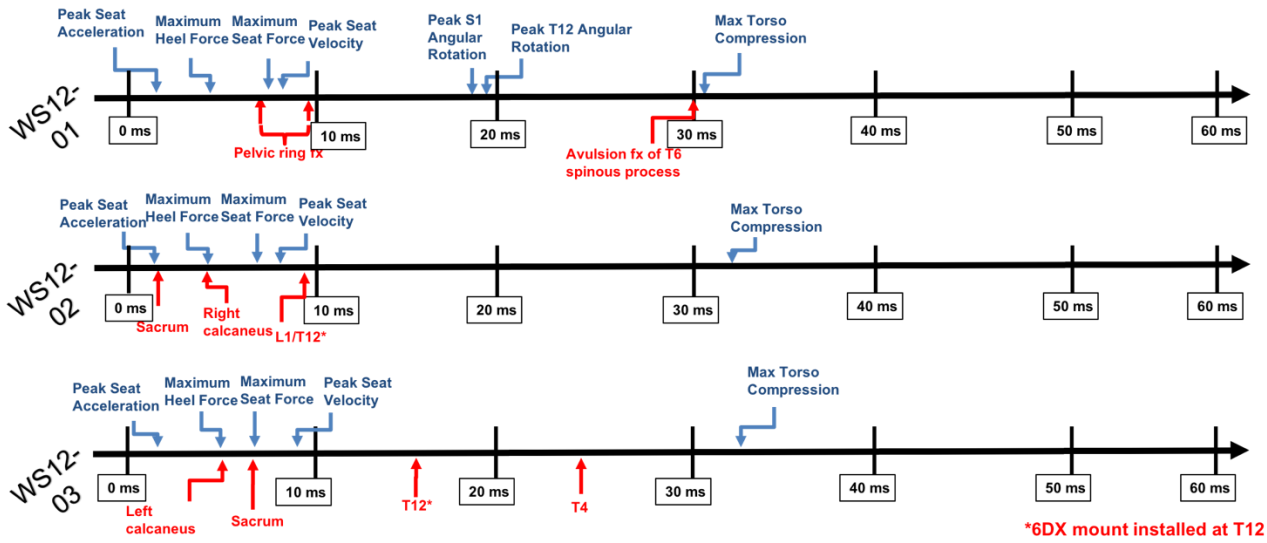

Figure 54. Injury timing relative to key events displayed as a timeline

4.2.4 Key Sensor Responses

Key sensor responses are shown in Figures 55–61. The drop in applied seat force under condition WS12, as shown in Figure 52, is likely associated with the initiation of pelvis fracture. Similarly spikes in sacrum acceleration responses and variability in pelvis rotations across tests are associated with the unstable pelvic ring fractures in WS12-01 and WS12-03.

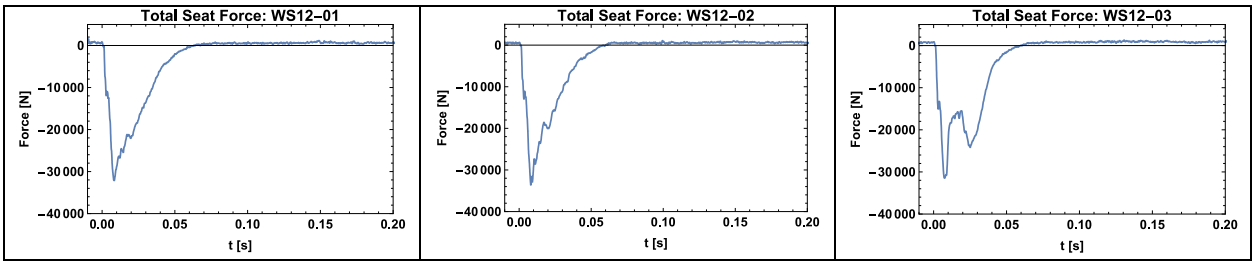

Figure 55. Seat force responses

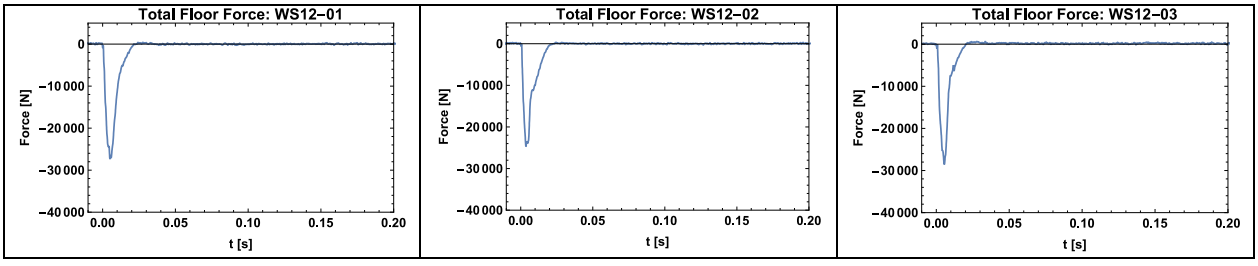

Figure 56. Floor force responses (sum of heel and forefoot loads)

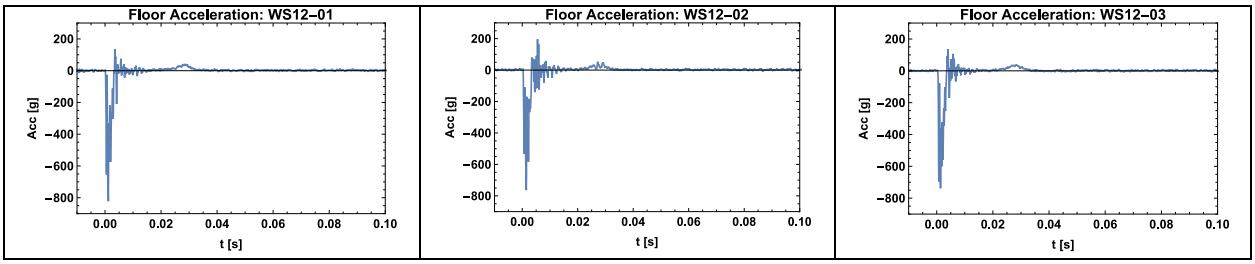

Figure 57. Floor vertical acceleration measurements (from heel plate accelerometer)

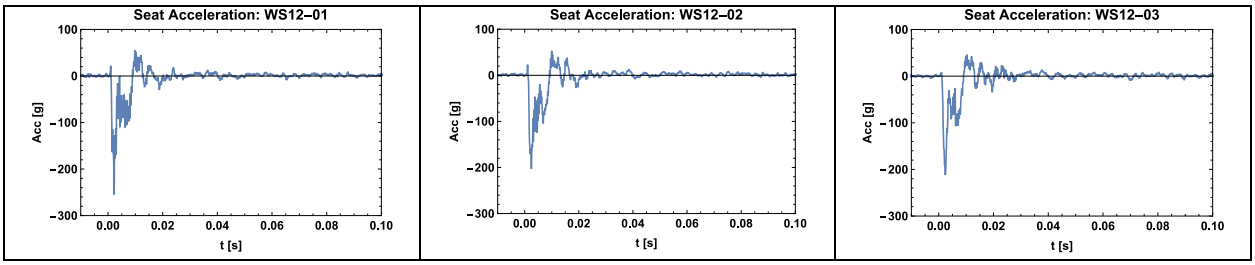

Figure 58. Seat vertical acceleration measurements

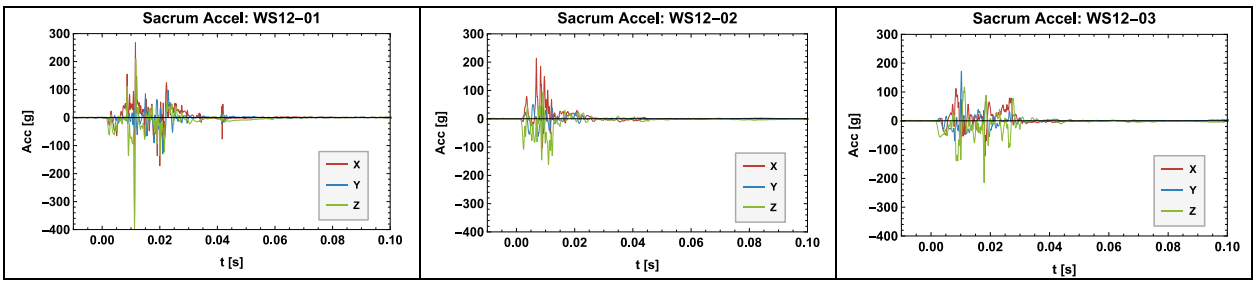

Figure 59. Sacrum acceleration measurements

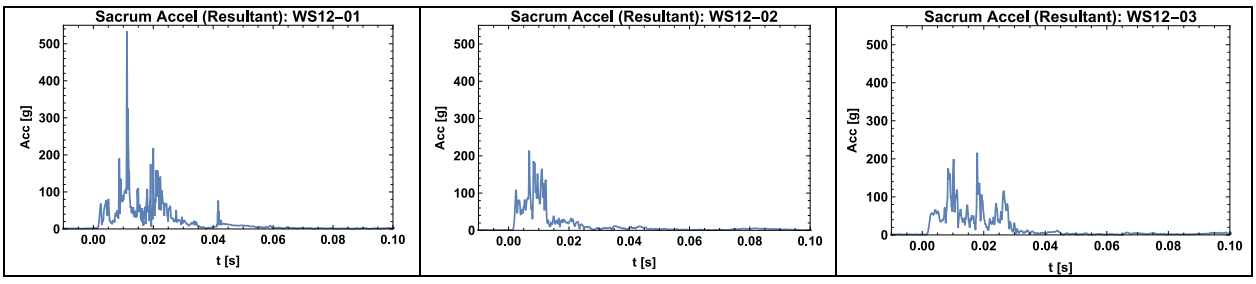

Figure 60. Resultant sacrum acceleration measurements

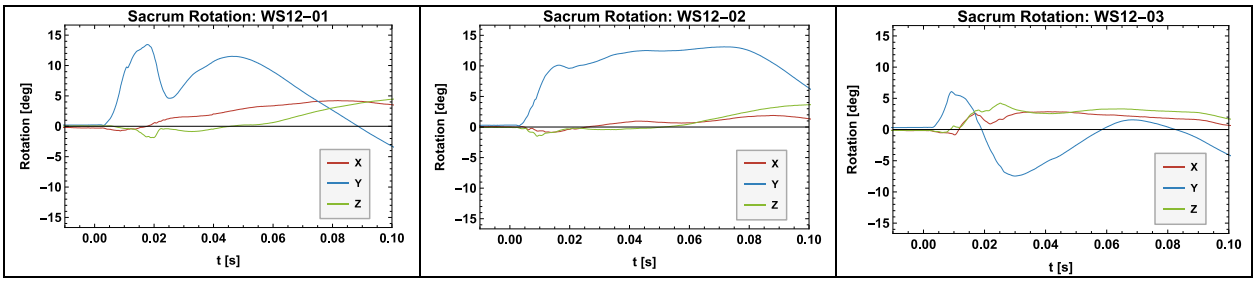

Figure 61. Pelvis (sacrum) rotation

4.2.5 Whole-Body Kinematics

Figures 62–64 provide X-Z (sagittal) and Y-Z (coronal) plane trajectories of markers attached to the knee, boot, shoulder, and head, as well as the frontal plane trajectories of the marker attached to the anterior knee. The observed trajectories have similar characteristics to those from tests in similar postures with less severe input conditions, although the magnitude of the motions in the WS12 series tests is much greater. All trajectories shown in Figures 62–64 are relative to the seat, so none of these reflect seat motion.

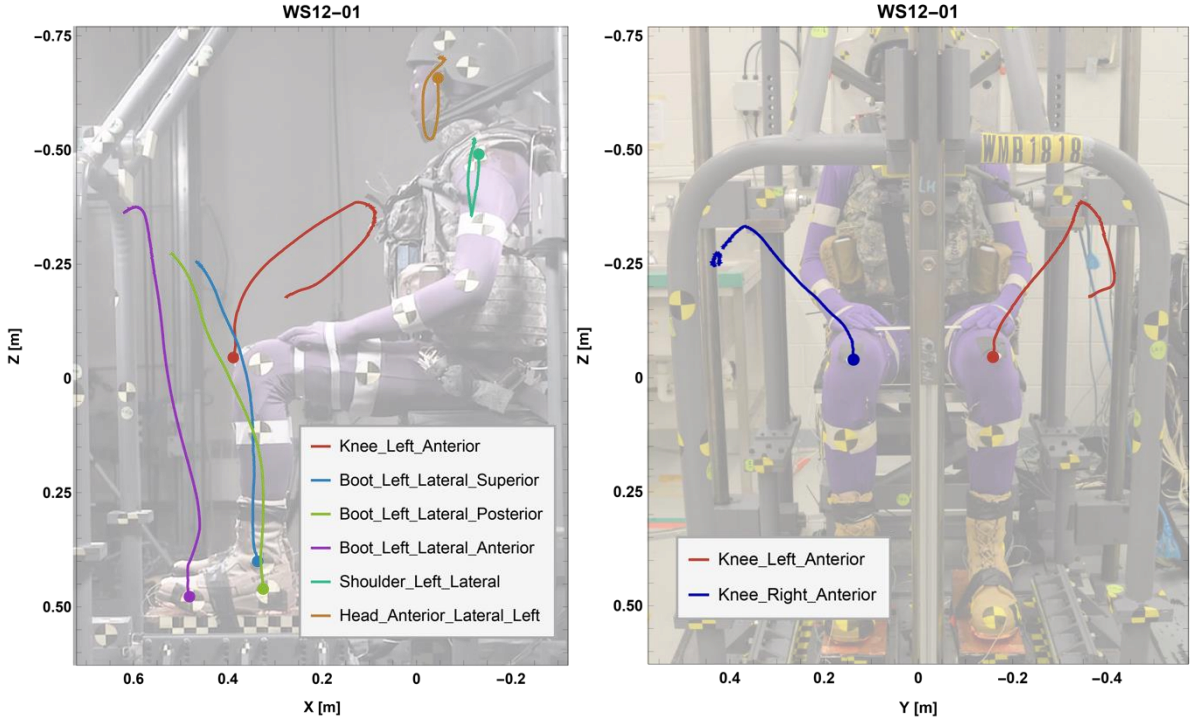

All motions are relative to a fixed point on the seat frame.

Figure 62. X-Z plane marker trajectories for knee, boot, shoulder, and head (left) and Y-Z marker trajectories for the anterior knee (right) from test WS12-01 overlaid with image showing initial position of the PMHS

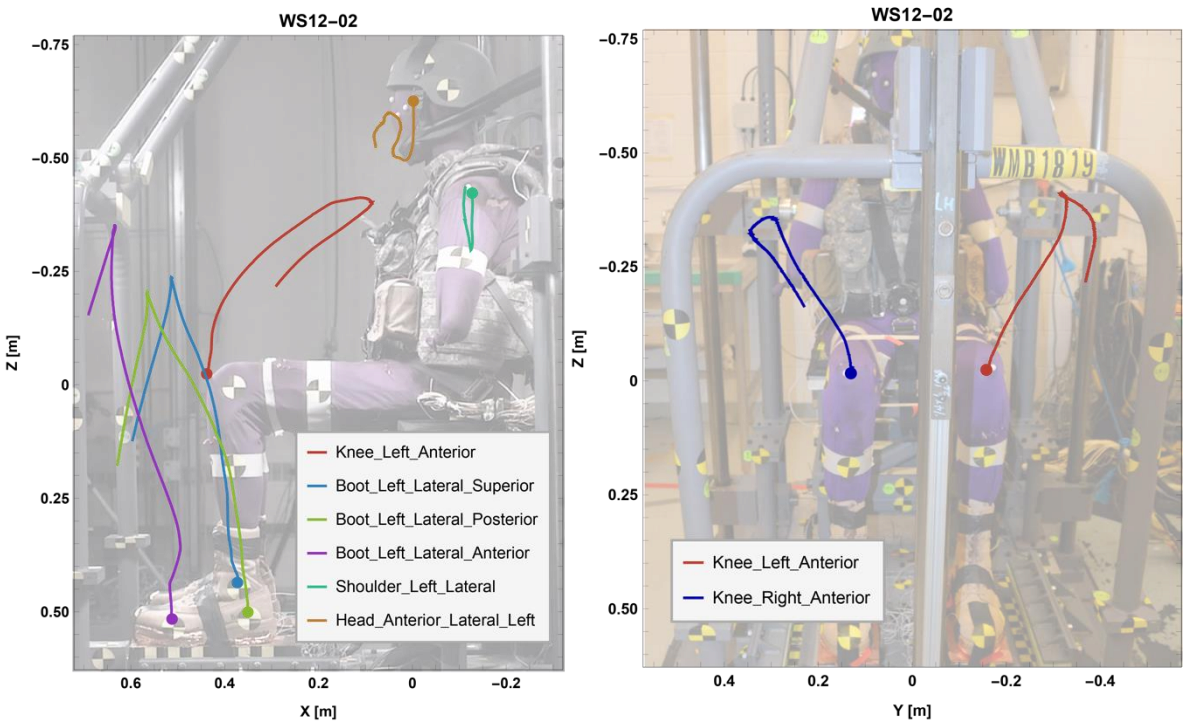

All motions are relative to a fixed point on the seat frame.

Figure 63. X-Z plane marker trajectories for knee, boot, shoulder, and head (left) and Y-Z marker trajectories for the anterior knee (right) from test WS12-02 overlaid with image showing initial position of the PMHS

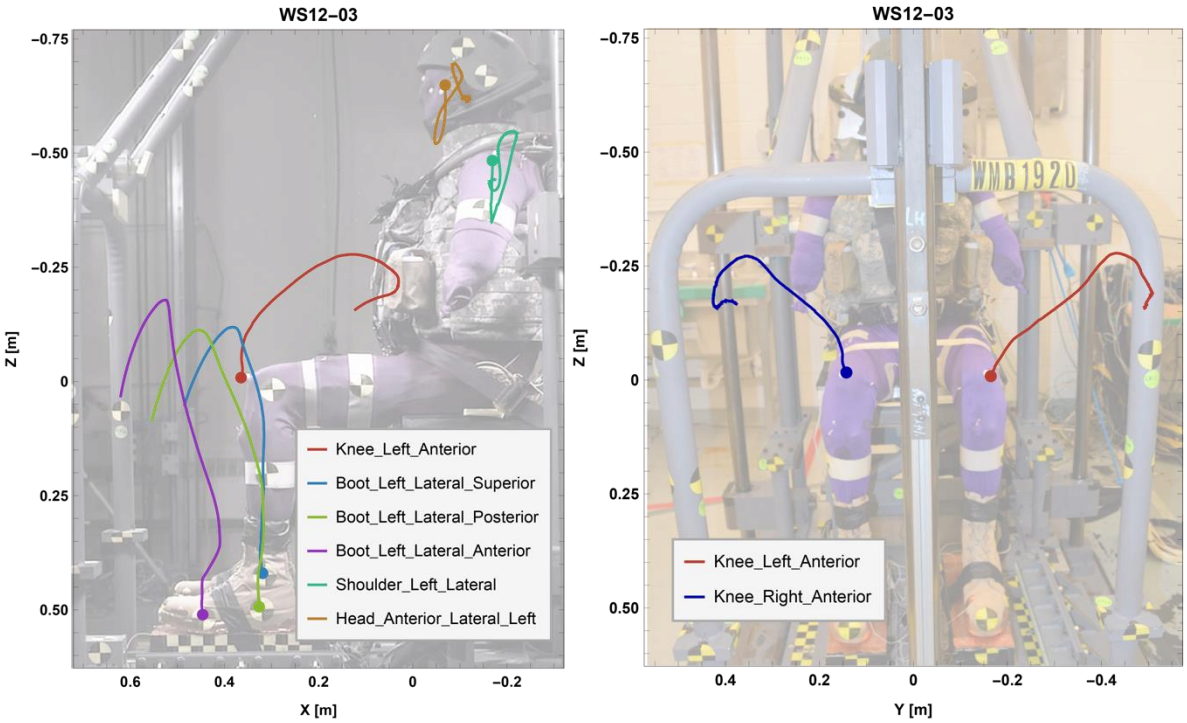

All motions are relative to a fixed point on the seat frame.

Figure 64. X-Z plane marker trajectories for knee, boot, shoulder, and head (left) and Y-Z marker trajectories for the anterior knee (right) from test WS12-03 overlaid with image showing initial position of the PMHS

5. DISCUSSION AND CONCLUSIONS

Three series of whole-body tests were completed using input conditions that targeted higher-severity portions of the full range of UBB relevant conditions than had been previously tested. These conditions were selected to represent input conditions of higher-severity tests that would likely result in multiple fractures to the body, including lumbar spine, pelvic ring, leg, and foot fractures. As shown in Figure 65, of the additional nine tests, four pelvic ring fractures, eight foot/ankle fractures, and one femur fracture were generated.

For the tests to be used in the validation and verification of injury prediction metrics, some criteria must be satisfied. Each test must achieve the prescribed test input conditions in terms of peak velocity and TTP of the seat and floor. Also, each test must identify and document injury outcomes of the experiments. On this basis, eight of the nine tests described in this report produced data that may be used for the validation and verification of injury prediction metrics. Future work may consider repeating an additional test in the WS11 condition to replace the single test that did not achieve the desired input conditions (WS11-03).

This report focuses only on documenting the whole-body PMHS tests results. Further analyses of test data are planned to determine if there is an association between injury patterns and test characteristics other than higher-severity input conditions increasing the likelihood of pelvis and foot/ankle fractures. IARC assessment is being performed in an independent Army effort. Match-paired WIAMan ATD tests for the conditions used in the tests described in this report will also be reported separately.

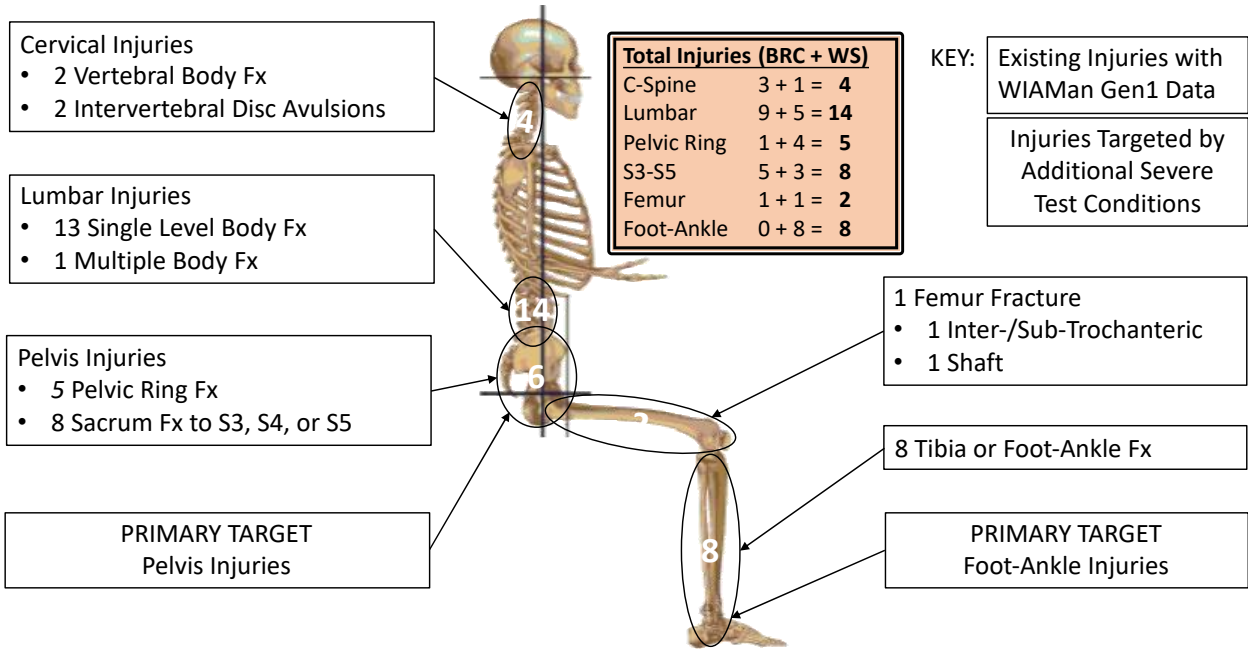

Figure 65. Distribution of injuries following WS10, WS11, and WS12 test series

6. REFERENCES AND DOCUMENTS

Bass, C. R., Danelson, K., Agnew, A., Gayzik, F. S., Rupp. J. D., Stitzel, J., Yoganandan, N., & Voo, L. (2013). *W0080: minimum pretest anthropometry requirements for scaling*.

Bass, C. R., Agnew, A., Gayzik, F. S., Rupp, J. D., Stitzel, J., Yoganandan, N., Marcus, I., & Voo, L. (2016). *W0084 PMHS scaling methods for biofidelity response corridors*.

Danelson, K., Watkins, L., Hendricks, J., Frounfelker, WIAMan Case Review Team, Pizzolato-Heine, K., Valentine, R., Loftis, K. (2018, November). Analysis of the frequency and mechanism of injury to warfighters in the under-body blast environment. *Stapp Car Crash J. 62*:489–513.

Gayzik, F. S., Pintar, F. A., Baker, A., Bass, C. R., Bannerjee, A., et al. (2017). *W0063: guidance document for HIPC development*.

Reed, M. P. & Ebert, S. M. (2013). *The seated soldier study: posture and body shape in vehicle seats*. Final Report (UMTRI-2013-13). Biosciences Group, University of Michigan Transportation Research Institute.

Rupp, J. R., & Reed, M. P. (2015). *Draft PMHS positioning procedures 9/Dec/2015*. Version 0.7.

Rupp, J. D., Miller, C. S., Zaseck, L. W., Orton, N., Bonifas, A., Slykhouse, L., & Reed, M. P. (2016). Forces applied to the foot and pelvis in high rate vertical accelerative loading. Summer Biomechanics, Bioengineering and Biotransport Conference, National Harbor, Maryland, June 30–July 2, 2016.

Slykhouse, L. R., Zaseck, L. W., Miller, C. S., Humm, J. R., Alai, A., Kang, Y. S., Dooley, C., Sherman, D. S., Bigler, B., Demetropolous, C. K., Reed, M. P., & Rupp, J.D. (2019, July). Anatomically-based skeletal coordinate systems for use with impact biomechanics data intended for anthropomorphic test device development. *J Biomech*. *19*(92):162–168.

Spink, R. (2014, September). *A simple method for processing measurements of vehicle response to underbody blast during live fire test and evaluation*. (Report No. ARL-TR-7030). U.S. Army Research Laboratory.

WIAMan Biomechanics Team. (2013a, September). *W0058: Warrior Injury Assessment Manikin (WIAMan) Project Helmet Fitting Procedures*. Version 1.1 [unpublished].

WIAMan Biomechanics Team. (2013b, September). *W0059: Warrior Injury Assessment Manikin (WIAMan) Project Vest Fitting Procedures*. Version 1.1 [unpublished].

WIAMan Biomechanics Team. (2013c, September). *W0060: Warrior Injury Assessment Manikin (WIAMan) Project Boot Fitting Procedures*. Version 1.0 [unpublished].

WIAMan Biomechanics Team. (2013d, October). *W0070: Warrior Injury Assessment Manikin (WIAMan) Project Belt Fitting Procedures.* Version 1.1 [unpublished].

Appendix A – Supplementary Information from WS10 Tests

A.1 Subject Anthropometry

Table A-1. WS10-001 Subject Anthropometry

Cadaver #	**16-10009**	Forearm Hand Length (cm)	41
Gender	M	Ankle Height (cm)	8
Age (years)	59		
Weight (kg)	86.2	Left Foot Length (cm)	23
Stature (cm)	176	Right Foot Length (cm)	23
Shoulder Height (cm)	--	Avg Foot Length (cm)	23
Vertex To Symphysis (cm)	103	Waist Back Length (cm)	39
Waist Height (cm)	83	Bicep Circumference (cm)	31
Crotch Height (cm)	46	Elbow Circumference (cm)	29
Tibial Height (cm)	16	Forearm Circumference (cm)	27
Head To Trochanter (cm)	--	Wrist Circumference (cm)	N/A
Vertex To Mentum (cm)	--	Thigh Circumference (cm)	49
Head Breadth (cm)	--	Lower Thigh Circumference (cm)	40
Bizygomatic Breadth (cm)	--	Knee Circumference (cm)	41
Biacromial Breadth (cm)	41	Calf Circumference (cm)	36
Chest Breadth (cm)	37	Ankle Circumference (cm)	24
Waist Breadth (cm)	40	Neck Circumference (cm)	48
Hip Breadth (cm)	39	Scye To Shoulder Circ. (cm)	104
Trochanter Breadth (cm)	43	Chest Circumference (cm)	92
Left Foot Breadth (cm)	10	Waist Circumference (cm)	90
Right Foot Breadth (cm)	10.5	Buttock Circumference (cm)	102
Avg Foot Breadth (cm)	10.3	Chest Depth (cm)	19
Head Length (cm)	9	Waist Depth (cm)	14
Menton-Sellion Length (cm)	16	Buttock Depth (cm)	18
Shoulder To Elbow (cm)	39		
Seated Measurements		**PPE Full Body Anthropometry**	
Biacromial Breadth (cm)	38	Chest Depth (cm)	19
Bideltoid Breadth (cm)	36	Waist Depth (cm)	14
Buttock-Knee Length (cm)	57	Chest Circumference (cm)	92
Hip Breadth Sitting (cm)	45	Chest Breadth (cm)	37
Knee Height Sitting (cm)	38	Waist Breadth (cm)	40
Sitting Height (cm)	81		

Table A-2. WS10-002 Subject Anthropometry

Cadaver #	**1612325R**	Forearm Hand Length (cm)	43
Gender	M	Ankle Height (cm)	6.5
Age (years)	54		
Weight (kg)	72.1	Left Foot Length (cm)	22
Stature (cm)	170.2	Right Foot Length (cm)	22
Shoulder Height (cm)	144	Avg Foot Length (cm)	22
Vertex To Symphysis (cm)	70	Waist Back Length (cm)	53
Waist Height (cm)	94	Bicep Circumference (cm)	26
Crotch Height (cm)	74	Elbow Circumference (cm)	25
Tibial Height (cm)	42.5	Forearm Circumference (cm)	23
Head To Trochanter (cm)	87	Wrist Circumference (cm)	16
Vertex To Mentum (cm)	16	Thigh Circumference (cm)	48.5
Head Breadth (cm)	23	Lower Thigh Circumference (cm)	41
Bizygomatic Breadth (cm)	7	Knee Circumference (cm)	38
Biacromial Breadth (cm)	40	Calf Circumference (cm)	33
Chest Breadth (cm)	46	Ankle Circumference (cm)	18.5
Waist Breadth (cm)	47	Neck Circumference (cm)	32
Hip Breadth (cm)	48	Scye To Shoulder Circ. (cm)	40.5
Trochanter Breadth (cm)	45	Chest Circumference (cm)	96
Left Foot Breadth (cm)	9	Waist Circumference (cm)	98
Right Foot Breadth (cm)	9	Buttock Circumference (cm)	102
Avg Foot Breadth (cm)	9	Chest Depth (cm)	18
Head Length (cm)	15.1	Waist Depth (cm)	17
Menton-Sellion Length (cm)	38	Buttock Depth (cm)	16
Shoulder To Elbow (cm)	37		
Seated Measurements		**PPE Full Body Anthropometry**	
Biacromial Breadth (cm)	36	Chest Depth (cm)	18
Bideltoid Breadth (cm)	37	Waist Depth (cm)	17
Buttock-Knee Length (cm)	53	Chest Circumference (cm)	96
Hip Breadth Sitting (cm)	33	Chest Breadth (cm)	46
Knee Height Sitting (cm)	58	Waist Breadth (cm)	47
Sitting Height (cm)	115		

Table A-3. WS10-003 Subject Anthropometry

Cadaver #	**F182258**	Forearm Hand Length (cm)	38
Gender	M	Ankle Height (cm)	7
Age (years)	65		
Weight (kg)	80.7	Left Foot Length (cm)	25
Stature (cm)	177.8	Right Foot Length (cm)	25
Shoulder Height (cm)	150	Avg Foot Length (cm)	25
Vertex To Symphysis (cm)	--	Waist Back Length (cm)	66
Waist Height (cm)	98	Bicep Circumference (cm)	37
Crotch Height (cm)	73.5	Elbow Circumference (cm)	39.5
Tibial Height (cm)	--	Forearm Circumference (cm)	36
Head To Trochanter (cm)	87	Wrist Circumference (cm)	28.2
Vertex To Mentum (cm)	18.4	Thigh Circumference (cm)	55
Head Breadth (cm)	30.9	Lower Thigh Circumference (cm)	49.5
Bizygomatic Breadth (cm)	--	Knee Circumference (cm)	46
Biacromial Breadth (cm)	47	Calf Circumference (cm)	40
Chest Breadth (cm)	45	Ankle Circumference (cm)	33.5
Waist Breadth (cm)	36	Neck Circumference (cm)	53
Hip Breadth (cm)	40	Scye To Shoulder Circ. (cm)	44
Trochanter Breadth (cm)	43	Chest Circumference (cm)	132
Left Foot Breadth (cm)	9	Waist Circumference (cm)	124
Right Foot Breadth (cm)	9	Buttock Circumference (cm)	120
Avg Foot Breadth (cm)	9	Chest Depth (cm)	32
Head Length (cm)	24.5	Waist Depth (cm)	28
Menton-Sellion Length (cm)	43	Buttock Depth (cm)	28
Shoulder To Elbow (cm)	45		
Seated Measurements		**PPE Full Body Anthropometry**	
Biacromial Breadth (cm)	--	Chest Depth (cm)	32
Bideltoid Breadth (cm)	--	Waist Depth (cm)	28
Buttock-Knee Length (cm)	--	Chest Circumference (cm)	132
Hip Breadth Sitting (cm)	--	Chest Breadth (cm)	45
Knee Height Sitting (cm)	--	Waist Breadth (cm)	36
Sitting Height (cm)	--		

A.2 Pre- vs. Posttest Radiology

A.2.1 Foot/Ankle Extremity Injuries

Table A-4. WS10-001 Lower Extremity Injuries

	Pretest	Posttest
Right Calcaneus Coronal View		
Left Calcaneus Coronal View		

Table A-4. WS10-001 Lower Extremity Injuries (continued)

	Pretest	Posttest
Right Talus Sagittal View	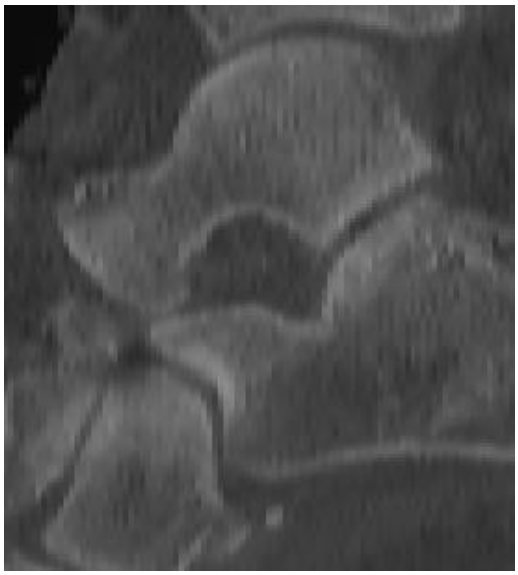	
Left Talus Sagittal View	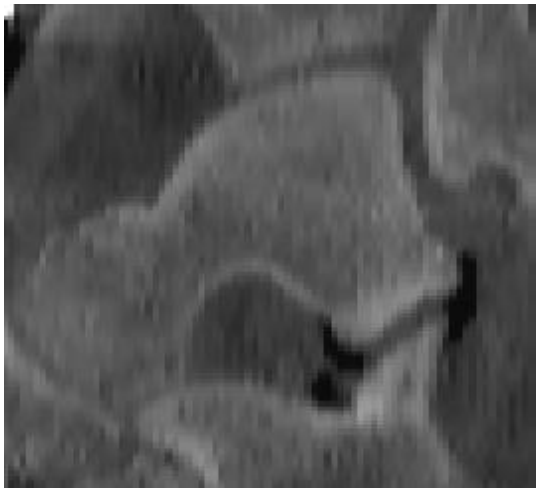	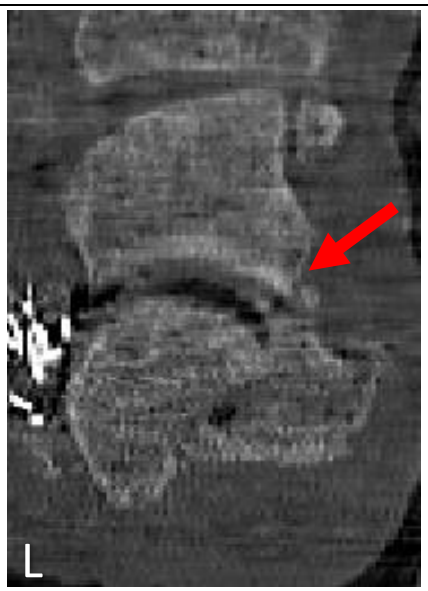

Table A-4. WS10-001 Lower Extremity Injuries (continued)

	Pretest	Posttest
Right Femur Axial View	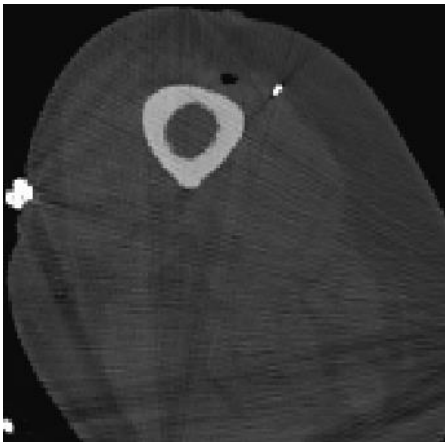	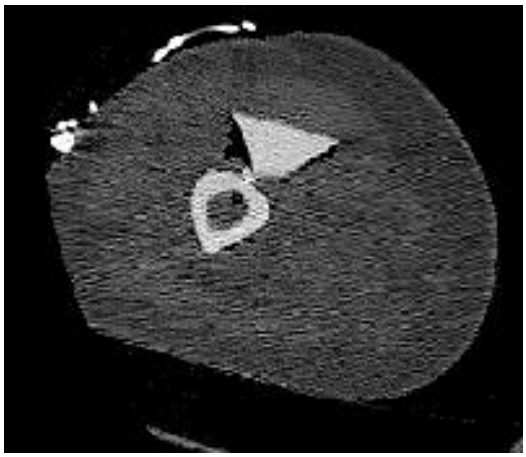

Table A-5. WS10-002 Lower Extremity Injuries

	Pretest	Posttest
Left Calcaneus Sagittal View	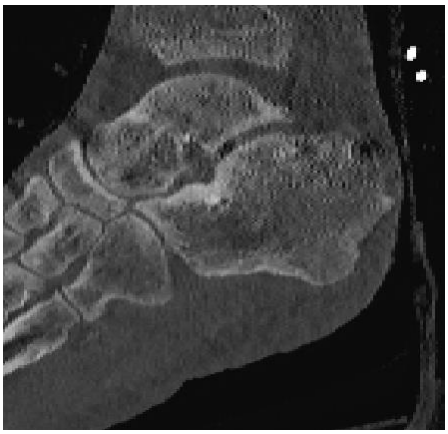	
Left Talus Coronal View	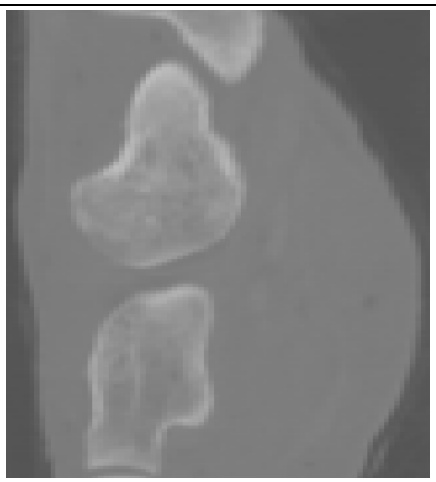	

Table A-6. WS10-003 Lower Extremity Injuries

	Pretest	Posttest
Left Calcaneus Sagittal View	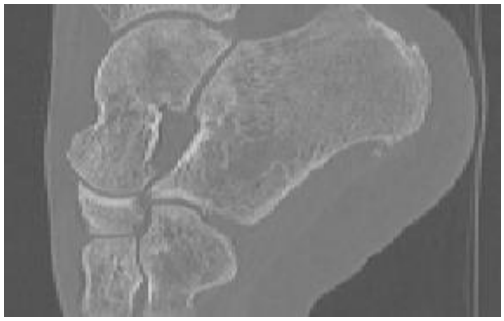	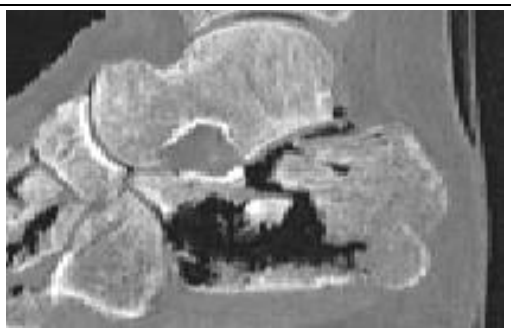
Left Talus Sagittal View		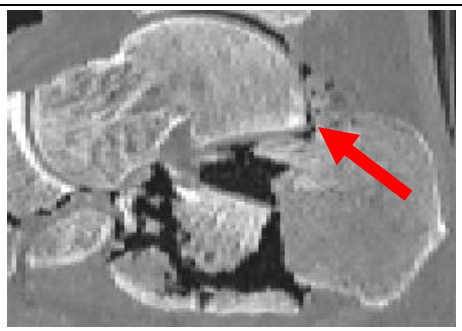
Right Calcaneus Sagittal View	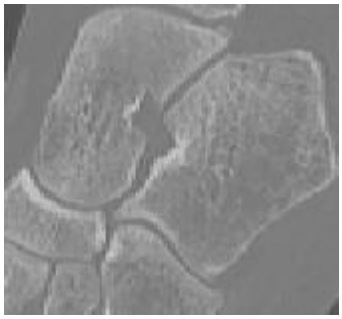	
Right Tibia Sagittal View		

Table A-6. WS10-003 Lower Extremity Injuries (continued)

	Pretest	Posttest
Right Fibula Sagittal View		
Left 3rd Metatarsal Sagittal View		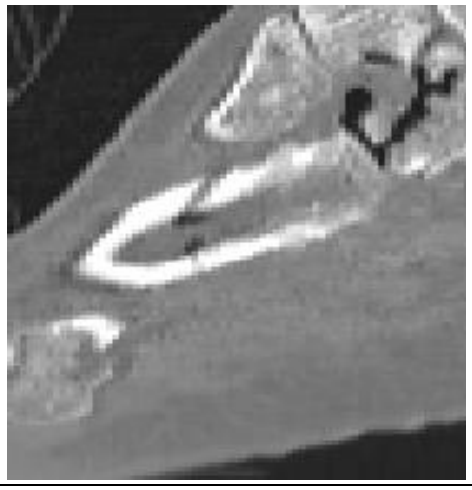
Left 4th Metatarsal Sagittal View	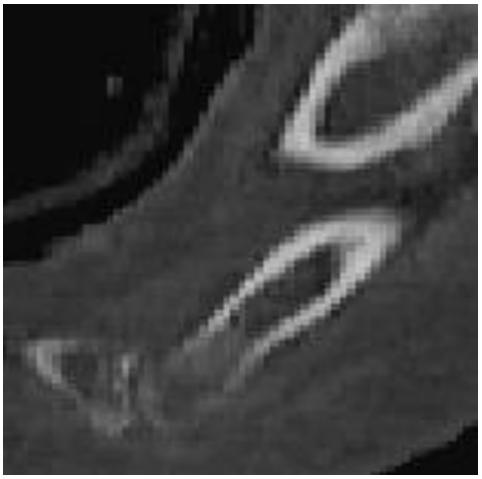	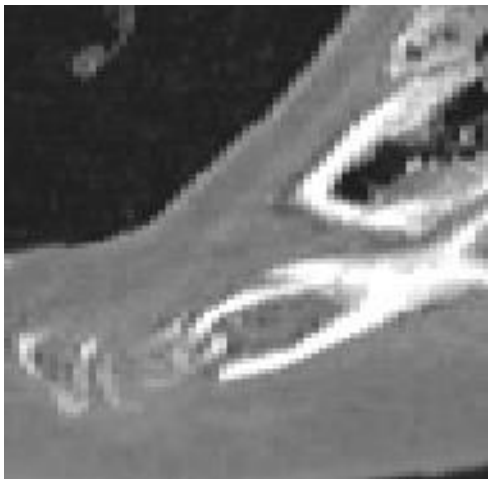

Table A-6. WS10-003 Lower Extremity Injuries (continued)

	Pretest	Posttest
Left 5th Metatarsal Sagittal View		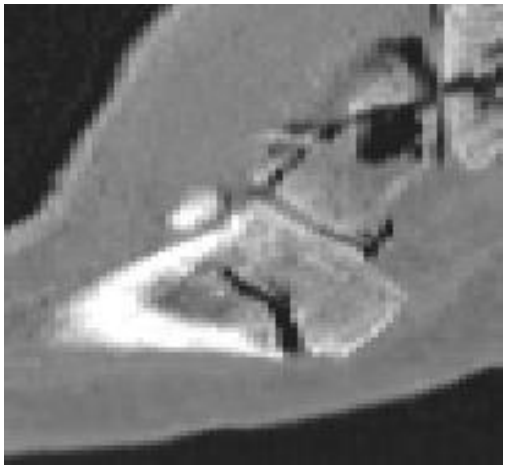
Left Medial Cuneiform Coronal View	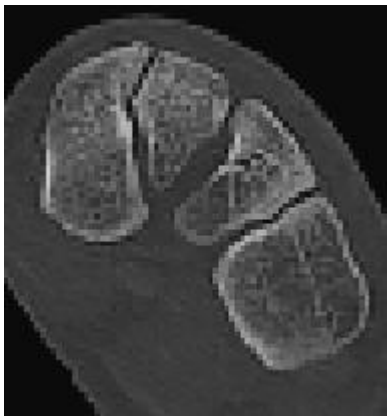	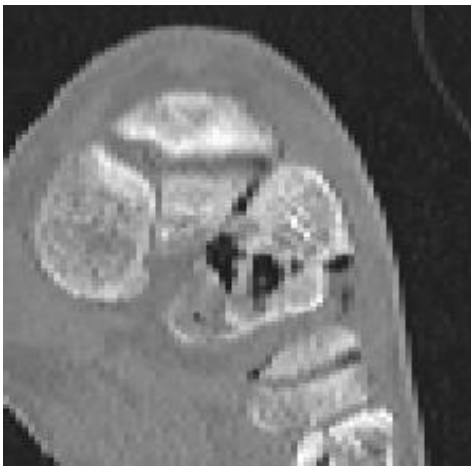
Left Cuboid Coronal View		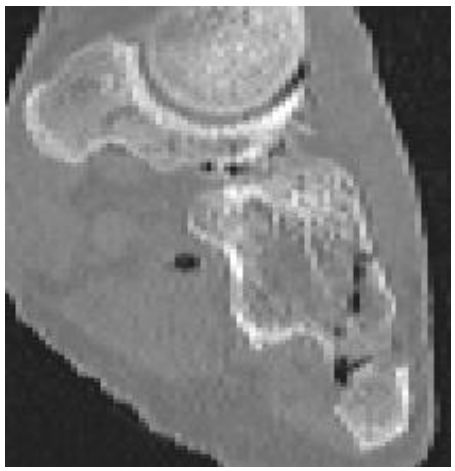

Table A-6. WS10-003 Lower Extremity Injuries (continued)

	Pretest	Posttest
Right 4th Metatarsal Sagittal View	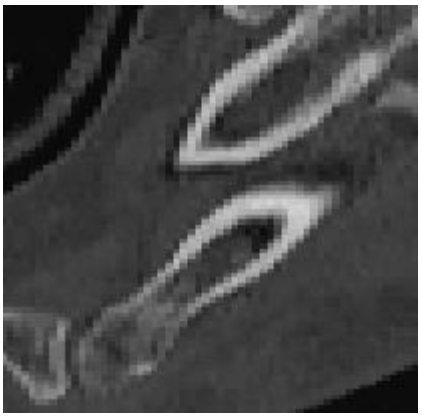	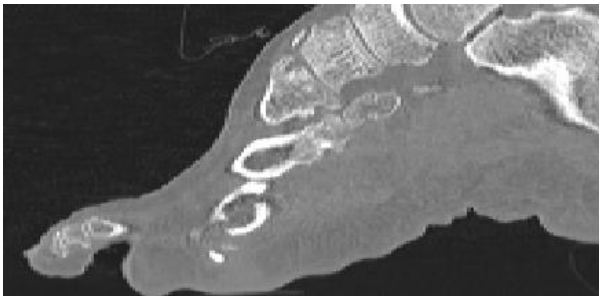
Right 5th Metatarsal Sagittal View	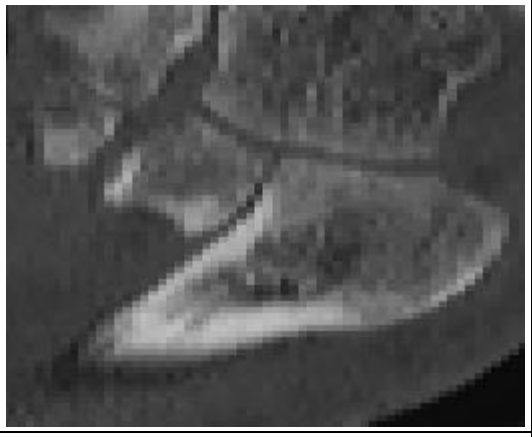	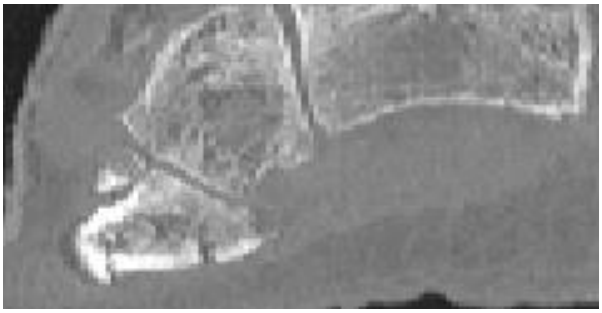
Right Cuneiform Sagittal View		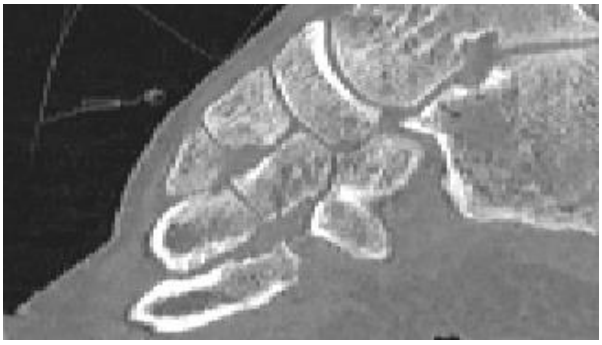

A.2.2 Pelvis Injuries

Table A-7. WS10-001 Pelvis Injuries

	Pretest	Posttest
Left Acetabulum Coronal View	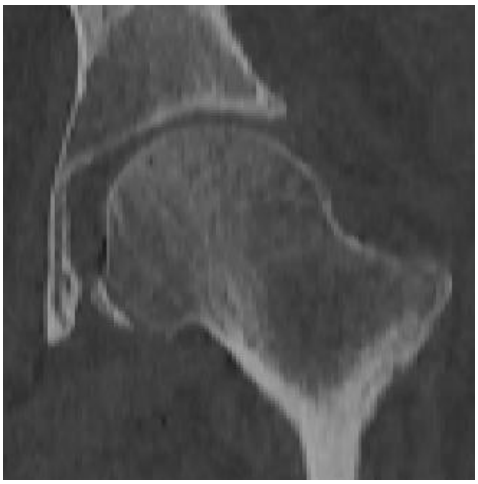	
Sacrum Axial View	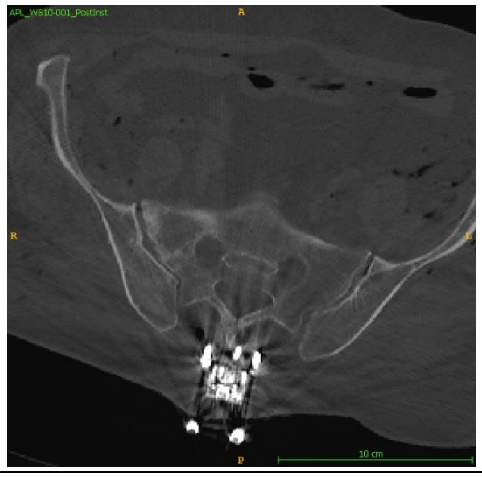	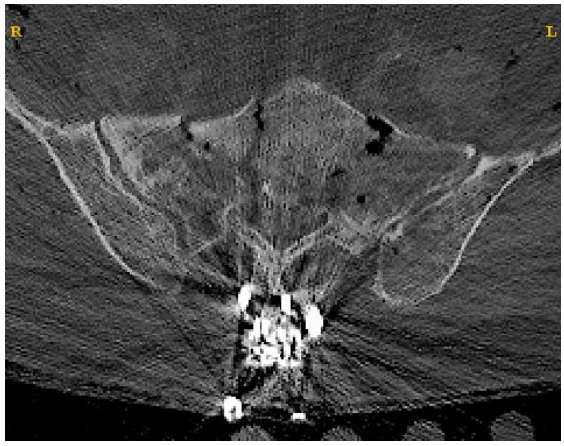
Coccyx Coronal View		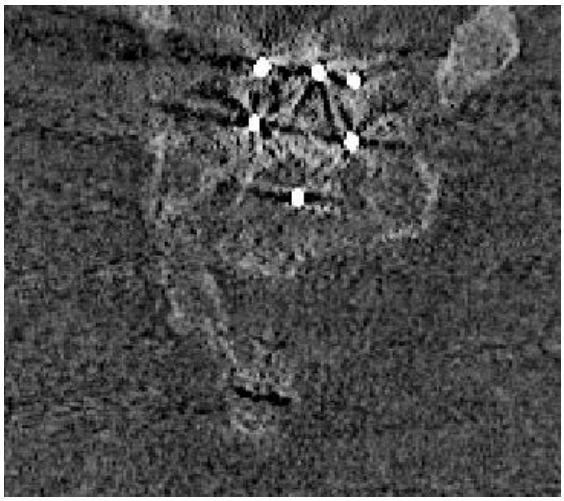

Table A-8. WS10-002 Pelvis Injuries

	Pretest	Posttest
Sacrum Axial View	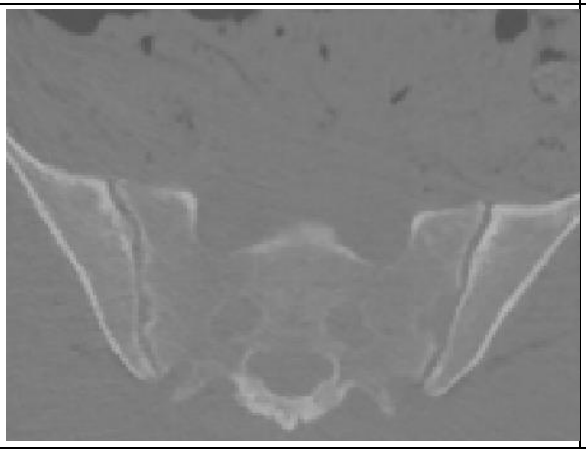	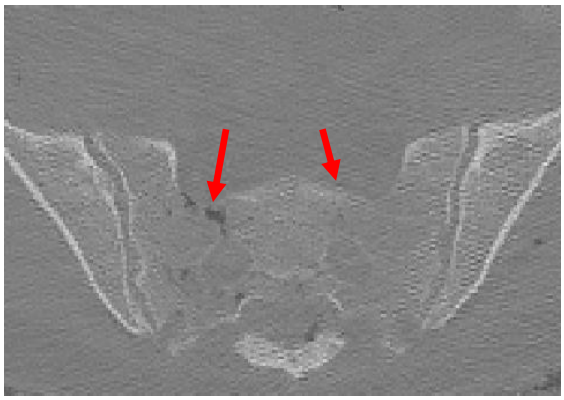

Table A-9. WS10-003 Pelvis Injuries

	Pretest	Posttest
Sacrum Sagittal View	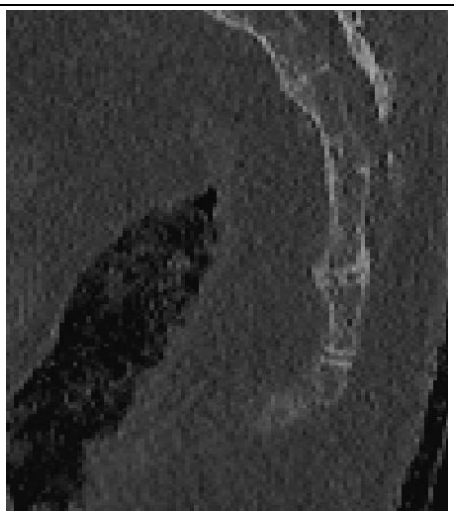	
Coccyx Sagittal View	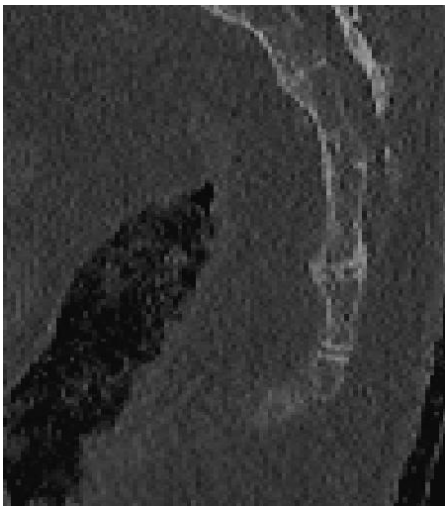	
Pubic Symphysis Axial View	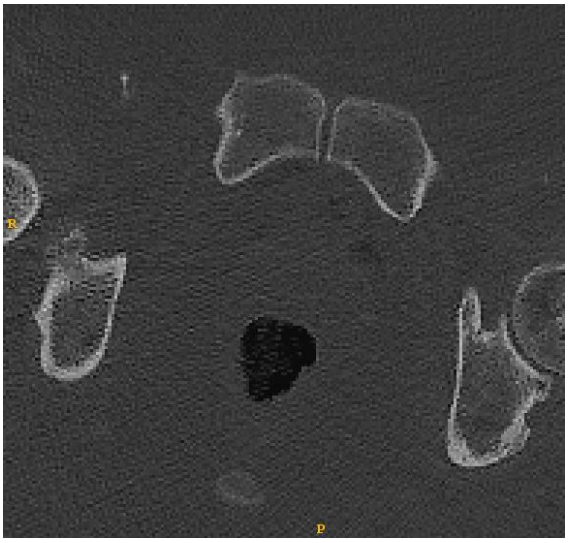	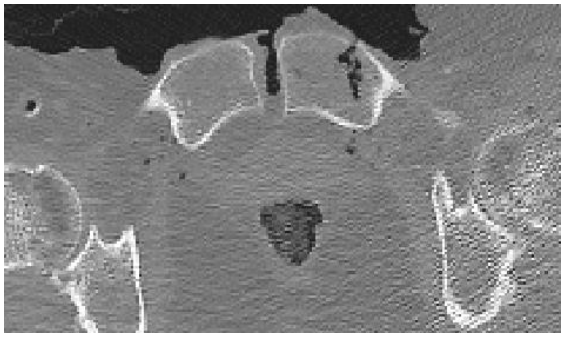

A.2.3 Spine Injuries

Table A-10. WS10-001 Lumbar Spine Injuries

	Pretest	Posttest
L5 Sagittal View		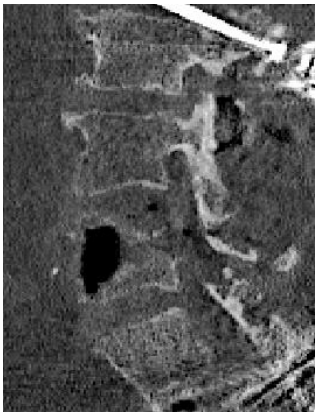
L1 Sagittal View	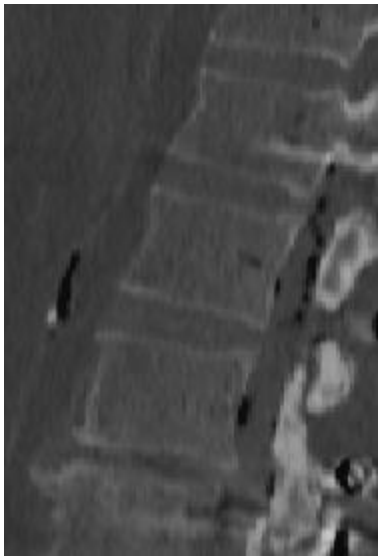	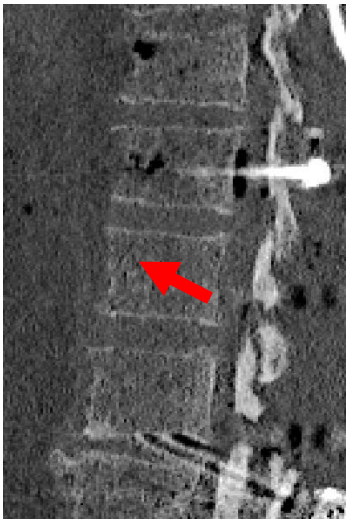

Table A-11. WS10-002 Lumbar Spine Injuries

	Pretest	Posttest
L5 Axial View		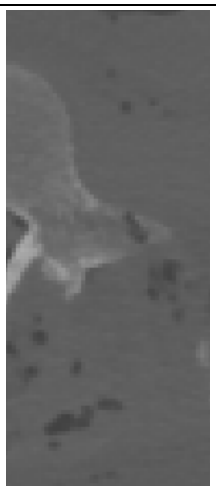
L5 Axial View		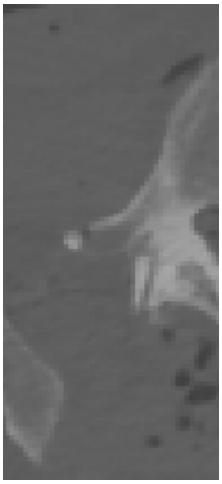
L4 Axial View		

Table A-11. WS10-002 Lumbar Spine Injuries (continued)

	Pretest	Posttest
L4 Axial View	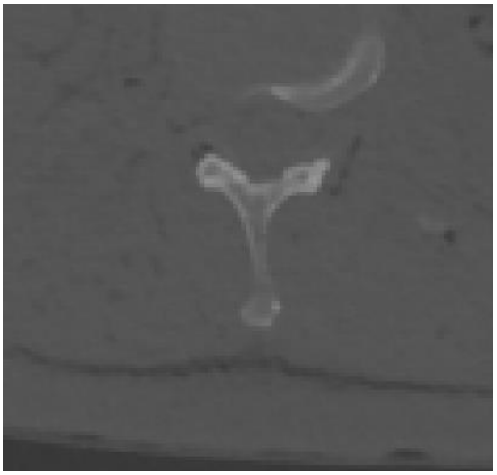	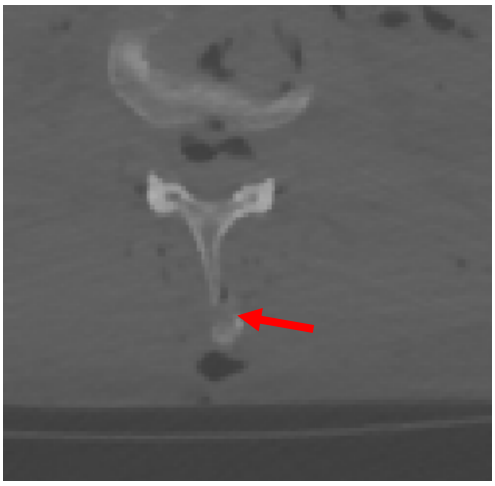
L1 Sagittal View	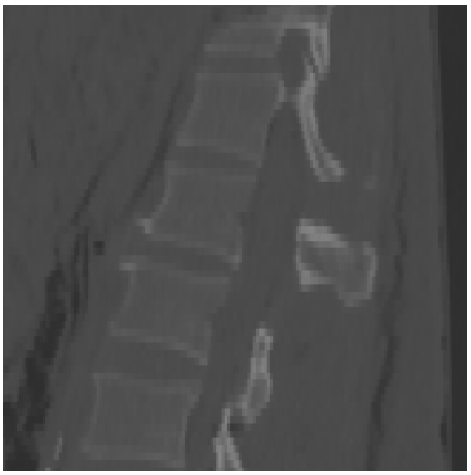	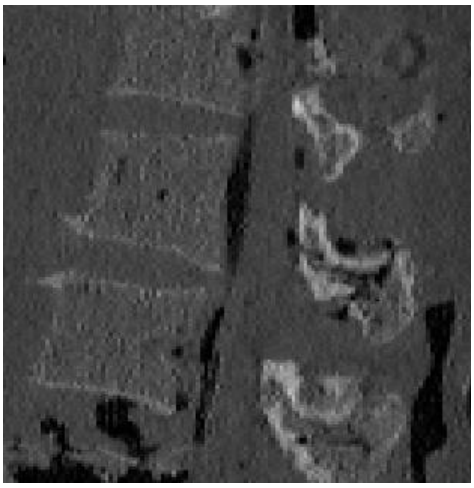
L1 Axial View	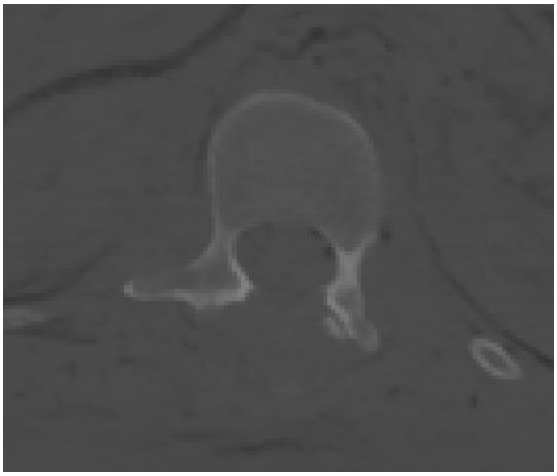	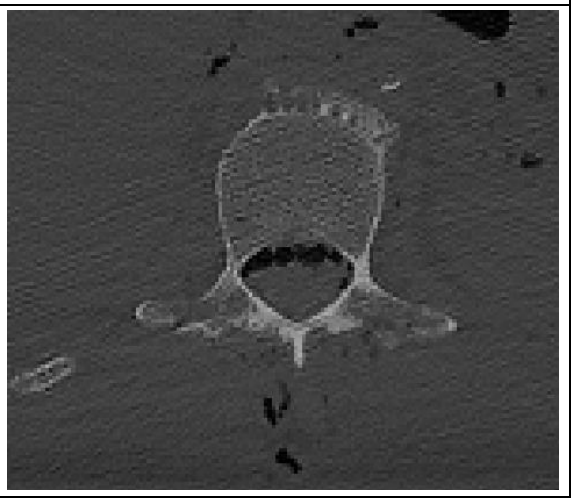

Table A-11. WS10-002 Lumbar Spine Injuries (continued)

	Pretest	Posttest
L3 Coronal View	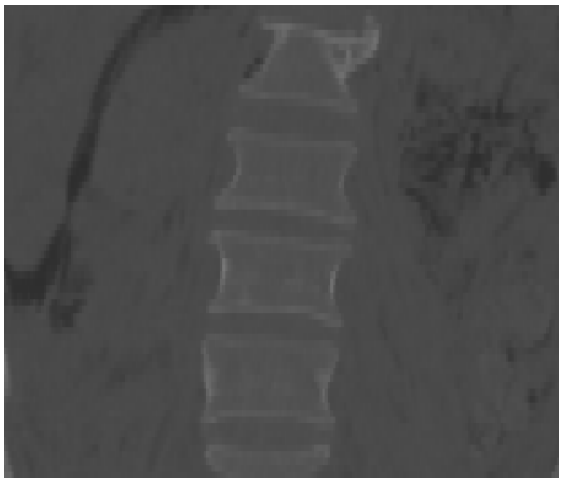	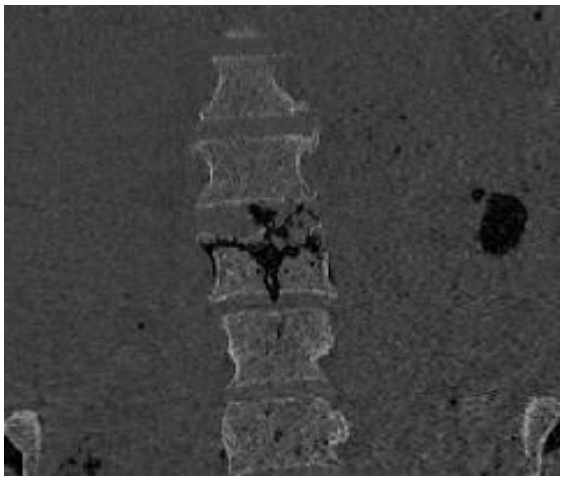

Table A-12. WS10-003 Lumbar Spine Injuries

	Pretest	Posttest
L2 Axial View		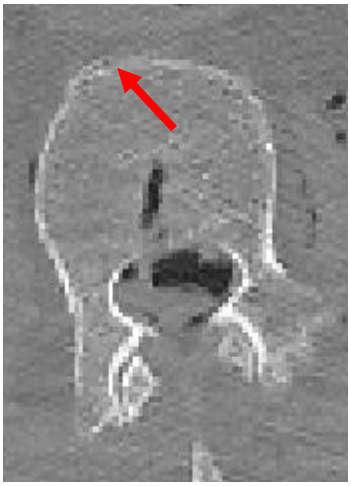

Table A-12. WS10-003 Lumbar Spine Injuries (continued)

	Pretest	Posttest
L5 Axial View	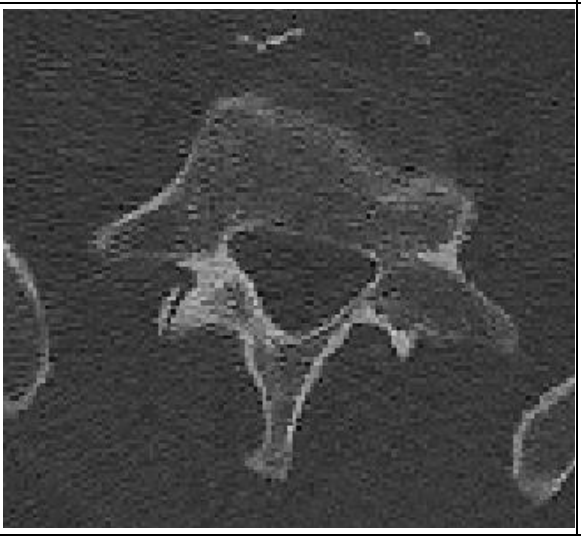	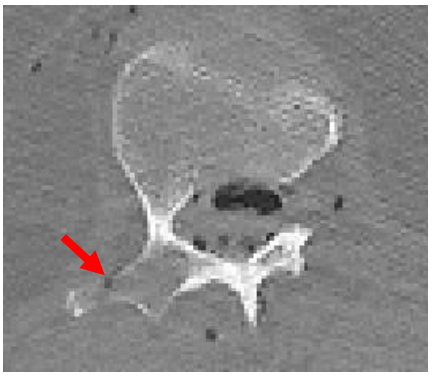
L5 Axial View	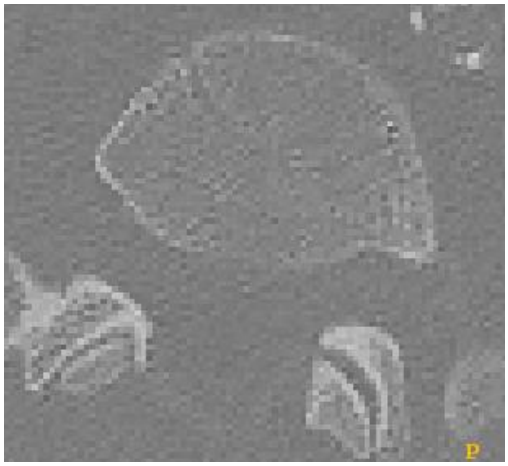	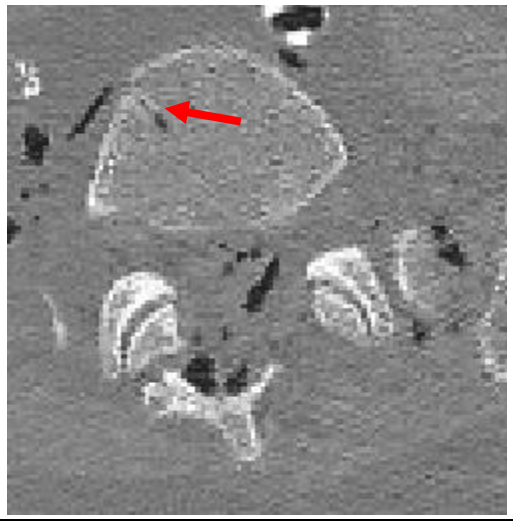
L5 Axial View	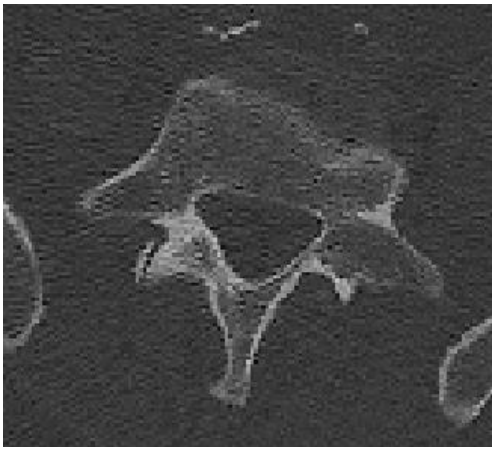	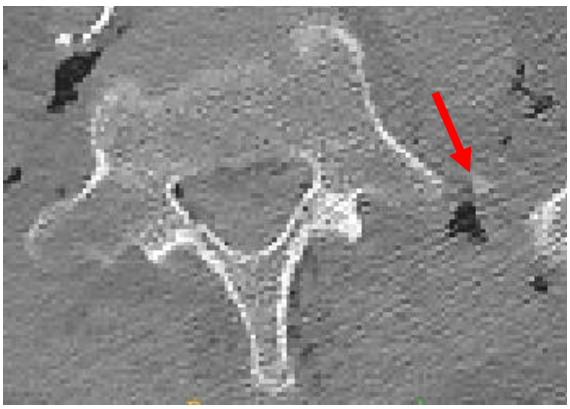

Table A-13. WS10-001 Thoracic Spine Injuries

	Pretest	Posttest
T11 Coronal View	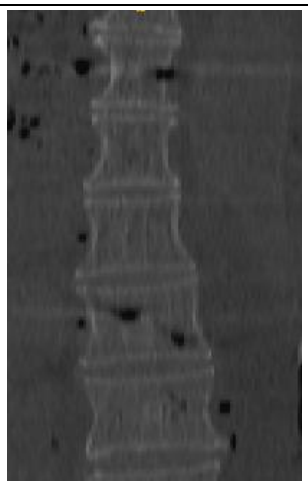	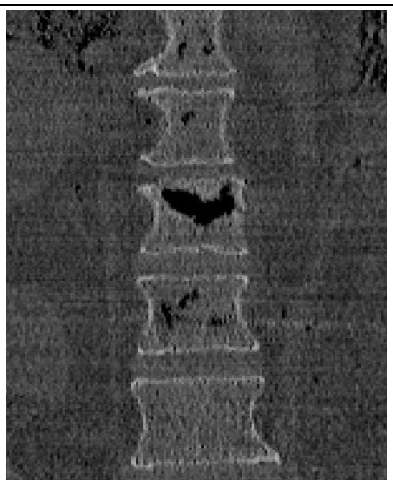

Table A-14. WS10-002 Thoracic Spine Injuries

	Pretest	Posttest
T8 Sagittal View		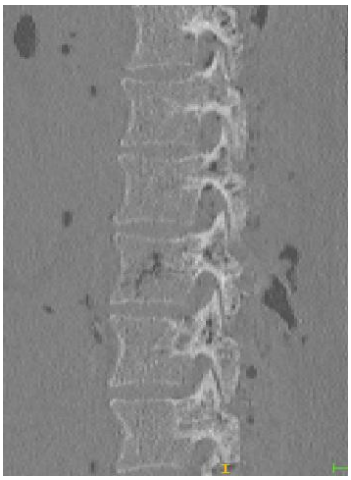

Table A-14. WS10-002 Thoracic Spine Injuries (continued)

	Pretest	Posttest
T1 Sagittal View	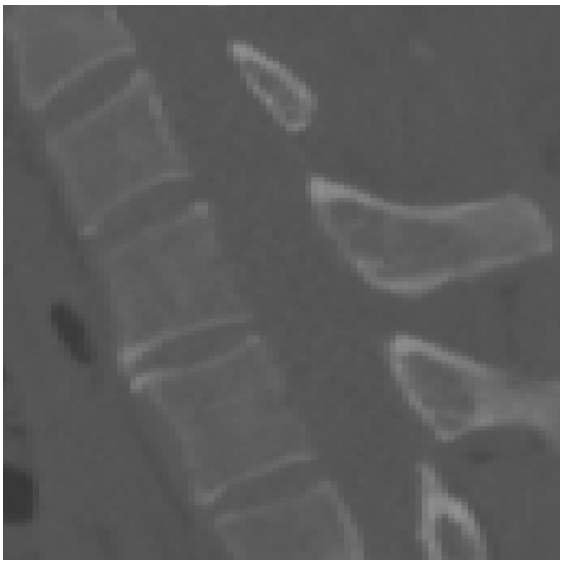	
C6 Sagittal View		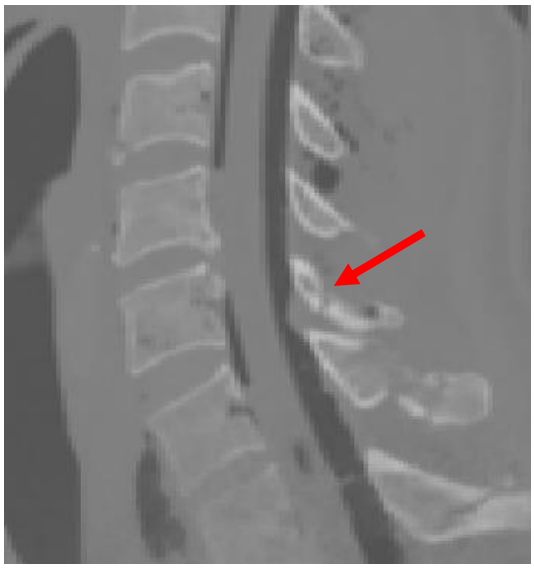

Table A-14. WS10-002 Thoracic Spine Injuries (continued)

	Pretest	Posttest
C4 Sagittal View		
Ribs Coronal View	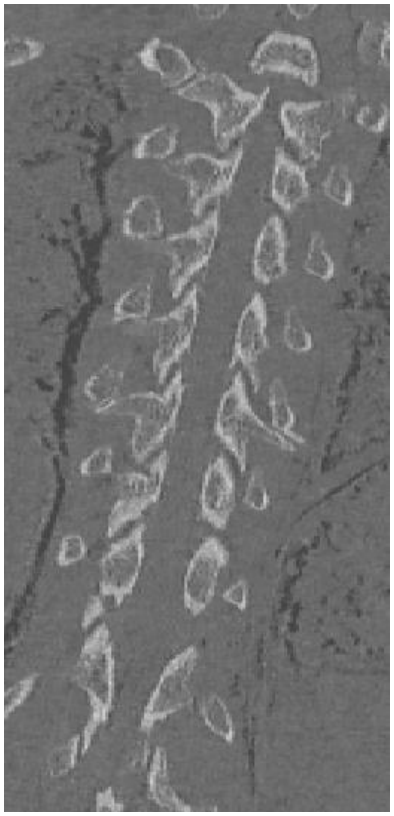	

Table A-15. WS10-003 Thoracic Spine Injuries

	Pretest	Posttest
T12 Sagittal View	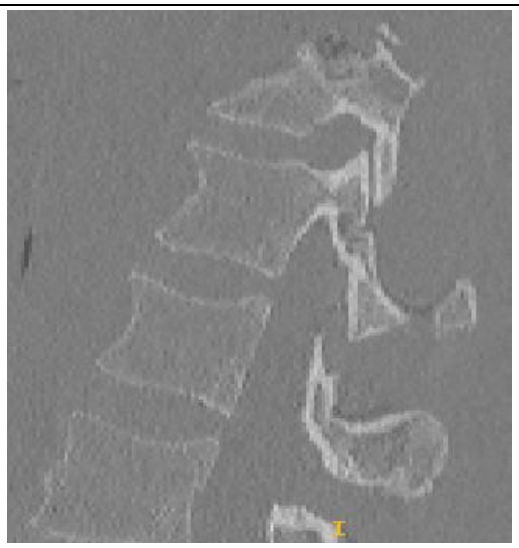	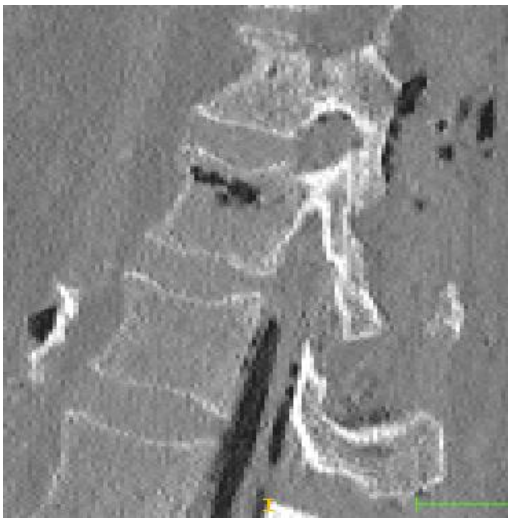

A.3 Injury Images

A.3.1 Foot/Ankle

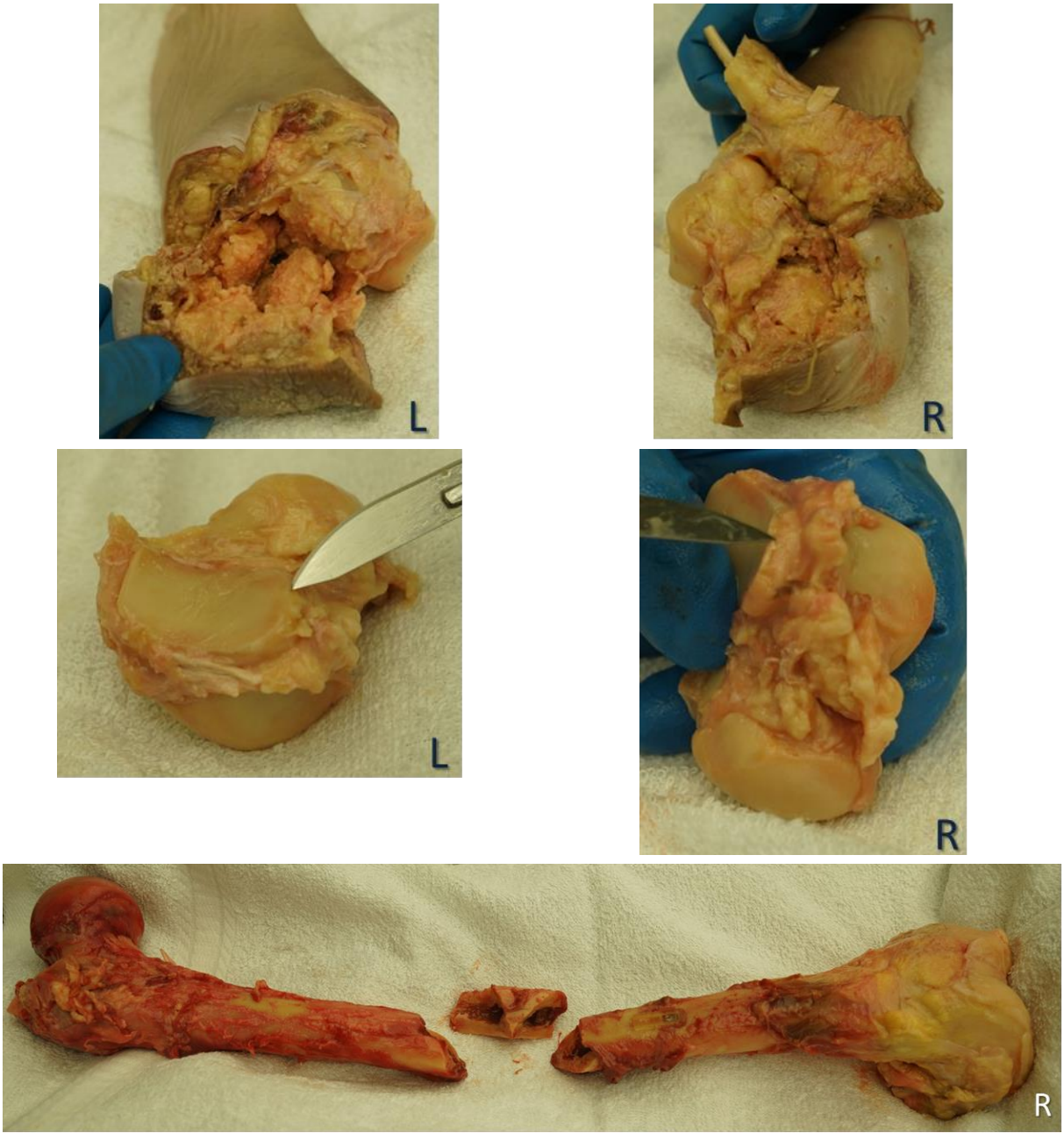

Figure A-1. WS10-001 lower extremity fractures

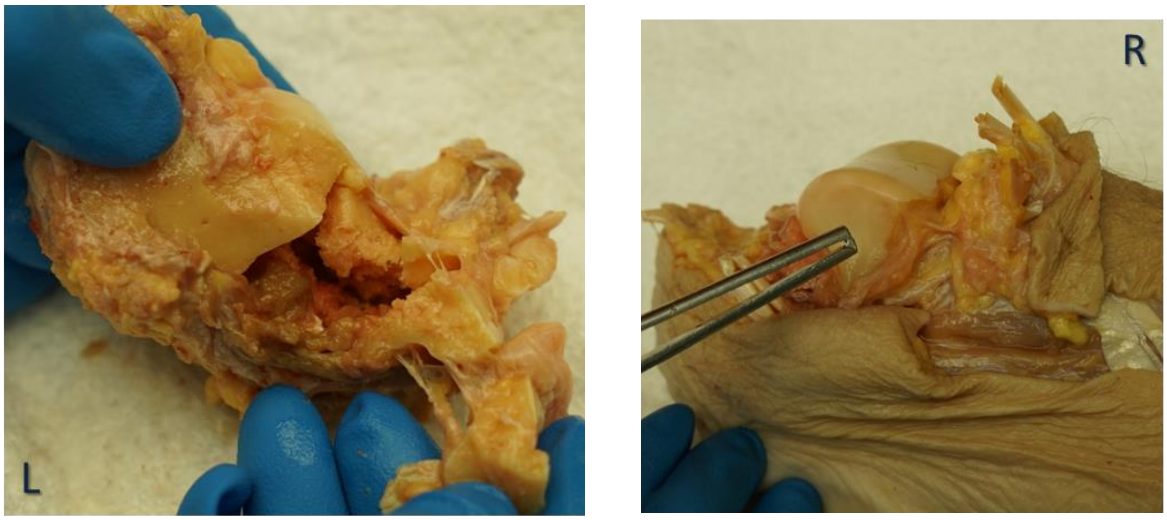

Figure A-2. WS10-002 lower extremity fractures

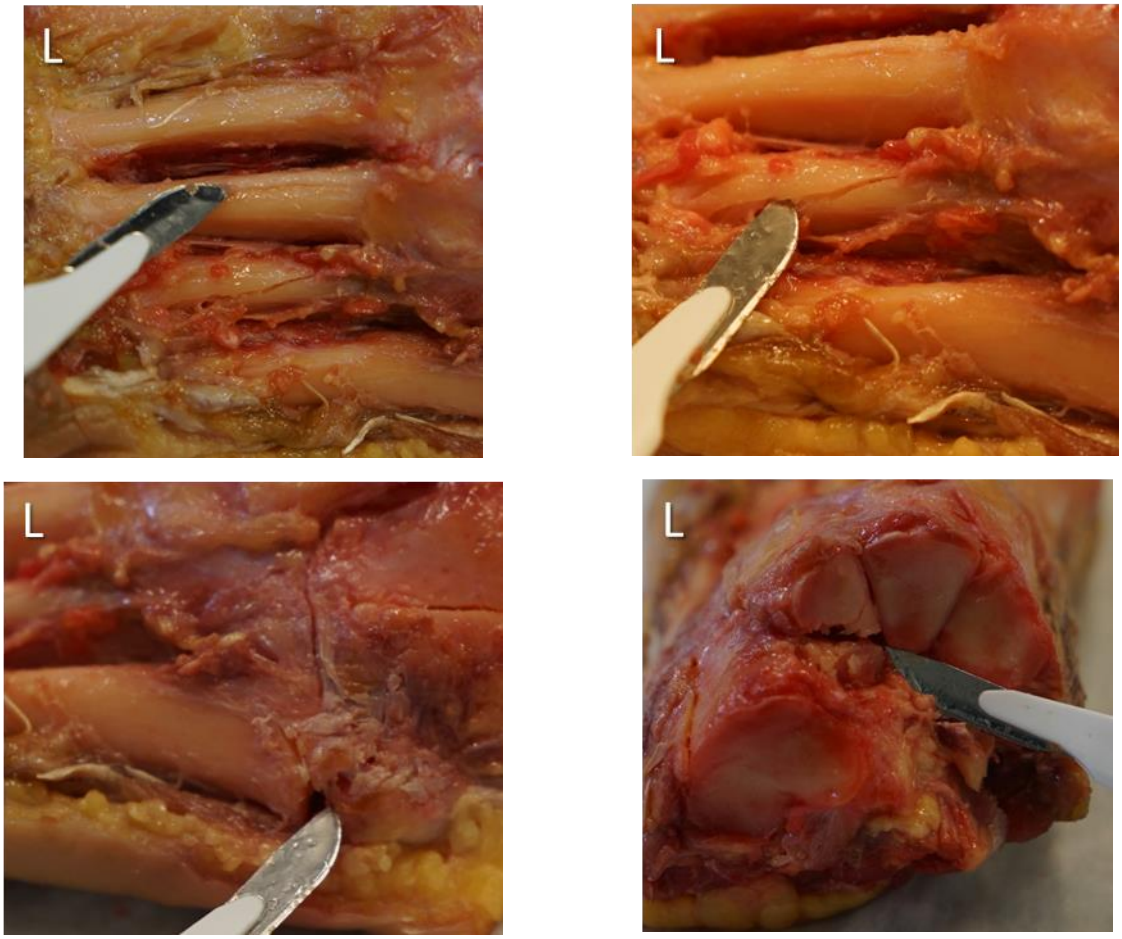

Figure A-3. WS10-003 lower extremity fractures

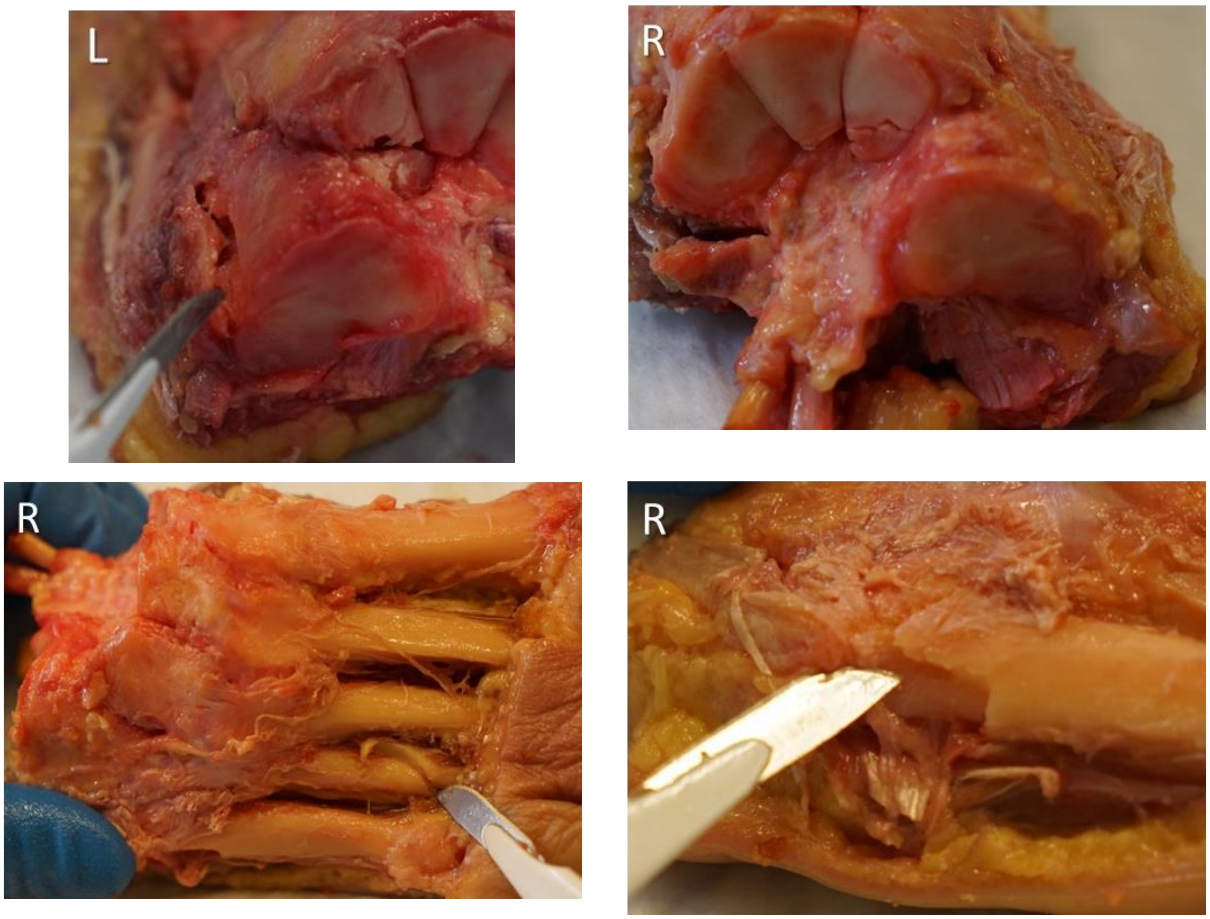

Figure A-3. WS10-003 lower extremity fractures (continued)

A.3.2 Pelvis

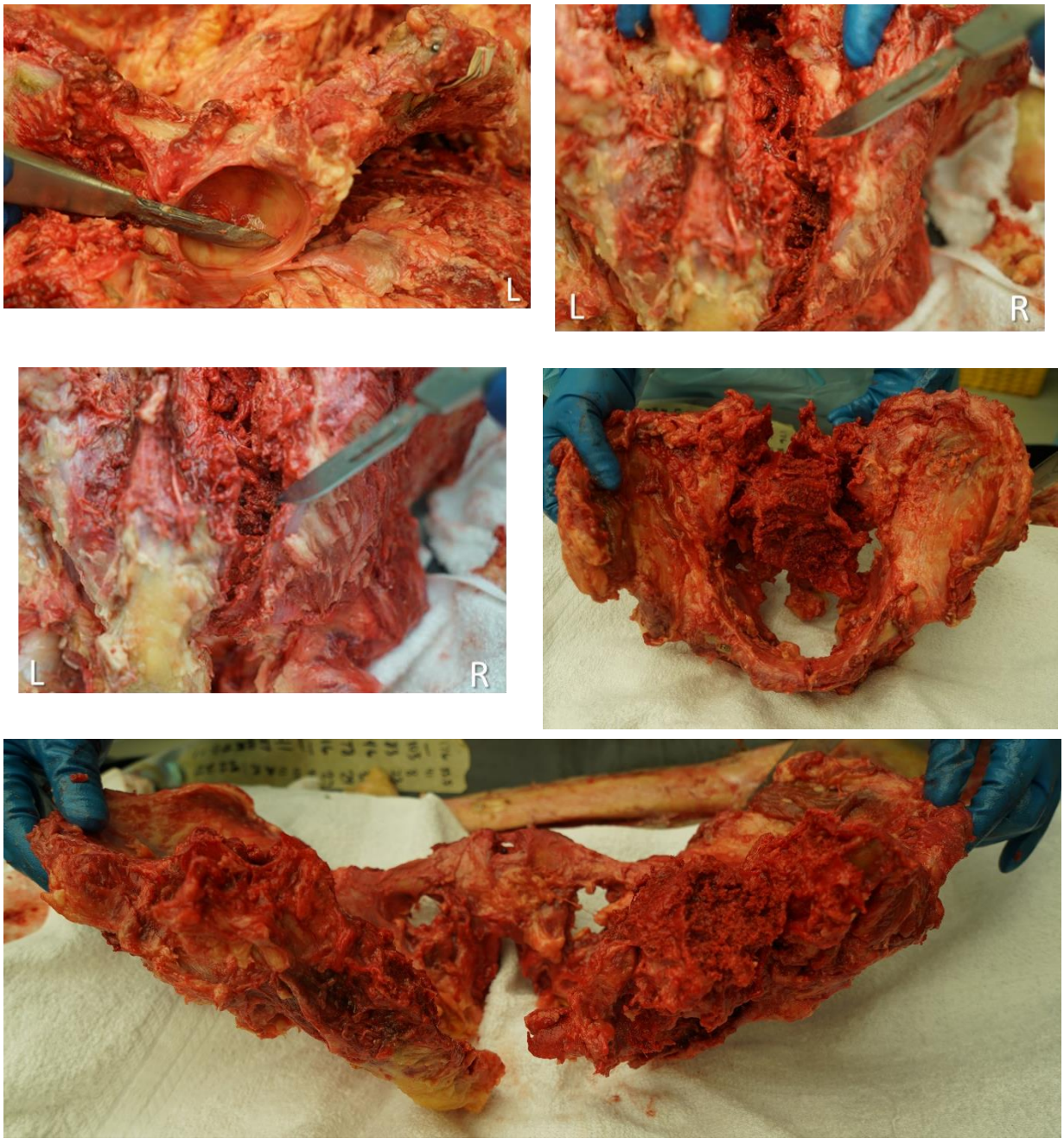

Figure A-4. WS10-001 pelvis fractures

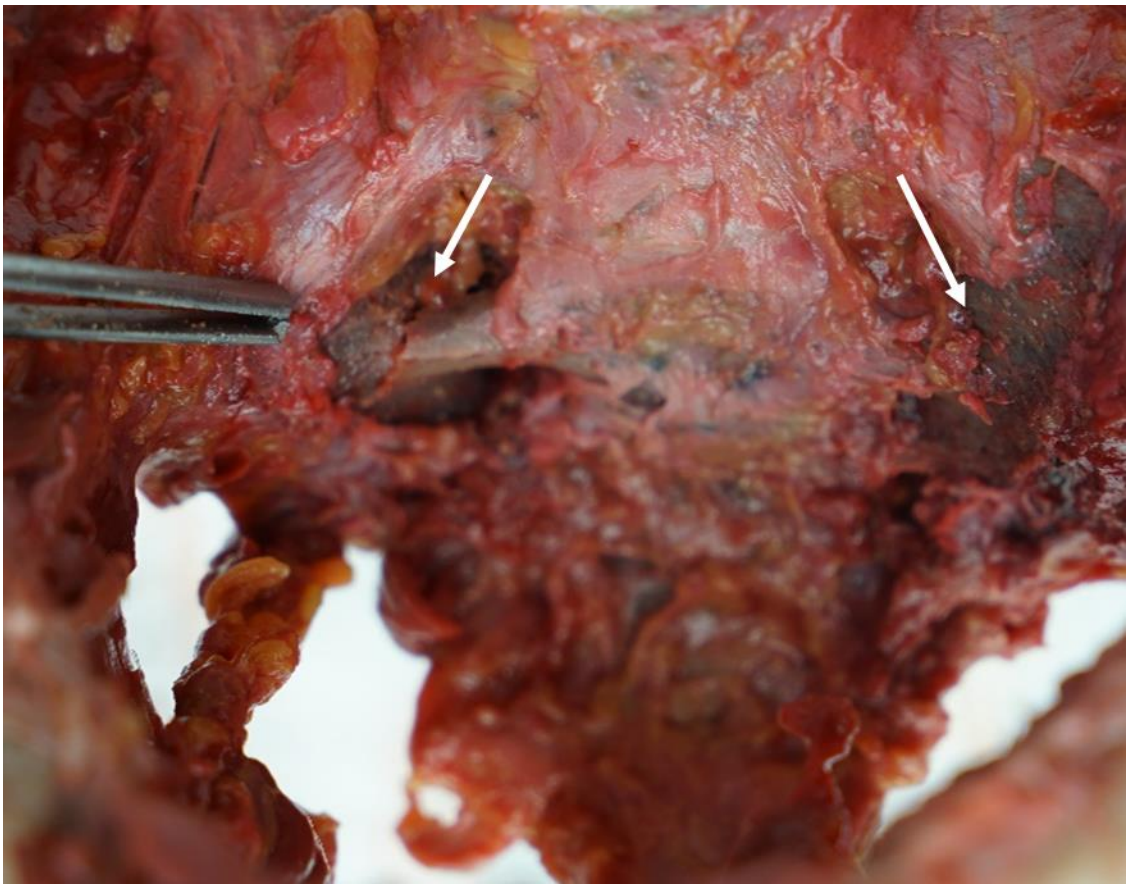

Figure A-5. WS10-002 pelvis fractures

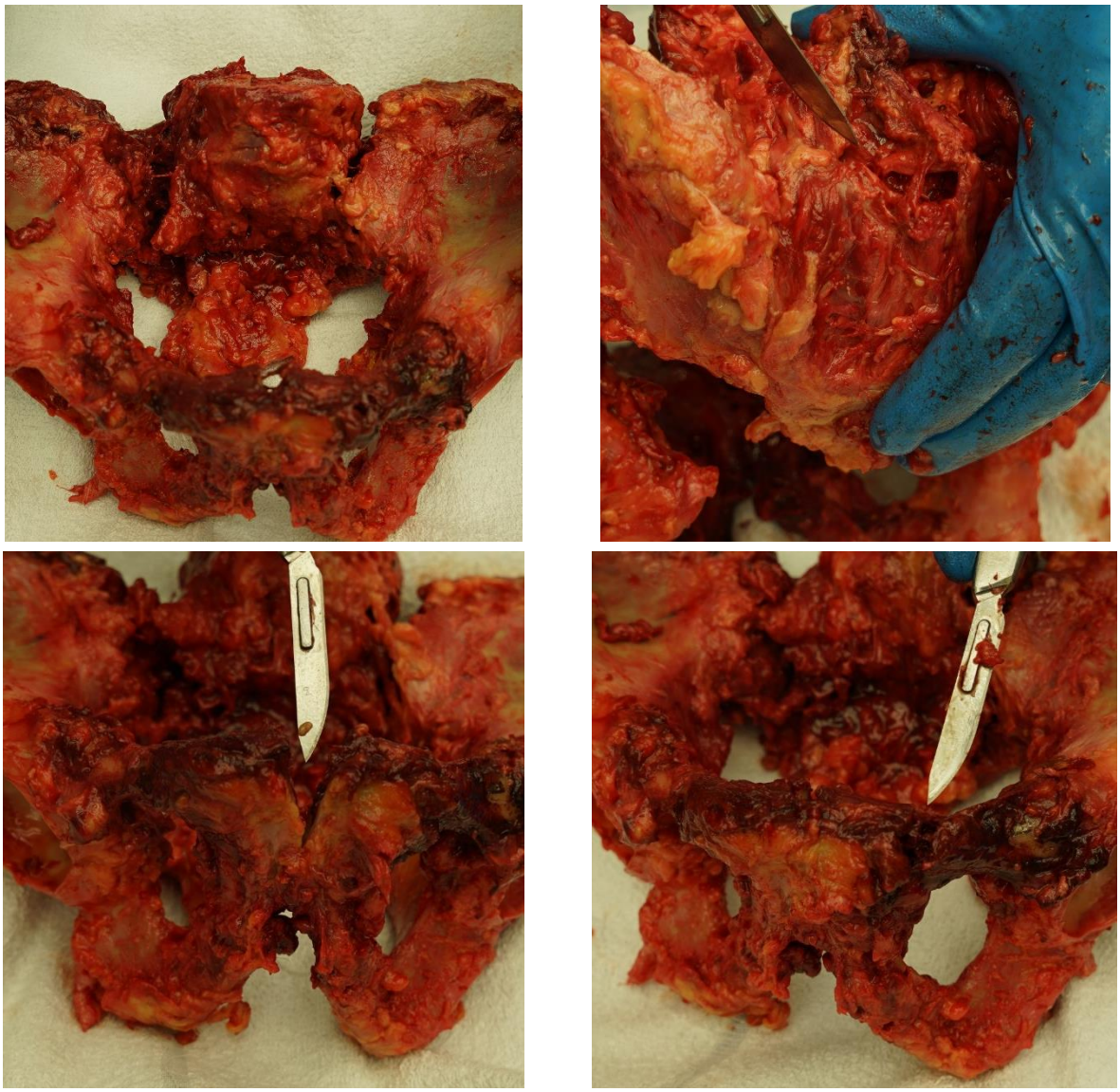

Figure A-6. WS10-003 pelvis fractures

A.3.3 Spine

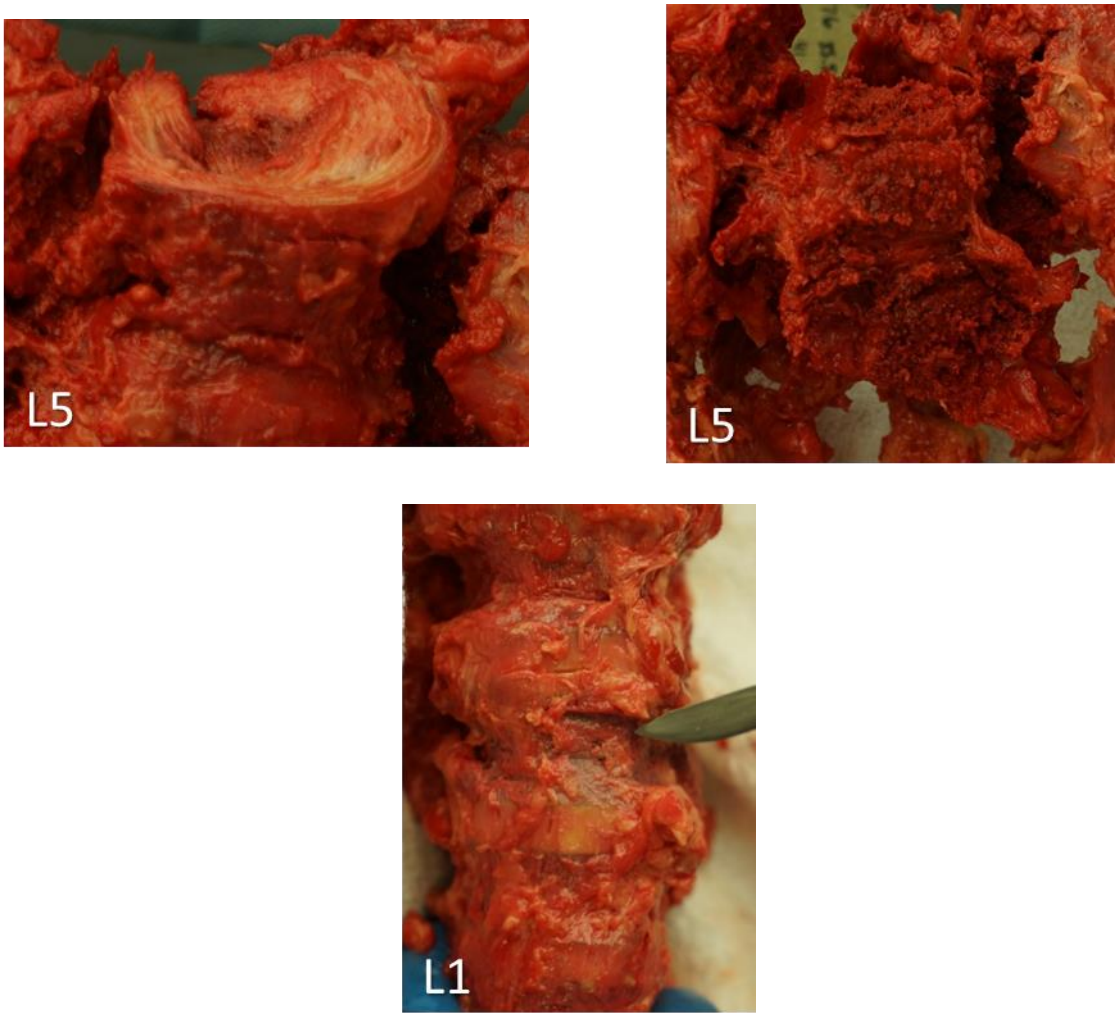

Figure A-7. WS10-001 lumbar spine fractures

Figure A-8. WS10-002 lumbar spine fractures

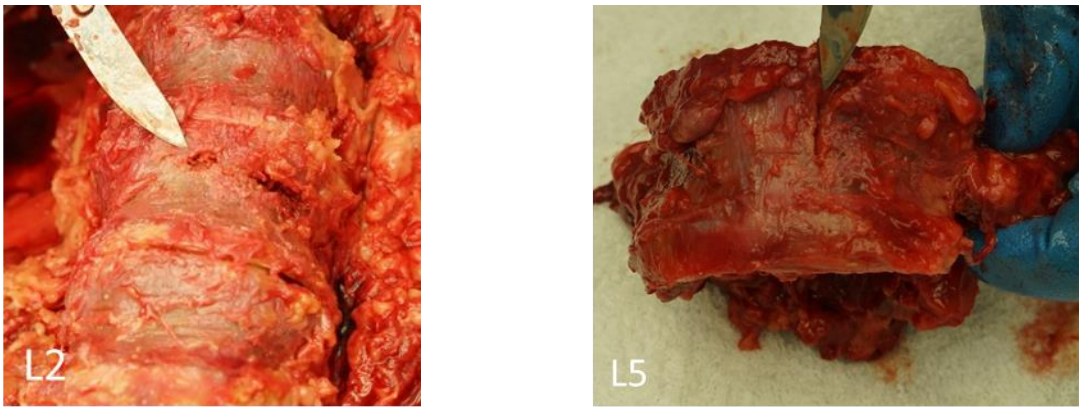

Figure A-9. WS10-003 lumbar spine fractures

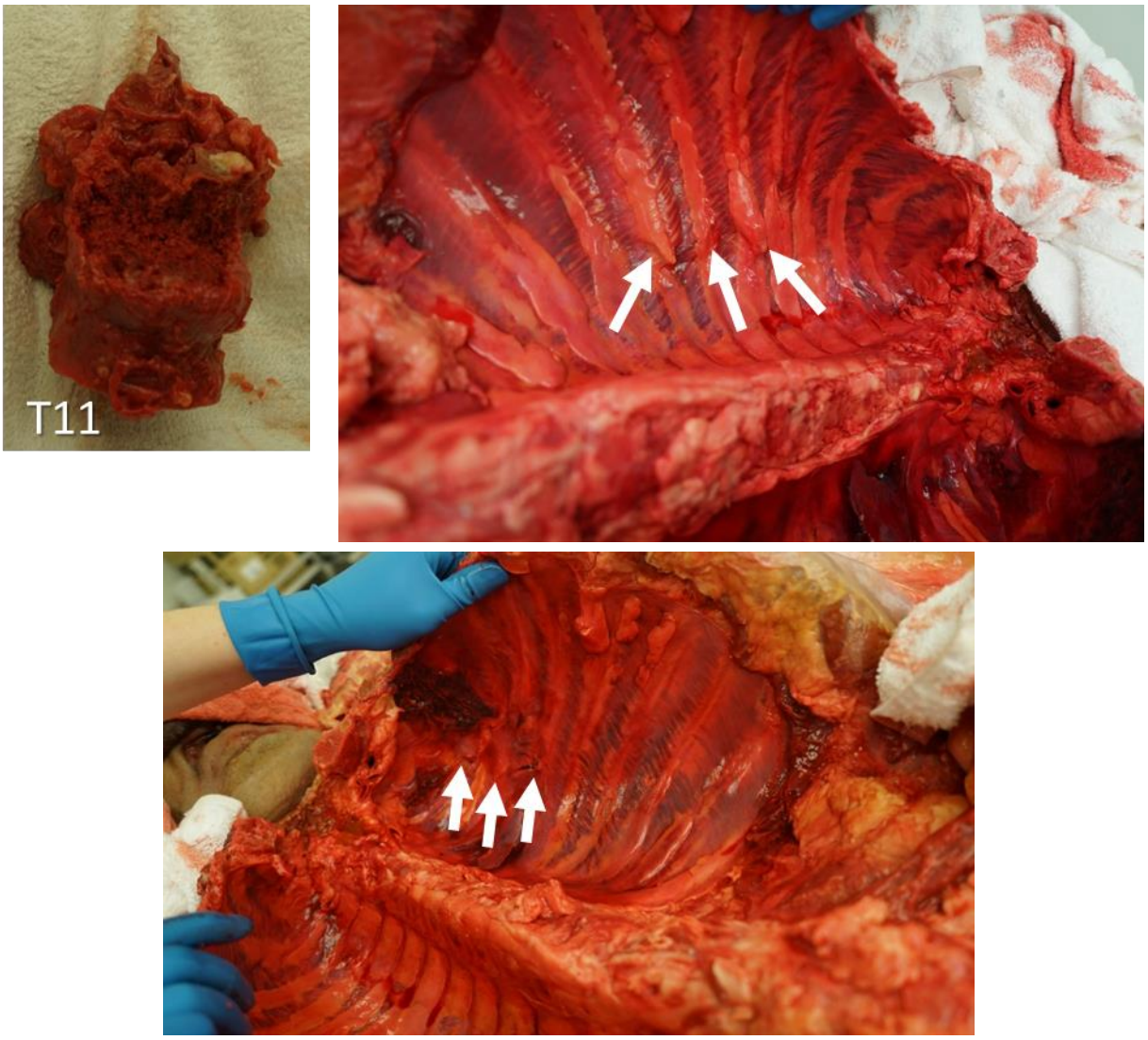

Figure A-10. WS10-001 thoracic spine fractures

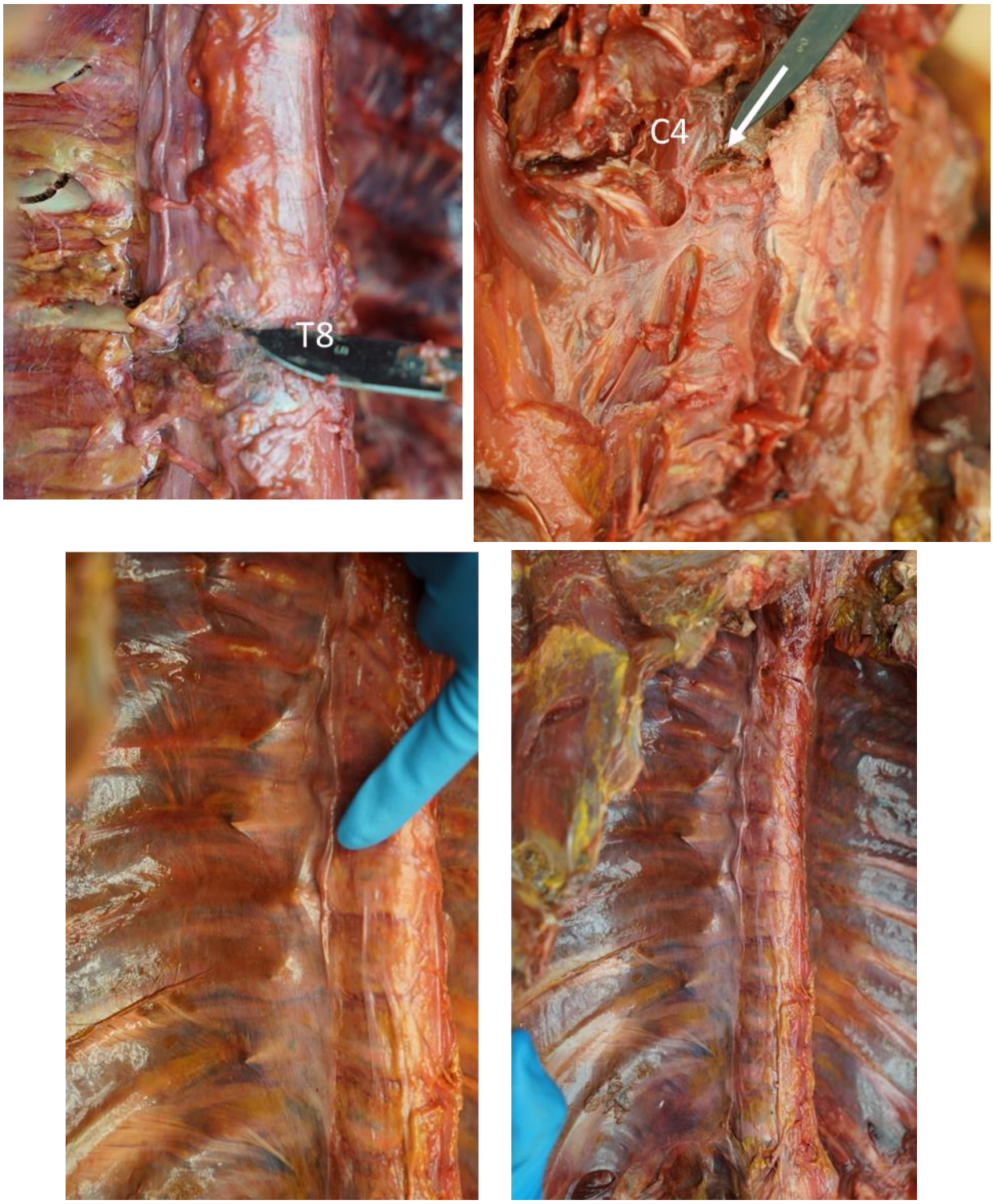

Figure A-11. WS10-002 thoracic spine fractures

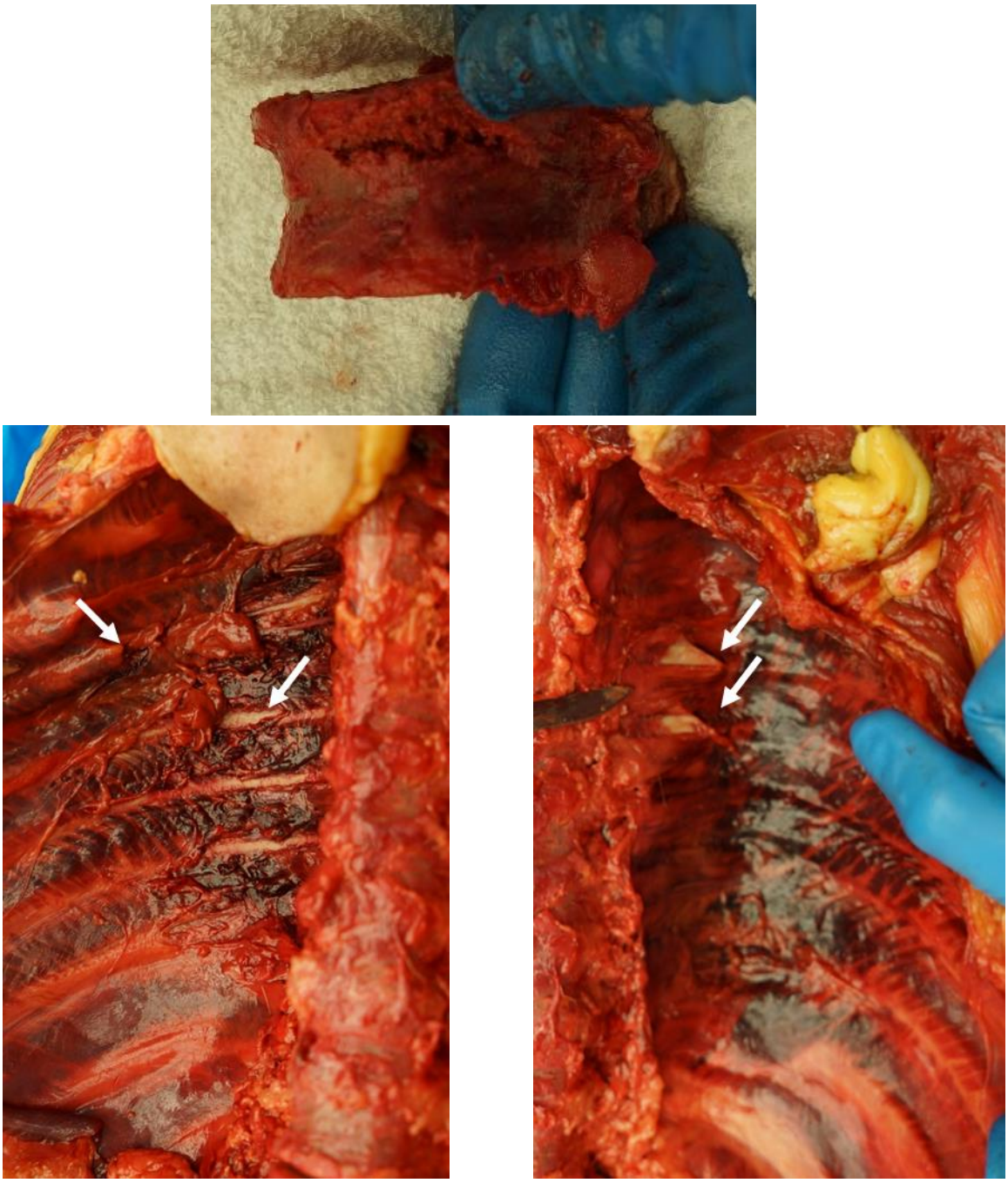

Figure A-12. WS12-03 thoracic spine fractures

Appendix B – Supplementary Information from WS11 Tests

B.1 Subject Anthropometry

Table B-1. WS11-01 Subject Anthropometry

Cadaver #	**L171491**	Forearm Hand Length (cm)	37.6
Gender	M	Ankle Height (cm)	9.5
Age (years)	62		
Weight (kg)	85	Left Foot Length (cm)	23.6
Stature (cm)	170.5	Right Foot Length (cm)	23.5
Shoulder Height (cm)	143.9	Avg Foot Length (cm)	23.55
Vertex To Symphysis (cm)	87.6	Waist Back Length (cm)	58
Waist Height (cm)	94.3	Bicep Circumference (cm)	32.65
Crotch Height (cm)	84	Elbow Circumference (cm)	30.2
Tibial Height (cm)	46	Forearm Circumference (cm)	29.4
Head To Trochanter (cm)	87.25	Wrist Circumference (cm)	17.5
Vertex To Mentum (cm)	21.8	Thigh Circumference (cm)	63.8
Head Breadth (cm)	16.7	Lower Thigh Circumference (cm)	42.9
Bizygomatic Breadth (cm)	12.8	Knee Circumference (cm)	43.5
Biacromial Breadth (cm)	36.2	Calf Circumference (cm)	34.5
Chest Breadth (cm)	31.75	Ankle Circumference (cm)	24.15
Waist Breadth (cm)	32.3	Neck Circumference (cm)	45.7
Hip Breadth (cm)	39.5	Scye To Shoulder Circ. (cm)	42.8
Trochanter Breadth (cm)	40.4	Chest Circumference (cm)	100.6
Left Foot Breadth (cm)	7.7	Waist Circumference (cm)	98.5
Right Foot Breadth (cm)	7.7	Buttock Circumference (cm)	106.2
Avg Foot Breadth (cm)	7.7	Chest Depth (cm)	22.8
Head Length (cm)	19	Waist Depth (cm)	22.3
Menton-Sellion Length (cm)	10.8	Buttock Depth (cm)	22.5
Shoulder To Elbow (cm)	36.35		
Seated Measurements		**PPE Full Body Anthropometry**	
Biacromial Breadth (cm)	42.5	Chest Depth (cm)	33.5
Bideltoid Breadth (cm)	57.5	Waist Depth (cm)	36.5
Buttock-Knee Length (cm)	56.1	Chest Circumference (cm)	147
Hip Breadth Sitting (cm)	40.5	Chest Breadth (cm)	35.6
Knee Height Sitting (cm)	42.15	Waist Breadth (cm)	34.5
Sitting Height (cm)	92.5		

Table B-2. WS11-02 Subject Anthropometry

Cadaver #	**S172105**	Forearm Hand Length (cm)	NA
Gender	Male	Ankle Height (cm)	9.85
Age (years)	35		
Weight (kg)	56.7	Left Foot Length (cm)	23.5
Stature (cm)	165.65	Right Foot Length (cm)	23.6
Shoulder Height (cm)	142	Avg Foot Length (cm)	23.55
Vertex To Symphysis (cm)	79.5	Waist Back Length (cm)	62.4
Waist Height (cm)	91.2	Bicep Circumference (cm)	26.25
Crotch Height (cm)	81.45	Elbow Circumference (cm)	NA
Tibial Height (cm)	37.45	Forearm Circumference (cm)	NA
Head To Trochanter (cm)	80.6	Wrist Circumference (cm)	NA
Vertex To Mentum (cm)	17.5	Thigh Circumference (cm)	47.5
Head Breadth (cm)	13.1	Lower Thigh Circumference (cm)	33.65
Bizygomatic Breadth (cm)	13.2	Knee Circumference (cm)	37.55
Biacromial Breadth (cm)	29.5	Calf Circumference (cm)	31.7
Chest Breadth (cm)	28.5	Ankle Circumference (cm)	22.25
Waist Breadth (cm)	22.5	Neck Circumference (cm)	38.5
Hip Breadth (cm)	34.7	Scye To Shoulder Circ. (cm)	39.7
Trochanter Breadth (cm)	32.8	Chest Circumference (cm)	92
Left Foot Breadth (cm)	7.6	Waist Circumference (cm)	80.9
Right Foot Breadth (cm)	7.5	Buttock Circumference (cm)	86.3
Avg Foot Breadth (cm)	7.55	Chest Depth (cm)	23.5
Head Length (cm)	17.5	Waist Depth (cm)	16.7
Menton-Sellion Length (cm)	12.3	Buttock Depth (cm)	18.5
Shoulder To Elbow (cm)	33.3		
Seated Measurements		**PPE Full Body Anthropometry**	
Biacromial Breadth (cm)	38.5	Chest Depth (cm)	28.4
Bideltoid Breadth (cm)	43.5	Waist Depth (cm)	37.6
Buttock-Knee Length (cm)	52.5	Chest Circumference (cm)	142.7
Hip Breadth Sitting (cm)	32.5	Chest Breadth (cm)	30.2
Knee Height Sitting (cm)	47	Waist Breadth (cm)	29.9
Sitting Height (cm)	99.5		

Table B-3. WS11-03 Subject Anthropometry

Cadaver #	**S160979**	Forearm Hand Length (cm)	NA
Gender	Male	Ankle Height (cm)	9.55
Age (years)	61		
Weight (kg)	91.6	Left Foot Length (cm)	25.7
Stature (cm)	175.5	Right Foot Length (cm)	25.7
Shoulder Height (cm)	151	Avg Foot Length (cm)	25.7
Vertex To Symphysis (cm)	86.6	Waist Back Length (cm)	61
Waist Height (cm)	99.3	Bicep Circumference (cm)	34.05
Crotch Height (cm)	89.5	Elbow Circumference (cm)	NA
Tibial Height (cm)	49.25	Forearm Circumference (cm)	NA
Head To Trochanter (cm)	88.6	Wrist Circumference (cm)	NA
Vertex To Mentum (cm)	24	Thigh Circumference (cm)	61.1
Head Breadth (cm)	12.6	Lower Thigh Circumference (cm)	46.7
Bizygomatic Breadth (cm)	11.4	Knee Circumference (cm)	44.35
Biacromial Breadth (cm)	31.5	Calf Circumference (cm)	42.2
Chest Breadth (cm)	33	Ankle Circumference (cm)	27.4
Waist Breadth (cm)	35.3	Neck Circumference (cm)	46.2
Hip Breadth (cm)	37.2	Scye To Shoulder Circ. (cm)	42.7
Trochanter Breadth (cm)	37.5	Chest Circumference (cm)	113.7
Left Foot Breadth (cm)	9.5	Waist Circumference (cm)	100.5
Right Foot Breadth (cm)	9.5	Buttock Circumference (cm)	101.7
Avg Foot Breadth (cm)	9.5	Chest Depth (cm)	27.6
Head Length (cm)	20	Waist Depth (cm)	24.6
Menton-Sellion Length (cm)	11.8	Buttock Depth (cm)	22.7
Shoulder To Elbow (cm)	32.85		
Seated Measurements		**PPE Full Body Anthropometry**	
Biacromial Breadth (cm)	40.5	Chest Depth (cm)	34.6
Bideltoid Breadth (cm)	51.3	Waist Depth (cm)	33.4
Buttock-Knee Length (cm)	48.3	Chest Circumference (cm)	136
Hip Breadth Sitting (cm)	36.8	Chest Breadth (cm)	36.3
Knee Height Sitting (cm)	51.95	Waist Breadth (cm)	34.4
Sitting Height (cm)	97.6		

B.2 Pre- vs. Posttest Radiology

B.2.1 Pelvis Injuries

Table B-4. WS11-01 Pelvis Injuries

	Pretest	Posttest
Sacrum Sagittal View	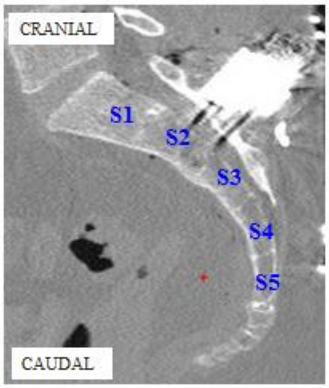	

B.2.2 Spine Injuries

Table B-5. WS11-03 Lumbar Spine Injuries

	Pretest	Posttest
L1 Sagittal View	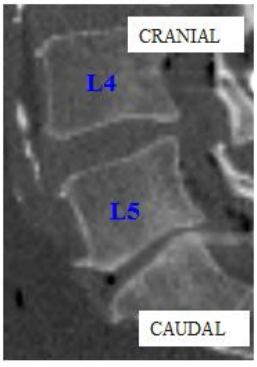	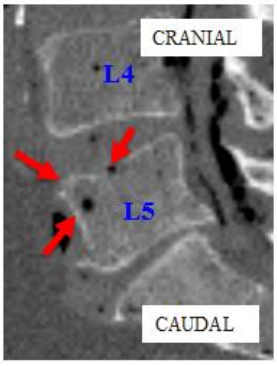

Table B-6. WS11-01 Thoracic Spine Injuries

	Pretest	Posttest
T4-T5 Sagittal View	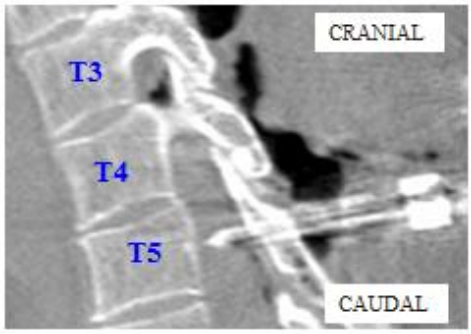	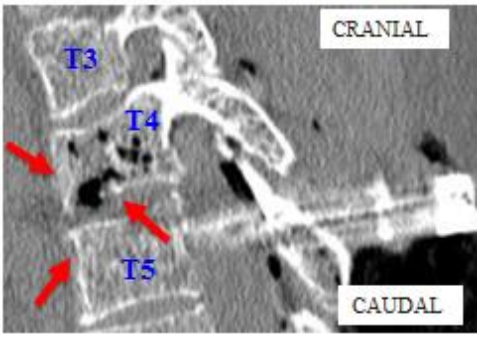
T10 Sagittal View	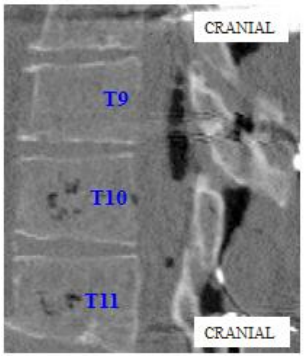	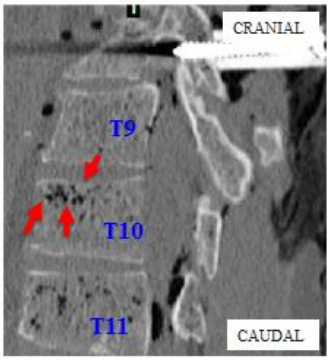

Table B-7. WS11-02 Thoracic Spine Injuries

	Pretest	Posttest
T5-T6 Sagittal View	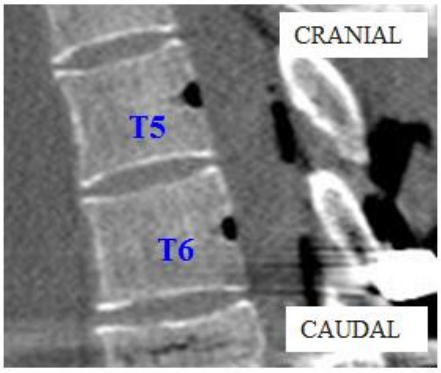	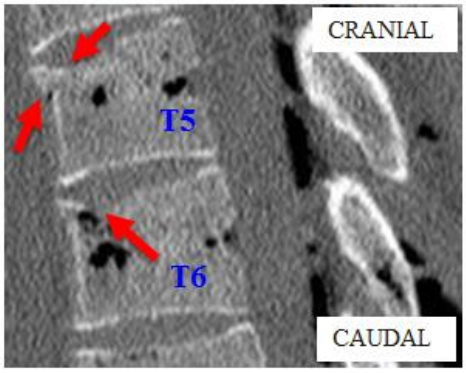

Table B-8. WS11-03 Thoracic Spine Injuries

	Pretest	Posttest
T4-T5 Sagittal View	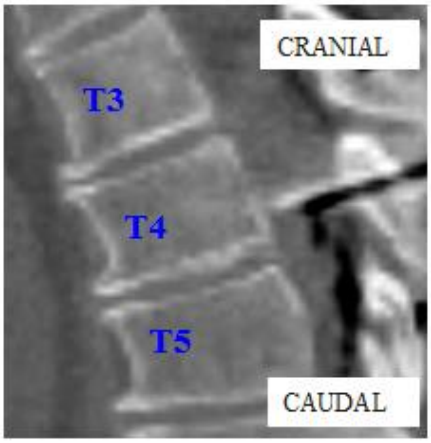	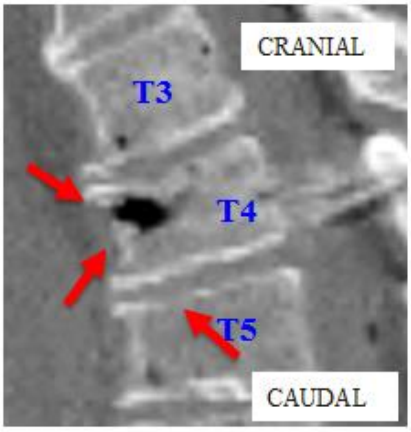
T7-T8 Sagittal View	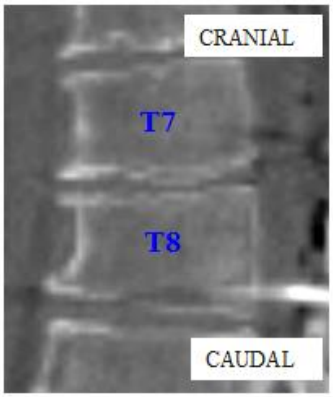	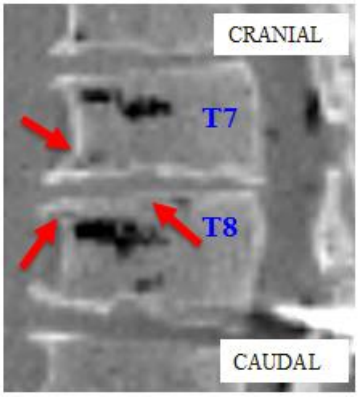

B.3 Injury Images

B.3.1 Pelvis

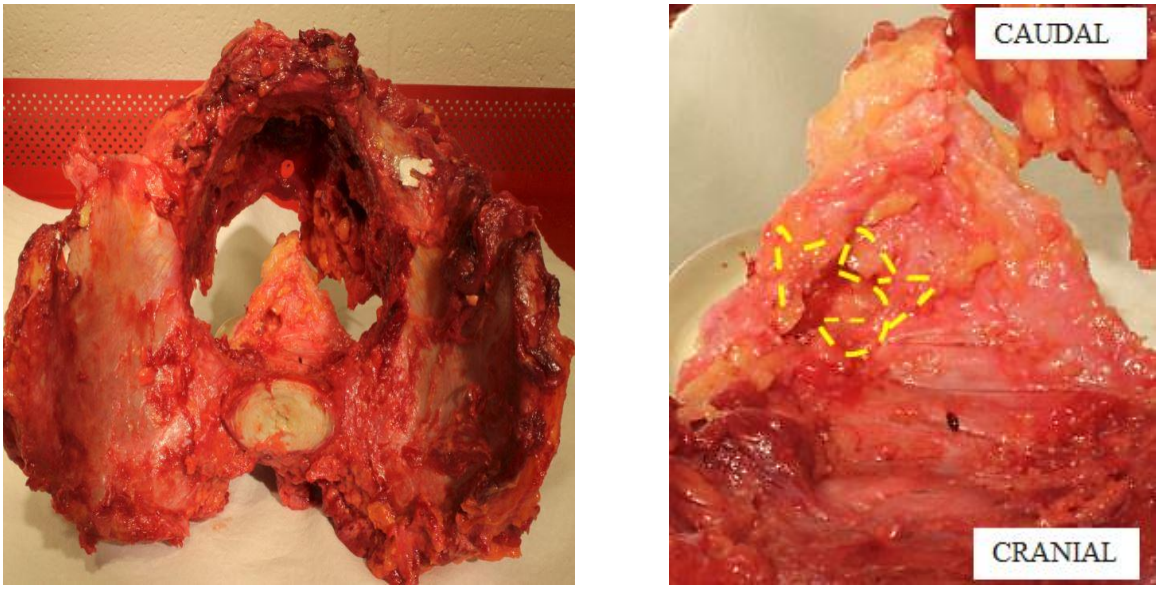

Figure B-1. WS11-01 pelvis fractures

B.3.2 Spine

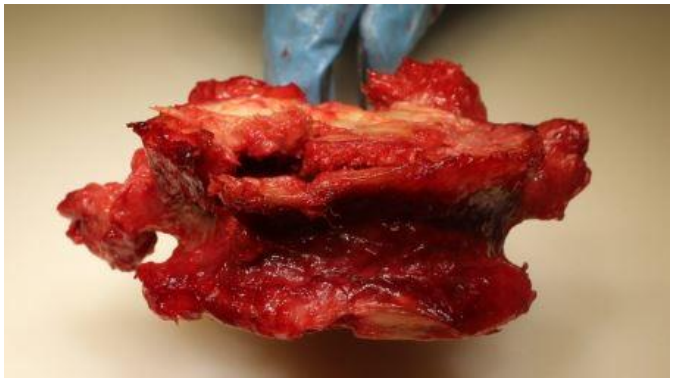

Figure B-2. WS11-03 lumbar spine fractures

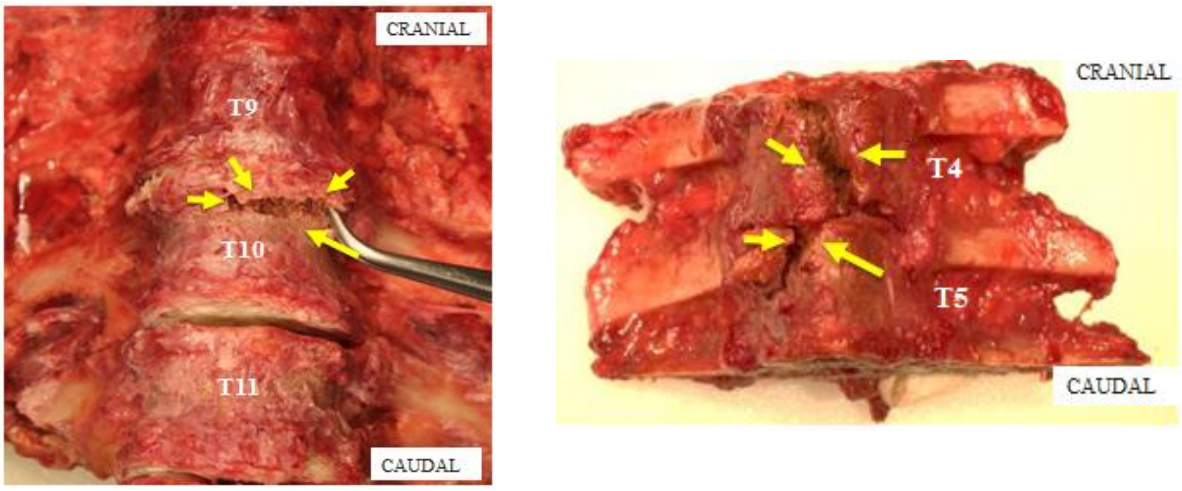

Figure B-3. WS11-01 thoracic spine fractures

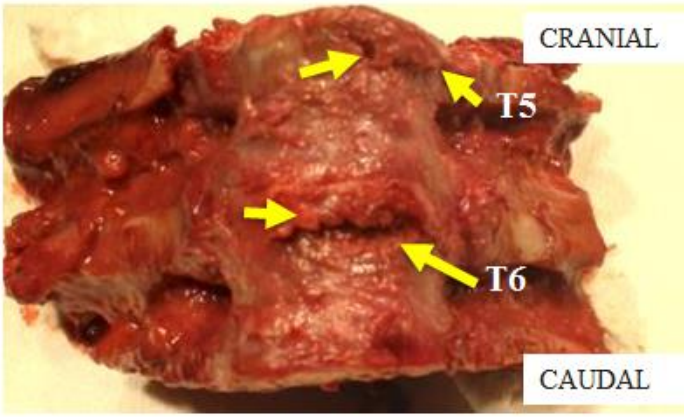

Figure B-4. WS11-02 thoracic spine fractures

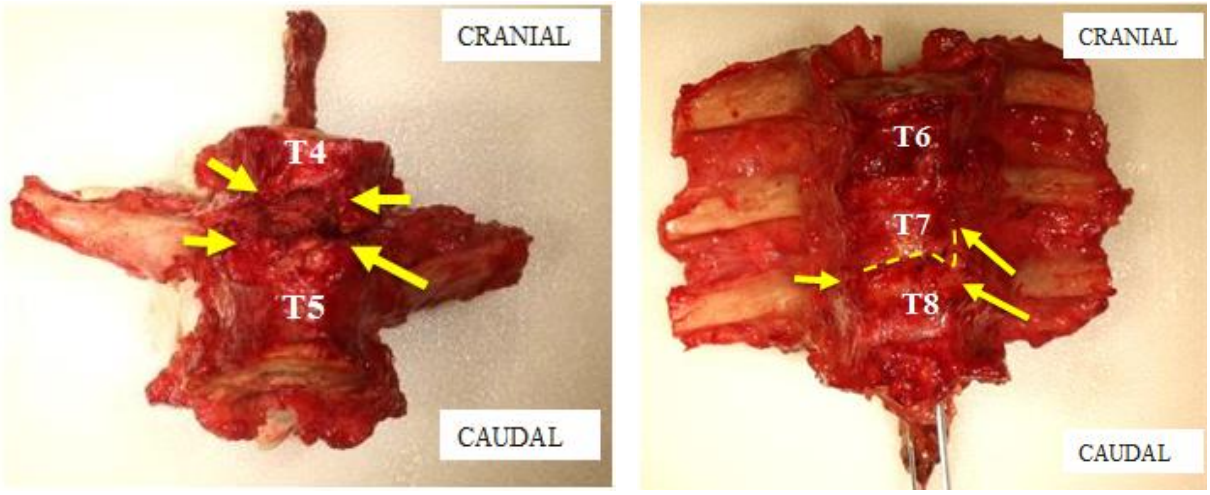

Figure B-5. WS11-03 thoracic spine fractures

Appendix C – Supplementary Information from WS12 Tests

C.1 Subject Anthropometry

Table C-1. WS10-003 Subject Anthropometry

Cadaver #	**35249**	Forearm Hand Length (cm)	46.2
Gender	M	Ankle Height (cm)	10.1
Age (years)	23.0		
Weight (kg)	72.0	Left Foot Length (cm)	25.1
Stature (cm)	172.3	Right Foot Length (cm)	25.0
Shoulder Height (cm)	147.9	Avg Foot Length (cm)	25.1
Vertex To Symphysis (cm)	86.0	Waist Back Length (cm)	
Waist Height (cm)	95.7	Bicep Circumference (cm)	26.5
Crotch Height (cm)	79.4	Elbow Circumference (cm)	25.0
Tibial Height (cm)	45.0	Forearm Circumference (cm)	24.2
Head To Trochanter (cm)	84.0	Wrist Circumference (cm)	16.7
Vertex To Mentum (cm)	20.8	Thigh Circumference (cm)	52.2
Head Breadth (cm)	14.3	Lower Thigh Circumference (cm)	38.2
Bizygomatic Breadth (cm)	17.8	Knee Circumference (cm)	37.5
Biacromial Breadth (cm)	30.7	Calf Circumference (cm)	32.9
Chest Breadth (cm)	29.8	Ankle Circumference (cm)	21.7
Waist Breadth (cm)	23.2	Neck Circumference (cm)	39.0
Hip Breadth (cm)	29.3	Scye To Shoulder Circ. (cm)	42.6
Trochanter Breadth (cm)	33.0	Chest Circumference (cm)	88.0
Left Foot Breadth (cm)	8.1	Waist Circumference (cm)	83.2
Right Foot Breadth (cm)	8.3	Buttock Circumference (cm)	90.0
Avg Foot Breadth (cm)	8.2	Chest Depth (cm)	22.2
Head Length (cm)	19.4	Waist Depth (cm)	16.7
Menton-Sellion Length (cm)	13.8	Buttock Depth (cm)	19.1
Shoulder To Elbow (cm)	36.3		
Seated Measurements		**PPE Full Body Anthropometry**	
Biacromial Breadth (cm)	38.4	Chest Depth (cm)	40.9
Bideltoid Breadth (cm)	43.2	Waist Depth (cm)	41.7
Buttock-Knee Length (cm)	57.7	Chest Circumference (cm)	129.7
Hip Breadth Sitting (cm)	37.6	Chest Breadth (cm)	30.6
Knee Height Sitting (cm)	53.2	Waist Breadth (cm)	39.9
Sitting Height (cm)	86.9		

Table C-2. WS10-003 Subject Anthropometry

Cadaver #	**L162663**	Forearm Hand Length (cm)	--
Gender	M	Ankle Height (cm)	12.0
Age (years)	75.0		
Weight (kg)	72.6	Left Foot Length (cm)	26.2
Stature (cm)	178.8	Right Foot Length (cm)	26.0
Shoulder Height (cm)	157.1	Avg Foot Length (cm)	26.1
Vertex To Symphysis (cm)	87.0	Waist Back Length (cm)	57.0
Waist Height (cm)	102.1	Bicep Circumference (cm)	30.1
Crotch Height (cm)	85.3	Elbow Circumference (cm)	--
Tibial Height (cm)	47.9	Forearm Circumference (cm)	--
Head To Trochanter (cm)	85.7	Wrist Circumference (cm)	--
Vertex To Mentum (cm)	22.7	Thigh Circumference (cm)	54.5
Head Breadth (cm)	15.7	Lower Thigh Circumference (cm)	41.0
Bizygomatic Breadth (cm)	11.6	Knee Circumference (cm)	42.5
Biacromial Breadth (cm)	31.8	Calf Circumference (cm)	34.1
Chest Breadth (cm)	30.7	Ankle Circumference (cm)	25.2
Waist Breadth (cm)	23.5	Neck Circumference (cm)	45.4
Hip Breadth (cm)	28.5	Scye To Shoulder Circ. (cm)	41.7
Trochanter Breadth (cm)	34.3	Chest Circumference (cm)	90.8
Left Foot Breadth (cm)	9.5	Waist Circumference (cm)	91.8
Right Foot Breadth (cm)	9.2	Buttock Circumference (cm)	97.4
Avg Foot Breadth (cm)	9.4	Chest Depth (cm)	21.7
Head Length (cm)	18.5	Waist Depth (cm)	17.3
Menton-Sellion Length (cm)	12.7	Buttock Depth (cm)	20.3
Shoulder To Elbow (cm)	36.9		
Seated Measurements		**PPE Full Body Anthropometry**	
Biacromial Breadth (cm)	40.2	Chest Depth (cm)	36.7
Bideltoid Breadth (cm)	43.0	Waist Depth (cm)	44.3
Buttock-Knee Length (cm)	64.9	Chest Circumference (cm)	119.5
Hip Breadth Sitting (cm)	37.4	Chest Breadth (cm)	29.6
Knee Height Sitting (cm)	55.4	Waist Breadth (cm)	41.2
Sitting Height (cm)	83.6		

Table C-3. WS10-003 Subject Anthropometry

Cadaver #	**L170249**	Forearm Hand Length (cm)	-
Gender	M	Ankle Height (cm)	12.2
Age (years)	79.0		
Weight (kg)	69.4	Left Foot Length (cm)	24.9
Stature (cm)	171.6	Right Foot Length (cm)	24.5
Shoulder Height (cm)	149.7	Avg Foot Length (cm)	24.7
Vertex To Symphysis (cm)	83.7	Waist Back Length (cm)	53.0
Waist Height (cm)	95.7	Bicep Circumference (cm)	29.4
Crotch Height (cm)	80.1	Elbow Circumference (cm)	-
Tibial Height (cm)	46.0	Forearm Circumference (cm)	-
Head To Trochanter (cm)	80.9	Wrist Circumference (cm)	-
Vertex To Mentum (cm)	21.2	Thigh Circumference (cm)	48.2
Head Breadth (cm)	16.0	Lower Thigh Circumference (cm)	36.6
Bizygomatic Breadth (cm)	11.4	Knee Circumference (cm)	38.1
Biacromial Breadth (cm)	32.5	Calf Circumference (cm)	31.4
Chest Breadth (cm)	32.3	Ankle Circumference (cm)	21.5
Waist Breadth (cm)	24.3	Neck Circumference (cm)	40.4
Hip Breadth (cm)	32.1	Scye To Shoulder Circ. (cm)	44.5
Trochanter Breadth (cm)	32.4	Chest Circumference (cm)	95.8
Left Foot Breadth (cm)	8.4	Waist Circumference (cm)	88.4
Right Foot Breadth (cm)	8.5	Buttock Circumference (cm)	91.0
Avg Foot Breadth (cm)	8.5	Chest Depth (cm)	22.3
Head Length (cm)	19.3	Waist Depth (cm)	16.8
Menton-Sellion Length (cm)	11.4	Buttock Depth (cm)	19.5
Shoulder To Elbow (cm)	34.4		
Seated Measurements		**PPE Full Body Anthropometry**	
Biacromial Breadth (cm)	36.2	Chest Depth (cm)	39.4
Bideltoid Breadth (cm)	43.4	Waist Depth (cm)	42.8
Buttock-Knee Length (cm)	56.4	Chest Circumference (cm)	141.5
Hip Breadth Sitting (cm)	37.2	Chest Breadth (cm)	31.2
Knee Height Sitting (cm)	56.2	Waist Breadth (cm)	45.4
Sitting Height (cm)	84.2		

C.2 Pre- vs. Posttest Radiology

C.2.1 Foot/Ankle Extremity Injuries

Table C-4. WS12-02 Lower Extremity Injuries

	Pretest	Posttest
Right Calcaneus Axial View	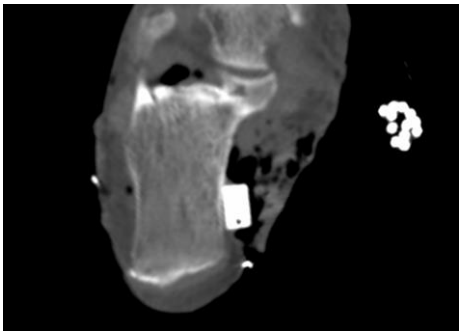	

Table C-5. WS12-03 Lower Extremity Injuries

	Pretest	Posttest
Left Calcaneus Axial View	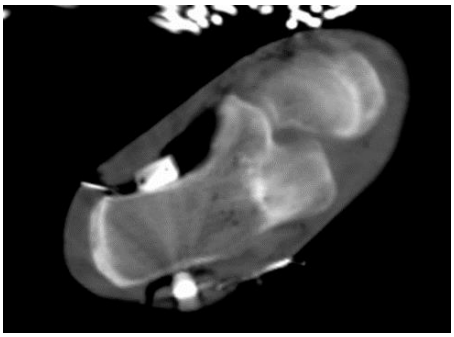	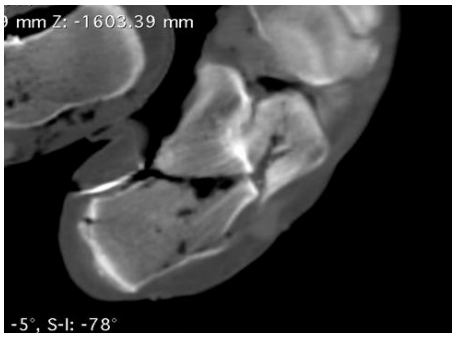

C.2.2 Pelvis Injuries

Table C-6. WS12-01 Pelvis Injuries

	Pretest	Posttest
Sacrum Axial View	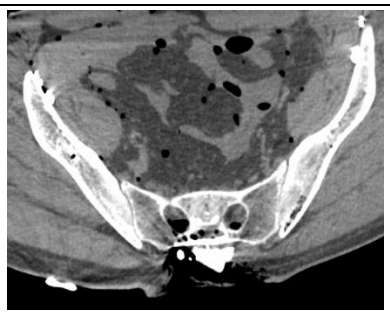	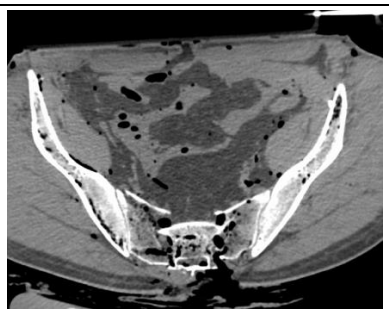
Sacrum Sagittal View	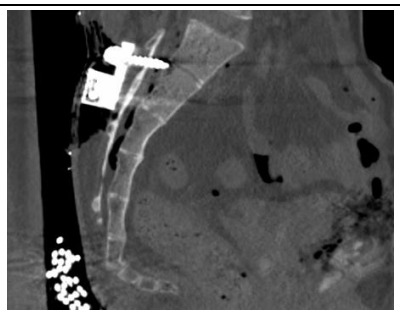	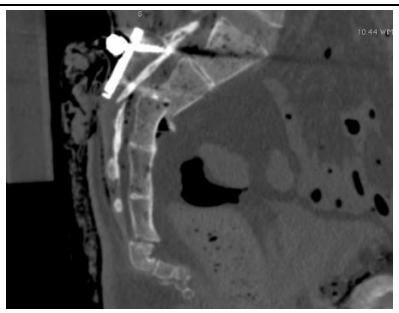

Table C-7. WS12-02 Pelvis Injuries

	Pretest	Posttest
Sacrum Coronal View	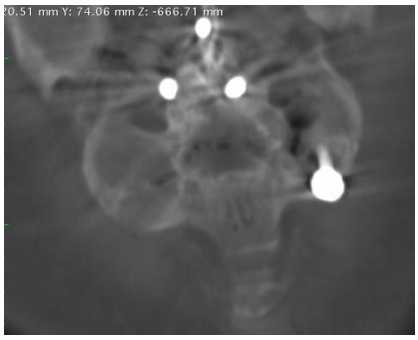	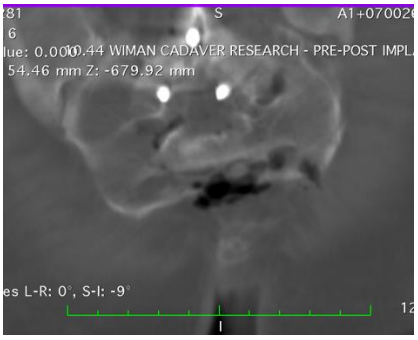
Sacrum Sagittal View	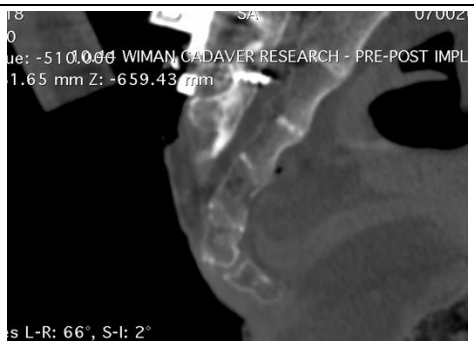	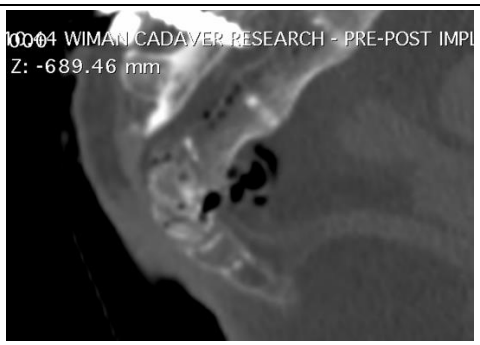

Table C-8. WS12-03 Pelvis Injuries

	Pretest	Posttest
Sacrum Sagittal View		
Left Iliac Wing Sagittal View	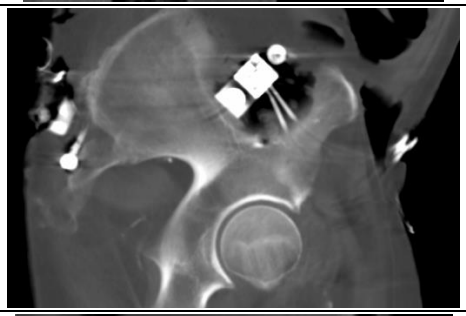	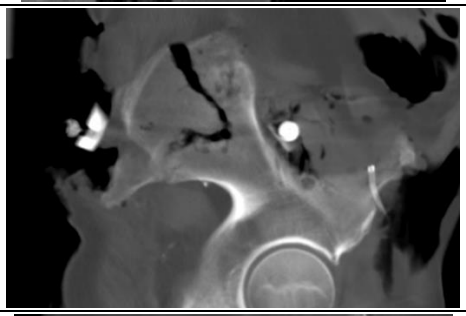
Right Iliac Wing Coronal View		
Right Pubic Ramus Axial View		
Right Ischial Tuberosity Coronal View	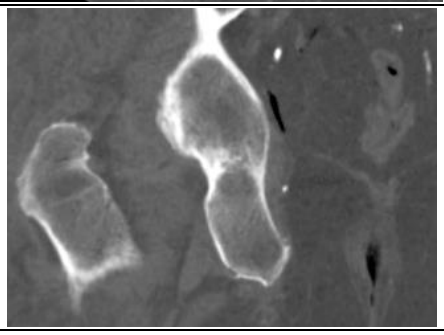	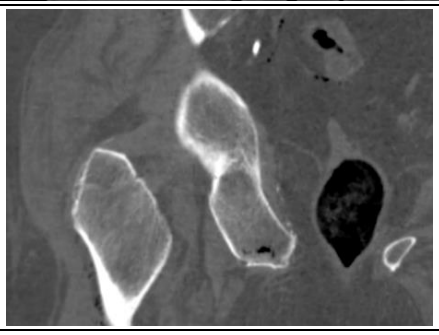

C.2.3 Spine Injuries

Table C-9. WS12-02 Lumbar Spine Injuries

	Pretest	Posttest
L1 Sagittal View	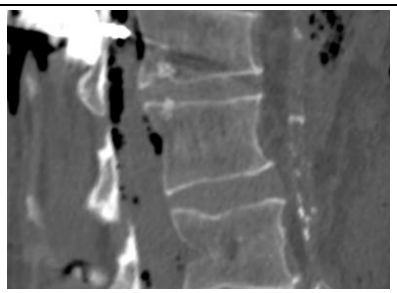	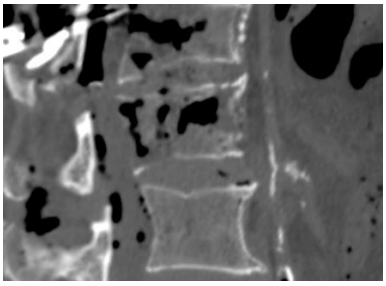
L1 Coronal View		

Table C-10. WS12-03 Lumbar Spine Injuries

	Pretest	Posttest
L1 Axial View	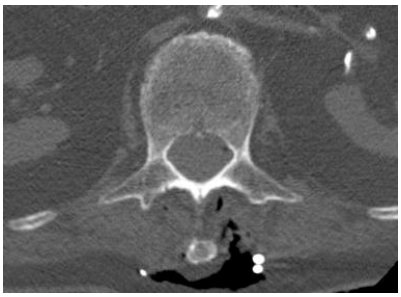	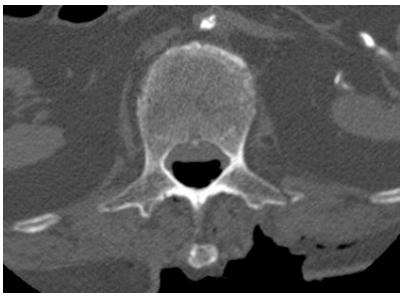
L4 Axial View	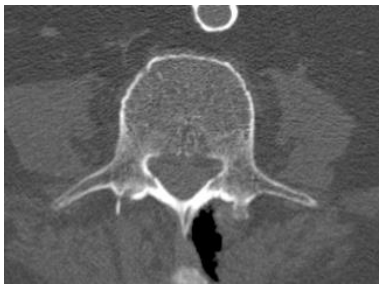	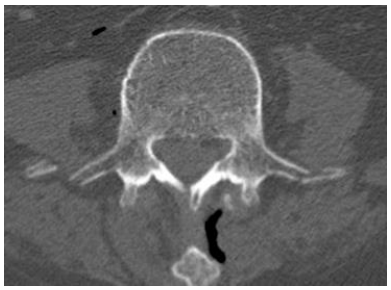

Table C-10. WS12-03 Lumbar Spine Injuries (continued)

	Pretest	Posttest
L5 Axial View	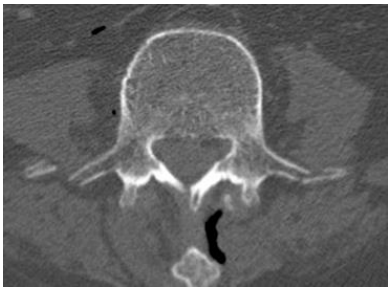	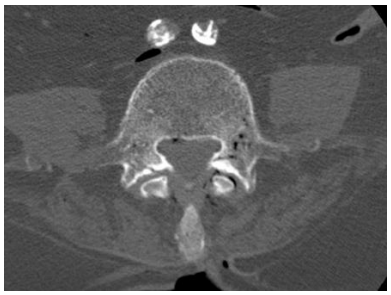

Table C-11. WS12-01 Thoracic Spine Injuries

	Pretest	Posttest
T6 Sagittal View	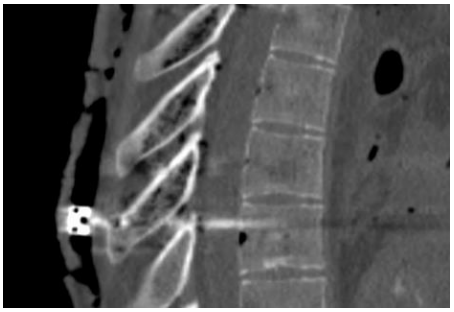	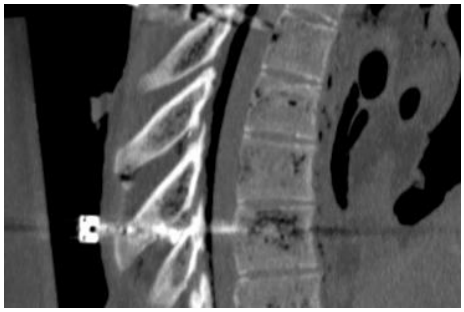

Table C-12. WS12-02 Thoracic Spine Injuries

	Pretest	Posttest
T12 Sagittal View	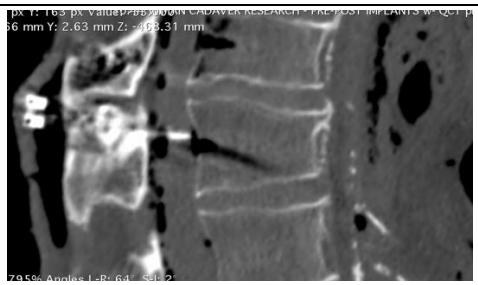	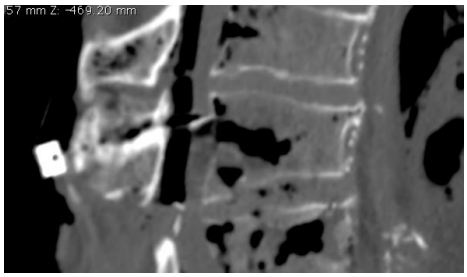
T12 Sagittal View	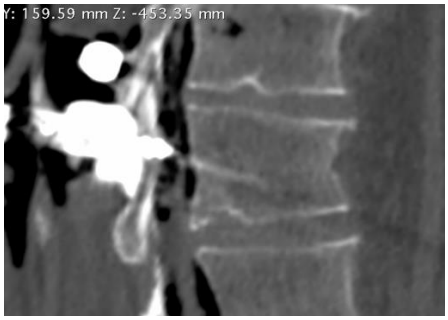	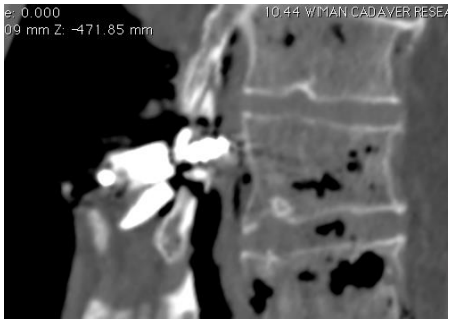
T12 Axial View	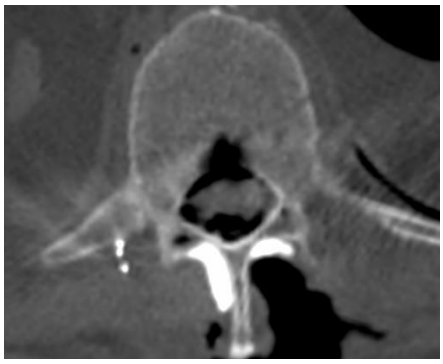	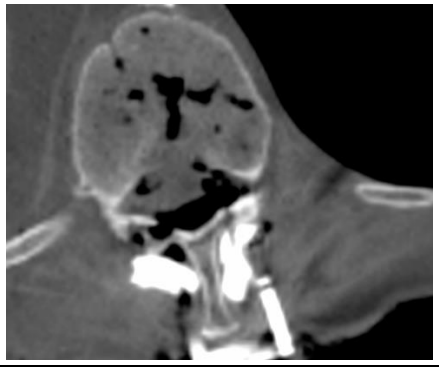

Table C-13. WS12-03 Thoracic Spine Injuries

	Pretest	Posttest
Right Rib 2 Axial View	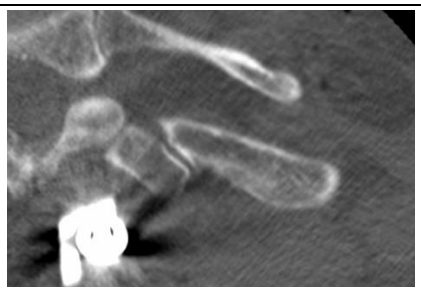	
T2/T3 Spinous Process Sagittal View	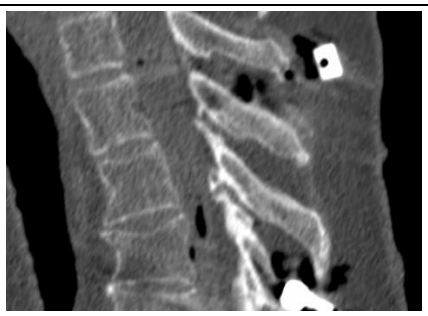	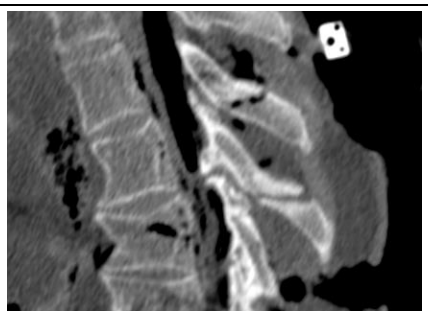
T4 Sagittal View	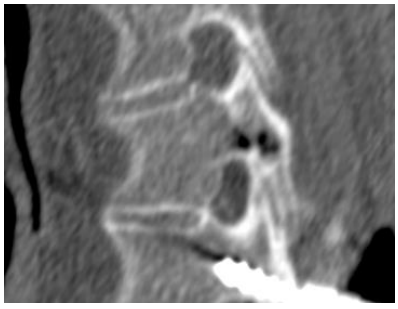	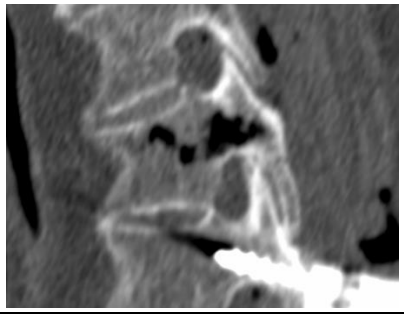
T4 Axial View	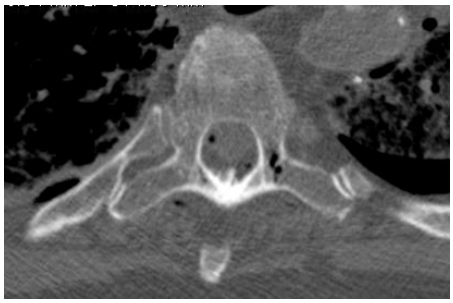	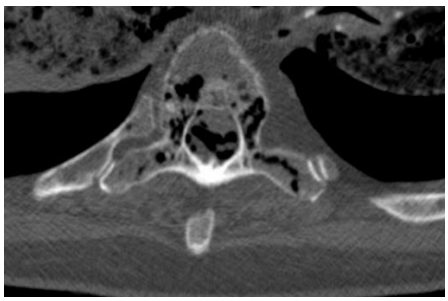
T12 Sagittal View	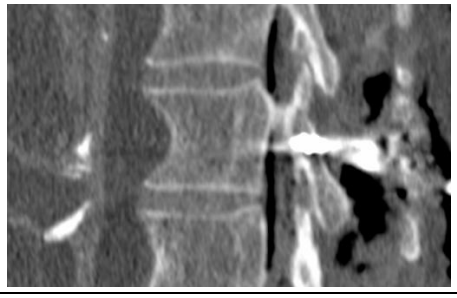	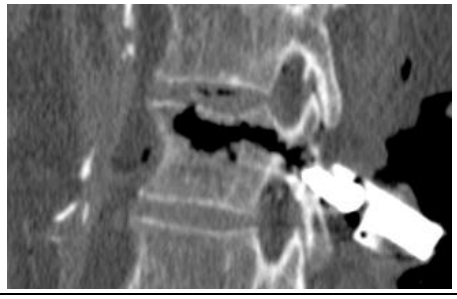

C.3 Injury Images

C.3.1 Foot/Ankle

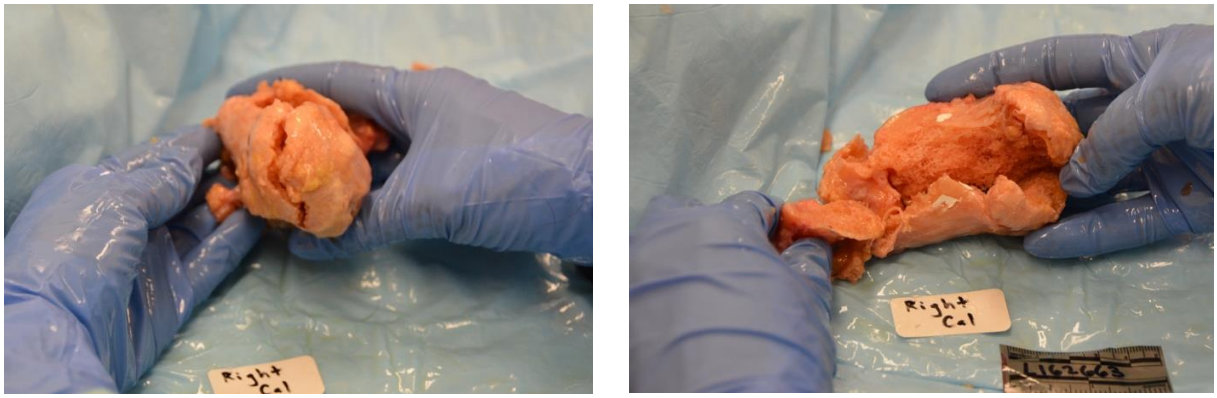

Figure C-1. WS12-02 lower extremity fractures

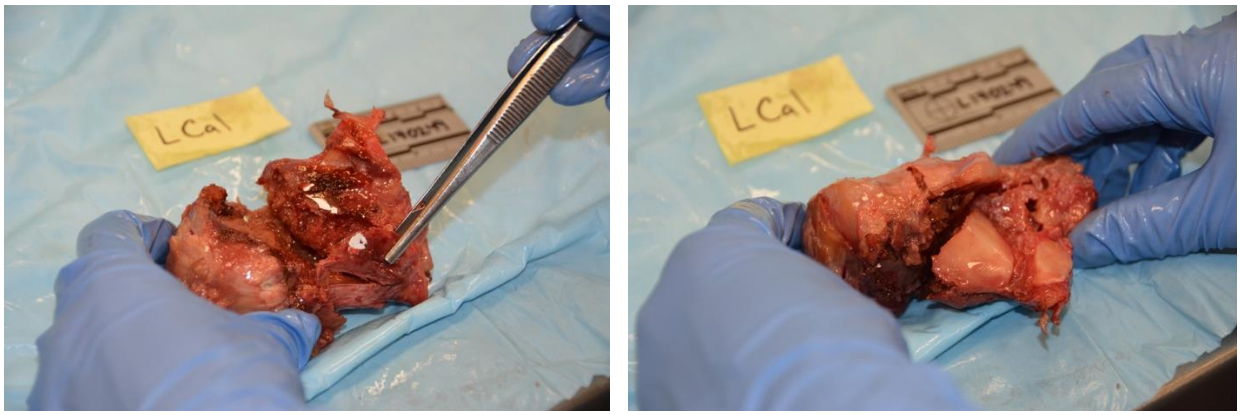

Figure C-2. WS12-03 lower extremity fractures

C.3.2 Pelvis

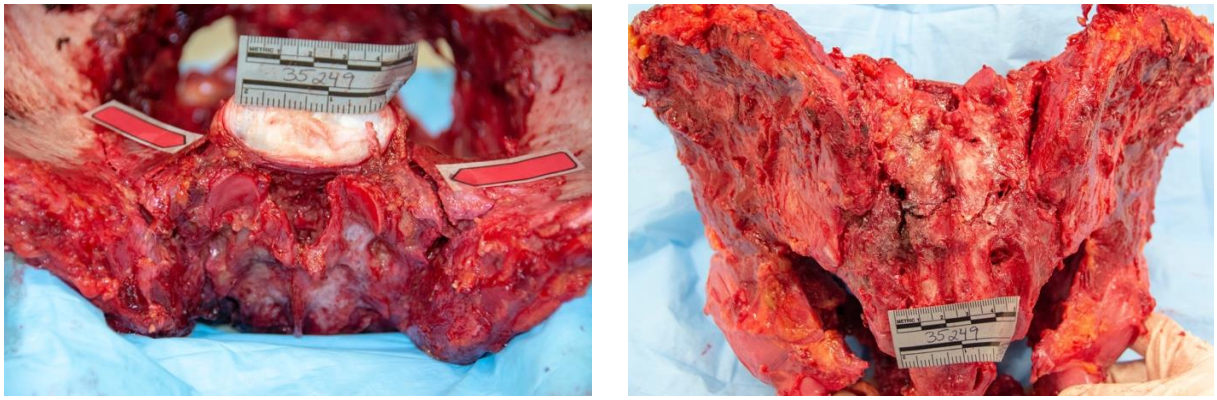

Figure C-3. WS12-01 pelvis fractures

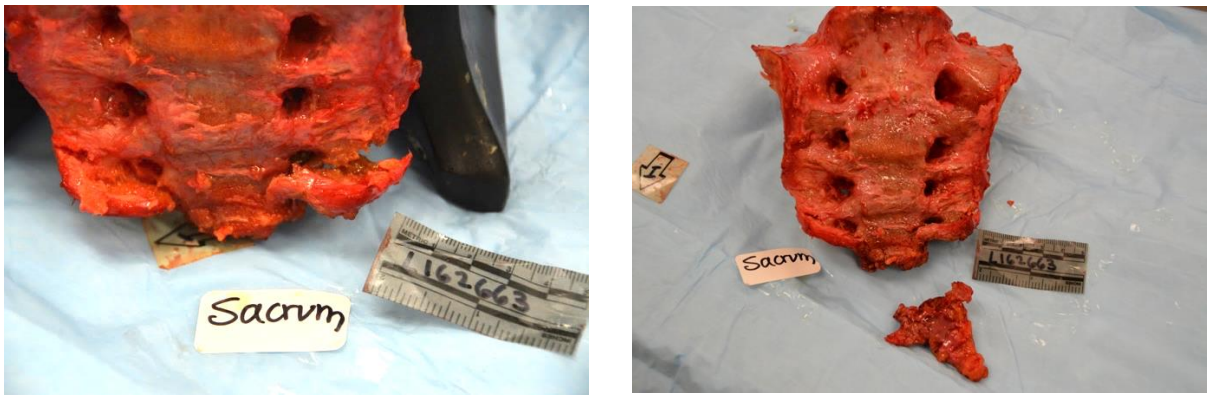

Figure C-4. WS12-02 pelvis fractures

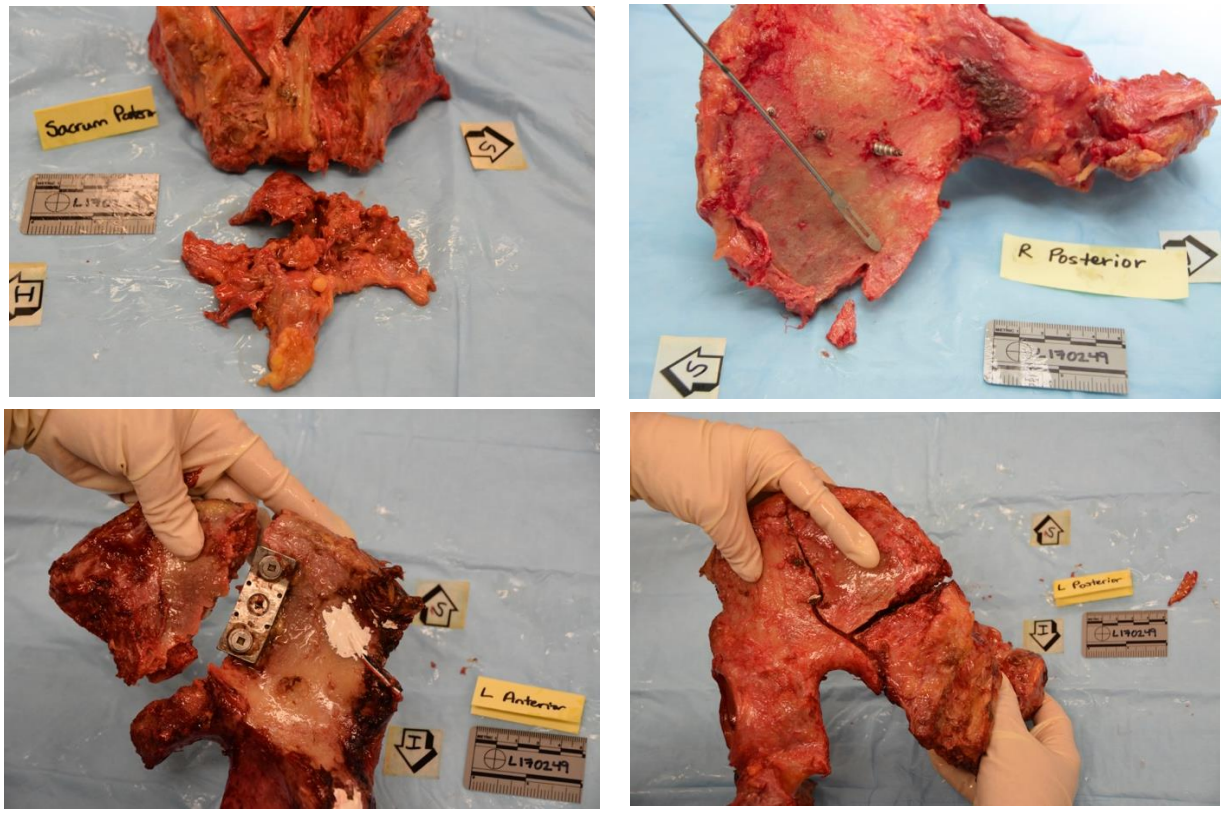

Figure C-5. WS12-03 pelvis fractures

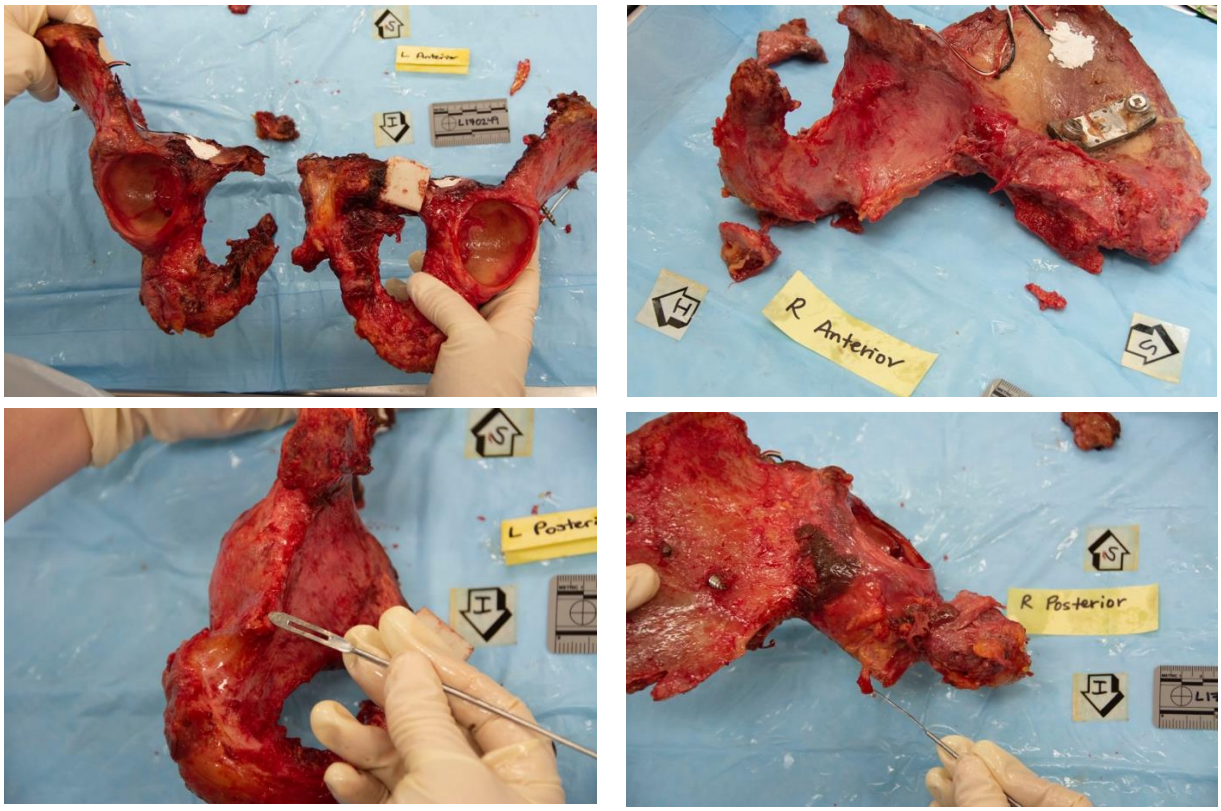

Figure C-5. WS12-03 pelvis fractures (continued)

C.3.3 Spine

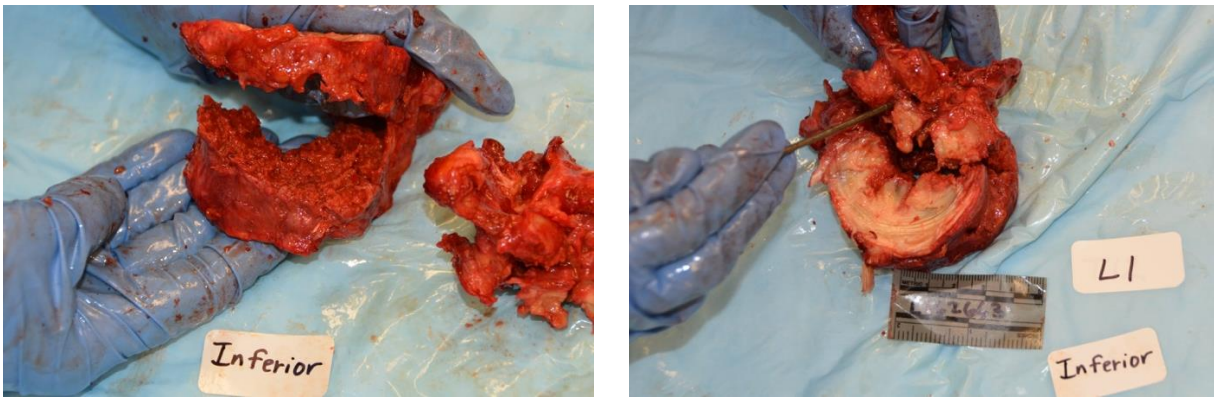

Figure C-6. WS12-02 lumbar spine fractures

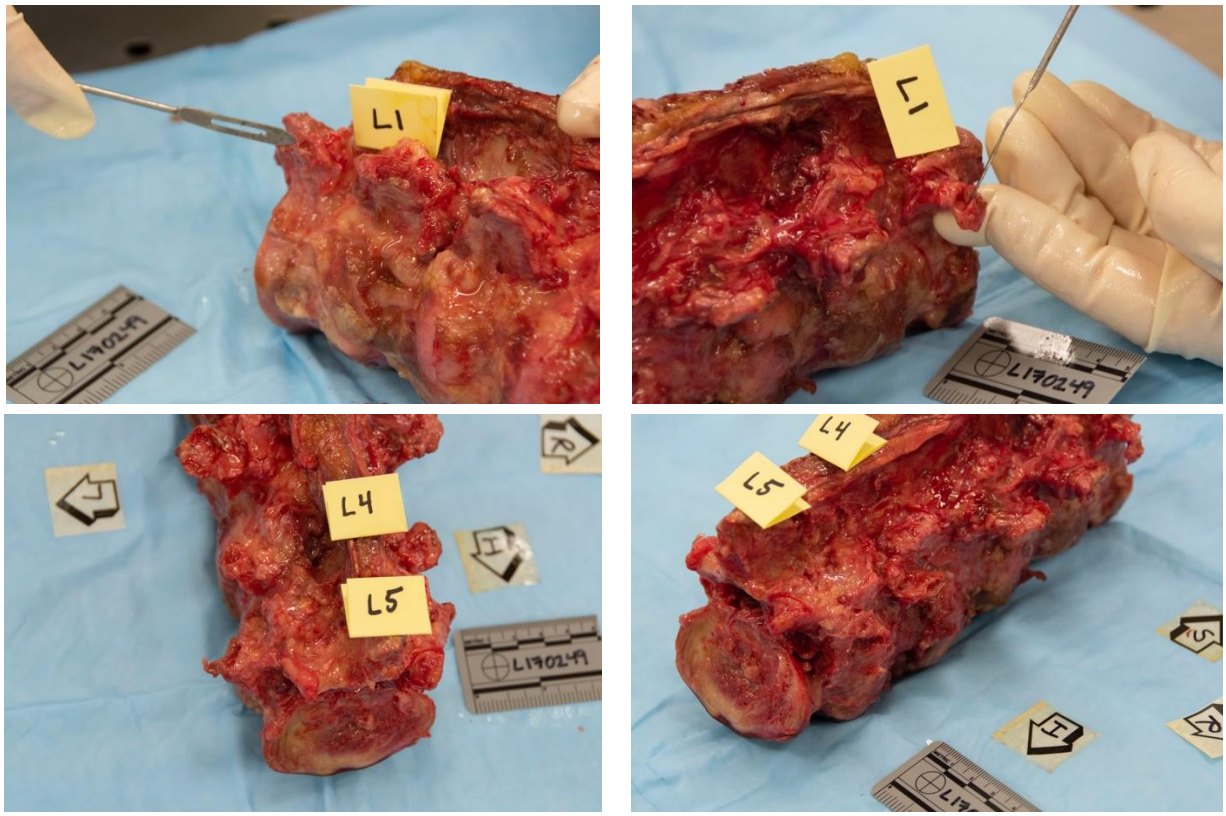

Figure C-7. WS12-03 lumbar spine fractures

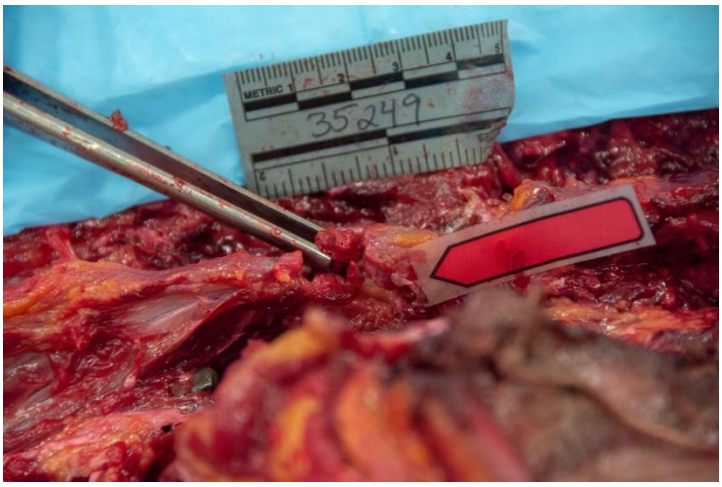

Figure C-8. WS12-01 thoracic spine fractures

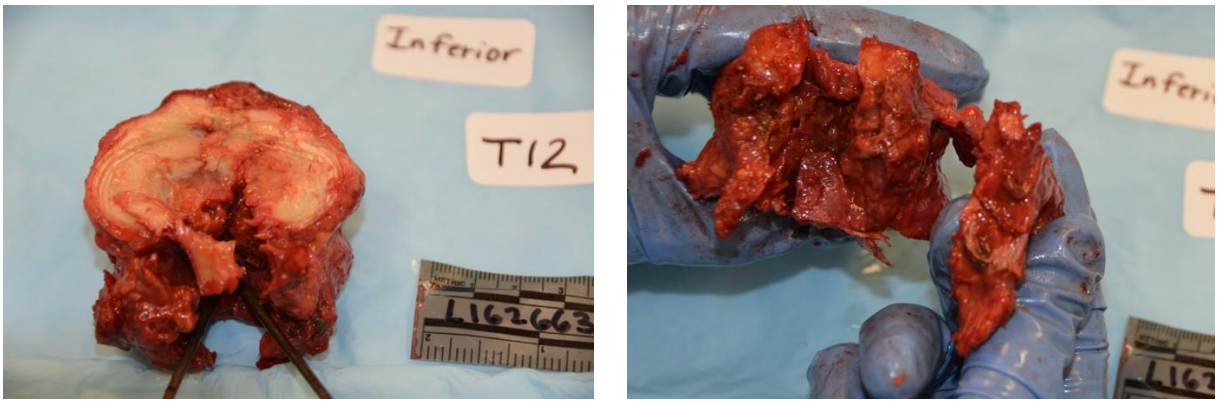

Figure C-9. WS12-02 thoracic spine fractures

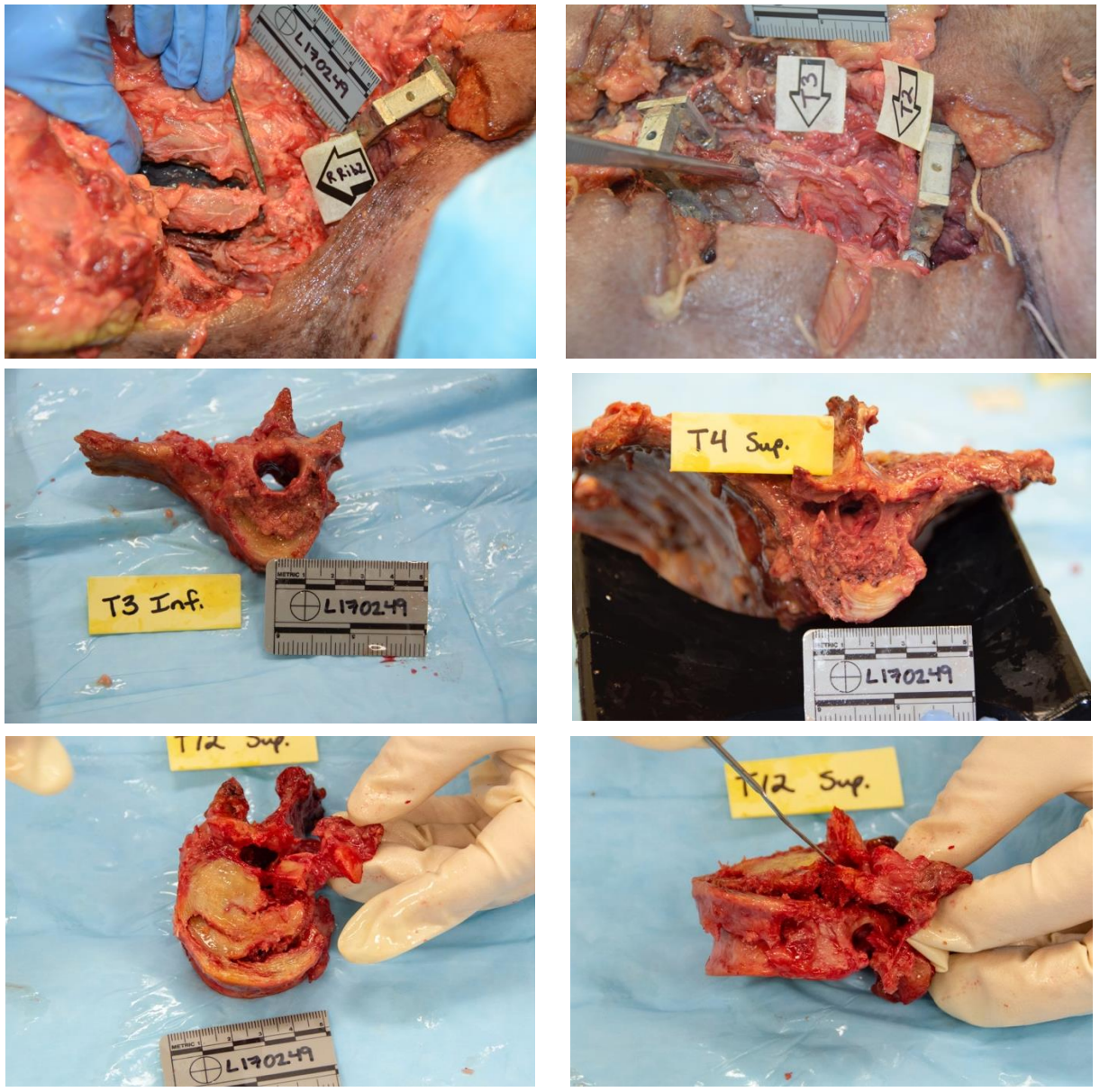

Figure C-10. WS12-03 thoracic spine fractures

Appendix D – List of Acronyms

3-D	three-dimensional
6DOF	six-degrees-of-freedom
ACH	advanced combat helmet
AE	acoustic emissions
AIS	Abbreviated Injury Scale
ARS	angular rate sensor
ASIS	anterior superior iliac spine
ATD	anthropomorphic test device
BRC	biofidelity response corridor
CG	center of gravity
CT	computed tomography
HIPC	Human Injury Probability Curve
IARC	Injury Assessment Reference Curve
IOTV	improved outer tactical vest
JHU-APL	Johns Hopkins University Applied Physics Laboratory
MP	match paired
PMHS	postmortem human subject
PPE	personal protective equipment
PSIS	posterior superior iliac spine
QCT	quantitative computed tomography
SCoTT	Signal Conversion Tiger Team
SOD	strength of design
TTP	time to peak
UBB	under-body blast
UMTRI	University of Michigan Transportation Institute
VALTS	Vertically Accelerated Load Transfer System
VisualAID	Visual Anatomical Injury Descriptor

WEO	WIAMan Engineering Office
WIAMan	Warrior Injury Assessment Manikin
WSU	Wayne State University

Appendix E – Glossary

Anthropomorphic Test Device (ATD): A physical device with size, shape, and biomechanical response characteristics representative of a target population of living humans. Embedded sensors within the ATDs enable the measurement of biomechanical responses associated with injury metrics-based Injury Assessment Reference Curves (IARCs). The correlation of these metrics to specific injuries enables ATD to predict the probability of specific injuries in test and evaluation applications.

Biometric: Term for body measurements and calculations. In this report, it is used to refer to measurements of the lumbar spine response under the applied loading conditions.

Human Injury Probability Curve (HIPC): A statistical relationship between the probability of a particular injury to a human and a continuous biometric directly measured or calculated from the measurements from physical tests of a postmortem human subject (PMHS).

Injury Assessment Reference Curve (IARC): A mathematical relationship between the probability of a particular injury to a human and a continuous biomechanical parameter measured in physical tests or simulations (or calculated from the results of physical tests) using an ATD. The measurement locations for biometric of interest could differ between the ones captured in ATD tests for IARCs versus PMHS tests for HIPCs.

Injury Metric: A biomechanical response quantity measured or derived from PMHS testing that has statistical correlation to injury outcome and severity for a given bone or anatomical component (e.g., force, moment, acceleration, or strain). When multiple relevant metrics are available, statistical methods are used to determine the best predictor of PMHS injury (Gayzik et al., 2017).

Match paired (MP): A matching pair of a PMHS test and an ATD test based on their anatomical representation, inertial properties, and test conditions.

Postmortem Human Subject (PMHS): A term for human cadaveric subjects serving as human surrogates in biomechanical tests that are partially representative of living human subjects of the target population.

Subject ID: A de-identified tracking number assigned by the tissue vendor to the subject.

Strength of Design (SOD): A test designed to prove out the capability of a device or fixture at or near the expected limits of device survivability.

Test ID: An internal tracking number assigned to the subject within the organization where it is being tracked and tested.

Time to Peak (TTP): The time from the start of a measured or calculated response until the signal reaches its peak. Calculated using the method defined in ARL-TR-7030 (Spink, 2014).

Warrior Injury Assessment Manikin (WIAMan): Army-sponsored program to develop an ATD specifically designed to predict injury risk in vertical loading environments.

Appendix F – Distribution List

ORGANIZATION

U.S. Army CCDC Data & Analysis Center
FCDD-DAD-OL/T Resetar-Racine
FCDD-DAS-LBW/K Loftis
6896 Mauchly St.
Aberdeen Proving Ground, MD 21005-5071

U.S. Army CCDC Army Research Laboratory
FCDD-RLD-CL/Tech Library
2800 Powder Mill Rd.
Adelphi, MD 20783

Defense Technical Information Center
ATTN: DTIC-O
8725 John J. Kingman Rd.
Fort Belvoir, VA 22060-6218